universität wien

DISSERTATION / DOCTORAL THESIS

Titel der Dissertation /Title of the Doctoral Thesis

New methods for the analysis of dislocations in semi-crystalline polymers

verfasst von / submitted by

Dipl.-Ing. Harald WILHELM

angestrebter akademischer Grad / in partial fulfilment of the requirements for the degree of

Doktor der Naturwissenschaften (Dr. rer. nat.)

Wien, 2017 / Vienna 2017

Studienkennzahl lt. Studienblatt / degree programme code as it appears on the student record sheet:	A 091411
Dissertationsgebiet lt. Studienblatt / field of study as it appears on the student record sheet:	Physik
Betreut von / Supervisor:	a.o. Univ. Prof. Dr. Michael Zehetbauer

Zusammenfassung

Trotz der großen wirtschaftlichen Bedeutung von teilkristallinen Polymeren ist das Wissen über die wesentlichen mikrostrukturellen Prozesse, die für die mechanischen Eigenschaften verantwortlich sind, vergleichsweise gering. Oberhalb der Glasübergangstemperatur ist für die makroskopischen Eigenschaften vor allem die Festigkeit der kristallinen Phase entscheidend. Dabei spielen vor allem lineare Gitterdefekte, wie Versetzungen, eine wichtige Rolle. Im Gegensatz zu Metallen ist die Untersuchung von Versetzungen in teilkristallinen Poly-meren schwierig, da nur sehr wenige Methoden mit zum Teil wesentlichen Einschränkungen zur Verfügung stehen.

Daher war es das Ziel dieser Dissertation, neue Charakterisierungsmethoden für Versetzungen in teilkristallinen Polymeren zu etablieren. In den letzten Jahren wurde eine spezielle Röntgendiffraktionsmethode entwickelt (Multi-reflection X-ray Profile Analysis (MXPA)), mit der die Dichte, die Anordnung und der Typ der Versetzung, und daneben auch die Kristallitgrösse bestimmt werden kann. Die erste Aufgabe der vorliegenden Dissertation war es, die MXPA Methode erstmals für die Anwendung an teilkristallinen Polymeren zu adaptieren. Zu diesem Zweck wurden spezielle Algorithmen geschaffen, die es erlauben, sich trotz des durch die Komplexität der polymertypischen Kristallsysteme signifikant erweiterten Lösungsraums rasch an das globale Minimum anzunähern. Damit konnte erstmalig an Polypropylen (PP) gezeigt werden, dass mit zunehmender plastischer Verformung die Versetzungsdichte von etwa 10^{15} auf 10^{16} m^{-2} ansteigt, womit die grosse Bedeutung der Versetzungen für die plastische Deformation von teilkristallinen Polymeren bestätigt wurde.

Ein wesentlicher Vorteil der MXPA ist die Möglichkeit, sie auch für in situ Röntgenbeugungsmessungen während der Deformation anwenden zu können. Im Rahmen der Dissertation wurden in situ Kompressions- und Entlastungsversuche an PP mit Synchrotron-Strahlung durchgeführt. Dabei hat sich gezeigt, dass die Versetzungen bei Entlastung zwar annihilieren, aber dass bereits in unverformten Proben genügend viele thermisch aktivierbare Versetzungen existieren, die für die plastische Verformung mobilisiert werden können. Erst ab Verformungen weit über der Streckgrenze müssen zusätzliche Versetzungen generiert werden.

Ein weiterer wichtiger Faktor für die mechanischen Eigenschaften von kristallinen Materialien ist die Kinetik der Versetzungen, welche in teilkristallinen Polymeren bisher ungeklärt war. Die bisher zur Untersuchung dieser Kinetik durchgeführten Nanoindentierungs-Kriechexperimente erscheinen wegen der in Ort und Zeit variierenden Spannungen, des kleinen Messvolumens und der unkontrollierbaren plastischen Verformung problematisch, weswegen in dieser Dissertation versucht wurde, eine alternative Testmethode auf Basis eines Torsions-Rheometers zu entwickeln, die all diese Nachteile der Nanoindentierung vermeidet. Somit wird eine eindeutige Trennung der Deformation in der amorphen von der Deformation in der kristallinen Phase gewährleistet und damit die direkte Bestimmung der

physikalischen Versetzungsmodellparameter ermöglicht. Durch umfangreiche Experimente mit Polyethylen (PE-HD) bei unterschiedlichen Temperaturen und Belastungen konnte die Aktivierungsenthalpie für die Generierung und Mobilisierung von Versetzungen mit 0.59 eV bestimmt werden. Dabei konnten bereits bei Spannungen < 1 % der Streckgrenze Versetzungsbewegungen in Form von Versetzungslawinen nachgewiesen werden.

Abstract

Despite the economic importance of semi-crystalline polymers the knowledge of the microstructural processes responsible for their mechanical properties is low. Beyond the glass transition temperature the strength of the crystalline phase is primarily responsible for the macroscopic one. In that case, linear lattice defects such as dislocations can play a decisive role. In contrast to metals, the investigation of dislocations in semi-crystalline polymers is challenging, as only few methods for dislocation analysis with partially strong limitations exist.

Thus it was the aim of this doctoral thesis to establish new characterization methods for dislocations in semi-crystalline polymers. In recent years, a special method of X-ray diffraction analysis was developed (Multi-reflection X-ray Profile Analysis (MXPA)) which is capable of measuring the density, arrangement and type of dislocations. The first task of the present thesis was to adapt the MXPA method, for the first time, also for the application in semi-crystalline polymers. For this purpose, special algorithms were created which allow for a fast approach to the global minimum, in spite of the significantly extended solution space due to the complexity of polymer-specific crystal systems. It could be shown for the first time on polypropylene (PP) that during plastic deformation the dislocation density increases from approximately 10^{15} to 10^{16} m^{-2} which confirmed the importance of dislocations for the plastic deformation of semi-crystalline polymers.

A major advantage of the MXPA is the possibility to carry out in situ X-ray diffraction measurements of dislocation parameters during deformation. In frame of this thesis, in situ compression and unloading experiments in PP have been performed by means of Synchrotron radiation. It has been found that the dislocations annihilate during unloading and that even in undeformed samples, a sufficient number of thermally activable dislocations are available which can be mobilized for the plastic deformation. Only for deformations far beyond the yield stress, additional dislocations are to be generated.

Another important factor for the mechanical properties of crystalline materials is the kinetics of dislocations which so far has been widely unclear in semi-crystalline polymers. Recent experiments achieving creep by nanoindentation to study this kinetics appear to be problematic because of stresses being not constant with respect to time and space, the small measuring volume, and the non-controllable plastic deformation. Therefore in this thesis, an alternative test method based on torsion experiments with a rheometer was developed, which avoids all these disadvantages, thus permitting a clear separation of the deformation in the amorphous and crystalline phase and a direct determination of the physical dislocation model parameters. By extensive experiments with polyethylene (PE-HD) at different temperatures and loads, an activation enthalpy of 0.59 eV for the generation and mobilization of dislocations could be determined. The experiments showed that dislocation movements in the form of dislocation avalanches occur even at stresses lower than 1 % of the yield stress.

Acknowledgements

When I met in 2000 Michael Zehetbauer the first time I had only a vague idea about the topic of my planned dissertation. As a polymer engineer and with a degree in physics, the topic should be in the area of polymer physics and, of course, be exciting. Michael Zehetbauer must have experienced the same about polymers. He had little knowledge about polymers, but a lot about dislocations. It quickly became clear that the available knowledge on dislocations in polymers was limited and therefore an exciting and challenging topic was born. His willingness to become interested in a relatively unknown material for him and to give support to this dissertation as a supervisor was decisive in making this "project" possible at all. Therefore I would like to thank him very much for this opportunity and, of course, for his special support during the last 17 years. It was very soon obvious that successful completion would be difficult without further support. Luckily, the polymer group has expanded rapidly, and through Florian Spieckermann, I always had someone available with advice and assistance. This has certainly contributed to the success of this work, thus I would also like to thank him very much. Equally my thanks go to Gerald Polt for his continuous help during his master's thesis and dissertation in the polymer group. He was always an important comrade-in-arms. Many thanks!

Even outside of the polymer group there were some colleagues who have supported me a lot. I would especially like to thank Michael Kerber and Erhard Schafler, for their support in countless synchrotron measurement terms and in the evaluation of the XRD measurement data.

Another important colleague was Alfred Paris who gave fundamental support to the first successful application of MXPA for polymers with his perseverance. But I would also like to thank the other members of the polymer group, Mohammad Zare Ghomsheh, Christopher Fischer, Cornelia von Baeckmann and Sabrina Strobel, who have given many inputs over the last years through their Bachelor's, Master's and Doctoral's theses. Not to forget Tanja Wagenknecht who has supported me in the realization of the countless nano-creep experiments.

Last but not least, I also have to thank my wife Uschi and my three children, Nina, Lukas and Tanja, who were always full of understanding when I (often) lacked time for them.

Contents

Part I.

Introduction

1. Motivation

Today polymers are the most important material group. At the beginning of the 1990s, more polymers by volume were processed than steel and with the end of the twentieth century even more than all metals together [1, 2]. This rapid growth has two main causes. On the one hand, the 5 bulk plastics polyethylene (PE), polypropylene (PP), polyvinyl chloride (PVC), polystyrene (PS) and polyethylene terephthalate (PET) mean that low-cost materials are available ($\sim 1.5\,€/dm^3$) and, on the other hand, injection-moulding and extrusion processing provide two cheap mass-production methods for these thermoplastics. Therefore high-precision parts (tolerances in the 1/100 mm range) with very good surface quality can be produced cost-effectively. Nevertheless, these standard thermoplastics have significantly lower strengths ($\sim 1/10$) and stiffnesses ($\sim 1/100$) compared to metals. While it is possible to improve the strength and stiffness of these polymers through molecular orientation and/or addition of reinforcing fibres, the intrinsic strength can only be improved by a small extent, e.g. by modifying the molecular mass distribution.

The situation for metals is totally different. Since many years it is well known that detects, especially line defects called dislocations, affect the strength essentially. By hindering the movemennt of these dislocations the strength can be dramatically increased. Many mechanisms for restricting the dislocation movement have been developed over the last decades [3]. For example, by adding suitable alloying elements in aluminum in combination with a heat treatment, these various mechanisms can be used to hinder the dislocation movement, which leads to an increase in strength from 50 MPa to above 600 MPa. In nanocrystalline aluminum, the strength can even be increased up to 800 MPa [4].

There are two groups of thermoplastics, the amorphous and semi-crystalline thermoplastics. The majority of engineering applications use semi-crystalline polymers (especially polyethylene and polypropylene) since they have better mechanical properties. Despite their commercial importance, the knowledge of the micro-structural processes during plastic deformation of semi-crystalline polymers is relatively low. This is due to their complex two-phase structure consisting of crystalline and amorphous regions. It is the crystalline phase that is primarily responsible for the strength. Therefore, the knowledge and understanding of the crucial micro-mechanical processes, especially about dislocations and their kinetic in the crystalline phase of semi-crystalline polymers, is of great importance.

2. State of the art

2.1. Semi-crystalline polymers

Semi-crystalline polymers consist of an amorphous and a crystalline phase. Due to the large chain length of the macromolecules, locking and entanglement occur which have essential influence on the crystallization behaviour. As a result, polymers crystallizing from the melt never reach 100 % crystallinity. From the melt crystallized semi-crystalline polymers consist of lamella crystals with intermediate amorphous layers. The lamella crystals form superstructures called spherulites. A typical spherulite can be seen in Figure 2.1a showing a characteristic Maltese cross in polarized light. Spherulites grow radially outwards from a nucleus (Figure 2.1b and c). The growth stops when two adjacent spherulites touch together. Spherulites typically have a diameter of several μm to some 100 μm.

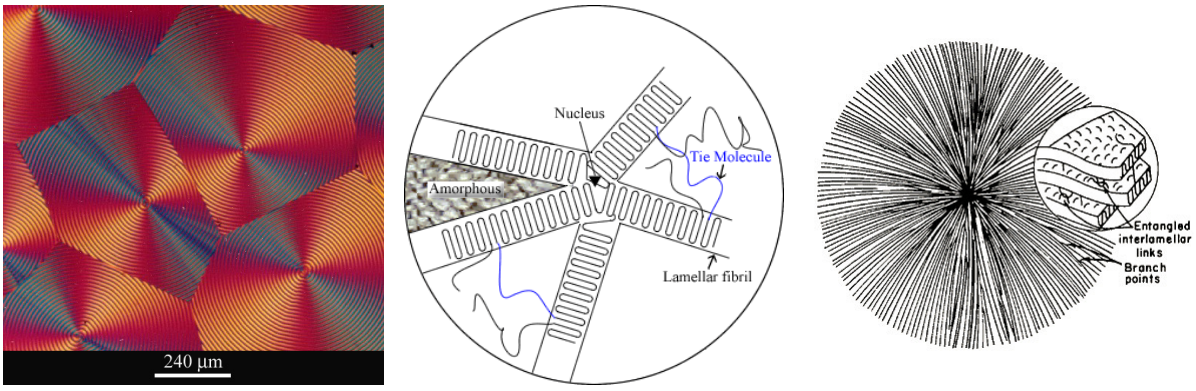

(a) (b) (c)

Figure 2.1.: *Spherulites.*
(a) Optical polarisation micrograph of polyhydrxybutyrate spherulites. From [5].
(b,c) Schematic representation of the crystalline lemellae arrangement in the spherulitic superstructure. From [6, 7].

The typical extinction patterns seen in polarized light are due to the orientation of the crystals within the spherulites. Analysis of the Maltese cross patterns has indicated that the molecules are normally aligned tangentially in polymer spherulites. It has been shown that the *b* crystal axis is radial in polyethylene spherulites and the *a* and *c* crystallographic directions are tangential. In some polymers, the spherulites in polarized light are seen to be ringed (Figure 2.1a), which has been attributed to a regular twist in the crystals. The

thickness of the lamellae is about 10 - 30 nm, which is similar to solution-grown lamella single crystals. Selected-area electron diffraction has shown that the polymer molecules are orientated approximately normal to the lamella surface (Figure 2.1b). This is also evidence of the similarity between melt-crystallized and solution-grown lamellae [8].

Since during the crystallization process the molecules do not completely disentangle, not all folded chains can return to the lamellae. It is therefore probable that individual chains extend over the intermediate amorphous regions from one to the next lamella (tie molecules, Figure 2.1 and 2.2). These tie molecules play an important role in plastic deformation, since they mechanically link the lamellae together.

The lamellae need not be of constant thickness and they are more or less curved, since the less dense and thus more space-consuming amorphous layers have to be incorporated between the lamellae (Figure 2.2).

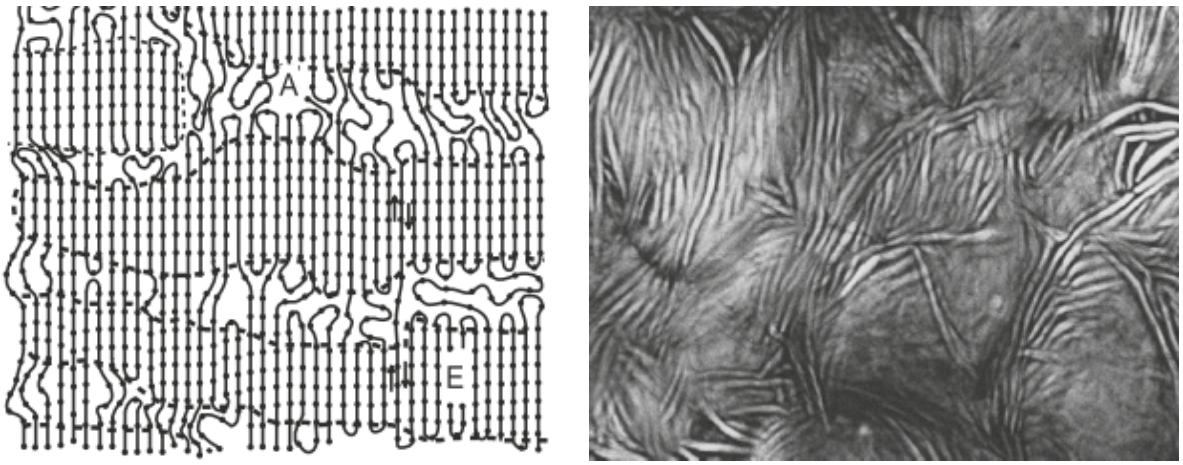

(a) (b)

Figure 2.2.: *Lamellae geometry.*
(a) Schematic representation of the chain arrangement. From [9].
(b) TEM micrograph of high density polyethylene. From [10].

Within the lamellae, the chains are arranged in parallel and almost perpendicular to the lamella surface. For example in polyethylene the symmetric zigzag chains in the plane are arranged in an orthorhombic crystalline form (Figure 2.3). Each chain is surrounded by four equally distant chains. These surrounding chains are rotated along their longitudinal axis by 82 ° to the central chain. The distance of the carbon atoms in the chain is 0.154 nm, the valence angle is 109 ° and the C-H distance is 0.11 nm. But even more complex, unsymmetrical macromolecules can form regular crystalline structures, such as polypropylene and polyethylene terephthalate.

In recent years it has been found that the transition between the amorphous and the crystalline phase is not abrupt. In the interface between the two phases there is still a few nm thick intermediate layer, the rigid amorphous phase (Figure 2.4) [12, 13]. This

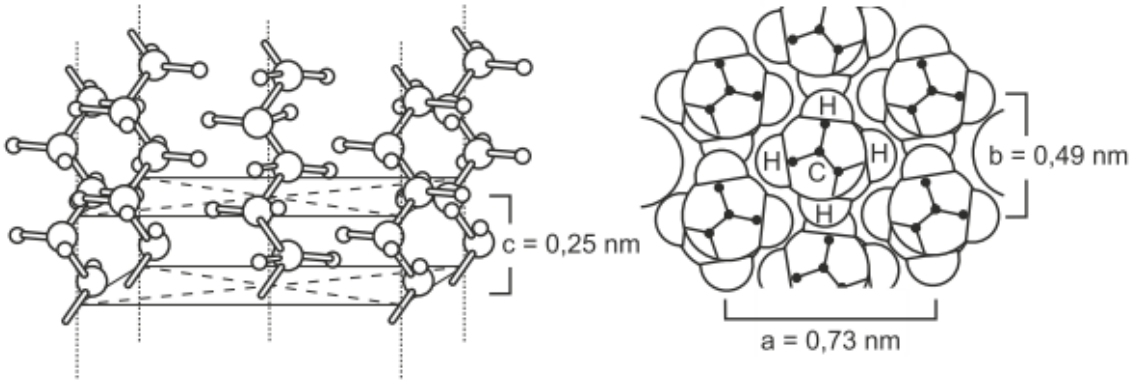

Figure 2.3.: *Crystalline structure of polyethylene. Left - orthorhombic unit cell. Right - section in the direction a b, atoms with Van der Waals radius. From* [11].

stiffer interface originates from geometrical constraints, because the density cannot change abruptly. This intermediate phase is non-crystalline and includes amorphous portions of macromolecules whose mobility is hindered by the near crystalline structures. The limited molecular mobility significantly increases the stiffness of this layer. This is particularly interesting, since dislocations are formed on the crystal surface and thus in the rigid amorphous phase.

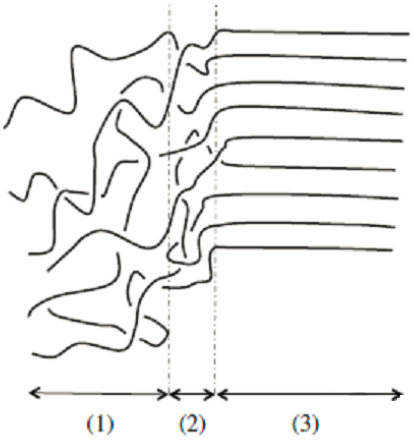

Figure 2.4.: *Rigid amorphous phase (2), the some few nm thick interface between the amorphous phase (1) and the crystalline phase (3). From* [14].

2.2. Plasticity of semi-crystalline polymers

Of course, the mechanical behaviour of the polymers was investigated intensively [15]. Especially the micro-structural changes during plastic deformation, such as orientations of the amorphous phase, lamella rotation, texture development, lamella deformation, lamella

fragmentation and formation of highly oriented structures, have all been studied in depth [16–19]. But because of their complex structure (amorphous and crystalline phases, superstructures, tie molecules) and the interaction of strong covalent bonding forces within the macromolecules and the much weaker Van der Waals bonds between the molecules there are still open questions.

There are strong differences in the mechanical properties of the amorphous and crystalline phases. This applies in particular to temperatures above the glass transition temperature T_g and leads to different distinct deformations in the amorphous and crystalline phase. Therefore a complete understanding of the mechanical properties is only possible if the micro-structural processes in both phases and their mutual influence are known. The phase fractions and size effects also play an important role.

2.2.1. Stress-strain characteristics of semi-crystalline polymers

The mechanical behaviour of materials is usually characterized by a stress-strain curve from a mechanical uniaxial deformation experiment. For semi-crystalline polymers above T_g, the stress-strain curve can be divided into four characteristic regions. The transition points A, B, C and D (Figure 2.5) can be determined by cyclic loading unloading experiments [20]. The deformation can be separated into elastic and plastic parts by means of intermediate complete unloads. An additional temperature treatment of the deformed samples allows the separation of the plastic deformation into reversible and residual parts. Combining these cyclic experiments with micro-structural observations, the transition points can be assigned to micro-structural processes [20, 21]. An important aspect is that these transition points are triggered by the applied strain instead of stress [19].

Point A
End of pure elastic deformation. From this point the plastic deformation starts. Normally, this point is not directly apparent in the stress-strain curve. However, some types of polyethylene display a double yield point [22] where the first yield point can be assigned to this transition. Before this point the deformation mainly takes place in the softer amorphous phase.

Point B
Macroscopic yield point. Begin of huge slip within lamellae and lamellae rotation. The crystalline deformation changes from a localized slip in a few lamellae with preferential orientation with respect to the applied strain, to a general slip in all lamellae. After this point ideal plastic flow or even softening can be observed.

Point C
Backstresses from the highly strained entangled amorphous network and tie molecules cause a partial fragmentation of the lamellae and thus a small reduction of crystallinity. In the following part of the stress strain curve, the highly oriented amorphous phase contributes essential to the macroscopic strength and a strong strain hardening occurs.

Point D
The formation of micro fibrils starts and the disentanglement of the chains leads to an unrecoverable deformation. Finally we get a fibrillar structure.

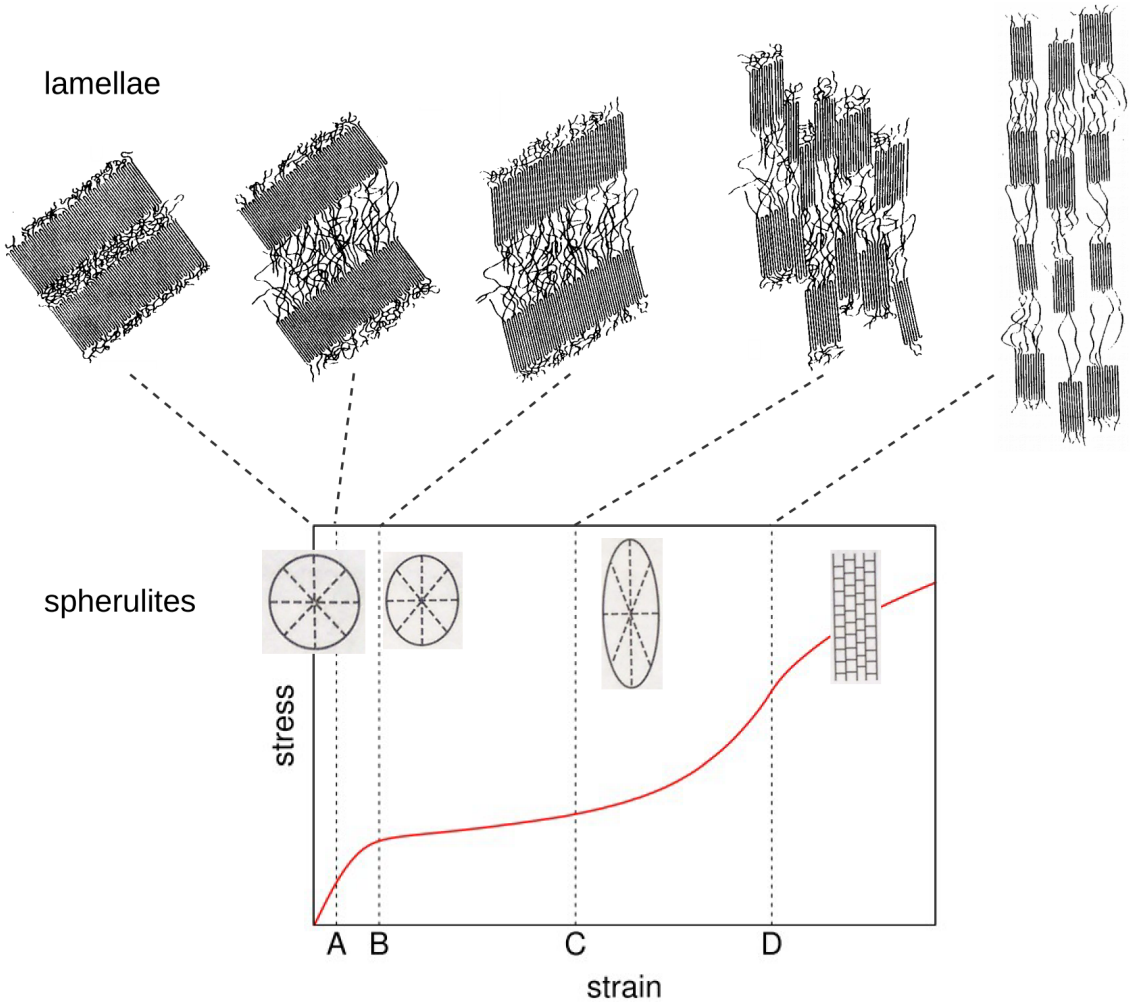

Figure 2.5.: *Transition points of the stress strain curve and the corresponding microstructure of a semi-crystalline polymer. Modified from* [23].

In principle, the compression test is equivalent to the tensile test with regard to micromechanical processes. But additional cavitation (crazing) occurs in tensile tests [24]. The differences in the stress-strain curve can be explained by the different texture development [15]. However, new molecular dynamics simulations [25] have shown that there could be at different strain rate levels differences depending on the type of deformation (extension, compression, shear). If the compression test is carried out as a plane strain compression experiment, very large deformations ($\varepsilon > 1$) can be attained. This can lead to the formation of a new lamella structure with a different lamella thickness [26].

2.2.2. Plasticity of the amorphous phase

The amorphous phase is formed from chains which are not immediately folded back into the same lamella. These chains can end in the amorphous phase or can also extend to adjacent lamellae and thus produce additional mechanical couplings between the lamellae (tie molecules). The embedding of the lamellae in the amorphous phase results in further degrees of freedom in the plastic deformation of the lamellae. This acts as an additional slip system for the crystalline deformation of the lamella crystals [27].

Basically, three deformation modes can be distinguished in the amorphous phase in semi-crystalline polymers (Figure 2.6) [28].

- interlamellar slip (shear)
- interlamellar separation
- lamellae stack rotation

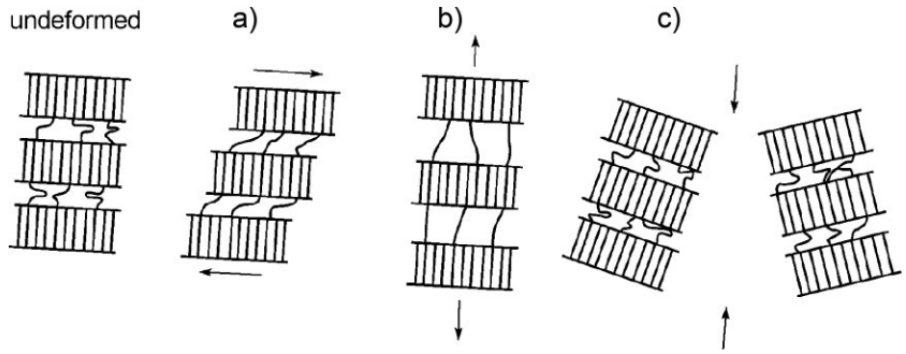

Figure 2.6.: *Deformation modes of the amorphous phase. Modified from* [28].
(a) interlamellar slip (shear), (b) interlamellar separation, (c) stack rotation.

Interlamellar slip (Figure 2.6a) allows shearing of the lamellae parallel to each other. This deformation mechanism is relatively easy to activate at temperatures above T_g and is therefore relevant for polyethylene [29] and polypropylene [30]. It was possible to show that the recoverable part of deformation can be almost entirely attributed to the reversible interlamellar slip [20]. The restoring forces result from the entropy elasticity of the amorphous phase [31]. The stretched tie molecules create a back stress, which returns the lamellae back to their original position when the sample is unloaded.

Interlamellar separation (Figure 2.6b) is induced by a tensile stress component perpendicular to the lamella surface [29]. As a result, the intermediate amorphous layer becomes thicker and the long period increases in the load direction. Since the amorphous phase behaves as a perfect rubber, this type of deformation is unlikely. A lamella separation simultaneously produces a transverse contraction, which is restricted by lateral constraints imposed by the souroundig crystalline phase. Thus, such a deformation must involve a

change in volume. Rubbers are resistant to volume changes (Poisson ratio = 0.5), since they generally have high bulk modulus and relative low shear modulus [19]. Therefore, this deformation mode leads to cavitation in the amorphous layer between lamella crystals [32] and further to the formation of voids or crazes. Whether and to what extent this deformation mode occurs depends strongly on the number of tie molecules and entanglement density in the amorphous phase.

Applied stress can always lead to *lamellae stack rotation* (Figure 2.6c). Due to the embedding of the lamellae in the softer amorphous phase this is always possible, especially at $T > T_g$ and does not lead to any increase of the strain. This results in an additional degree of freedom in the deformation, which reduces the number of necessary slip systems for the plastic deformation of the lamellae. Therefore the lamellae rotation does not occur individually, but in stacks of up to ten lemellae. These lamella stacks behave like a single body.

During the deformation, the various deformation modes in the amorphous phase can occur simultaneously. Which mechanism is preferred depends on the position in the spherulite relative to the load direction (Figure 2.7).

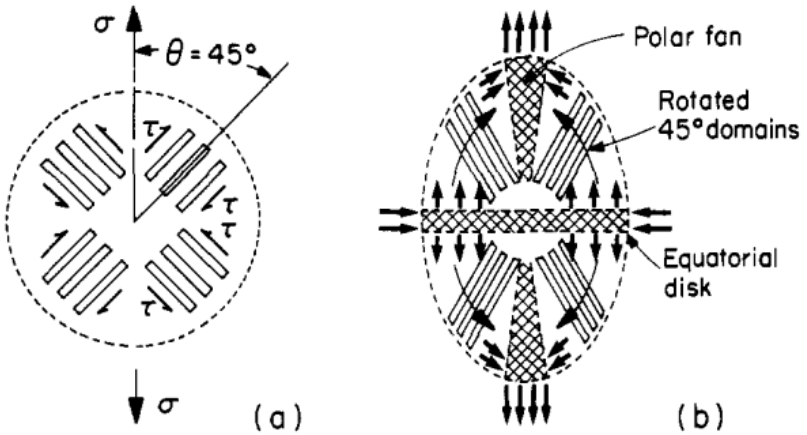

Figure 2.7.: *Possible deformation modes within a spherulite, depending on the psition. Modified from* [33].
(a) the 45 ° domains in an undeformed spherulite.
(b) lattice rotations due to simple shear in 45 ° segments subject equatorial regions to enhanced tension and radial compression and polar regions to enhanced compression.

Interlamellar separation occurs mainly in the equatorial region of the spherulites. Amorphous layers tilted by 45 ° towards the applied stress undergo interlamellar shear which leads to interlamellar slip and simultaneously to a rotation towards the polar region (lamellae stack rotation). A compression stress acts on the vertical lamellae in the polar region which can lead to interlamellar slip [18, 33].

Due to the low strength of the amorphous phase above T_g, it deforms at very low stresses. Thereby the molecules are increasingly oriented with the increase in deformation. This

causes a considerable increase in strength and stress in the amorphous phase. As a result, the stress is transferred to the crystalline phase. If the critical resolved shear stress (CRSS) for the easiest slip system is reached, a plastic deformation occurs in the crystalline phase.

The stress in the two phases is very different. Figure 2.8 shows the stress development of the equivalent stress in crystalline and amorphous components in polyethylene. During deformation, the amorphous network is stretched and the chains are oriented in the load direction. An ever larger tension is necessary for the increasing orientation. In case of still larger deformations, the stress in the amorphous phase exceeds the stress in the crystalline phase.

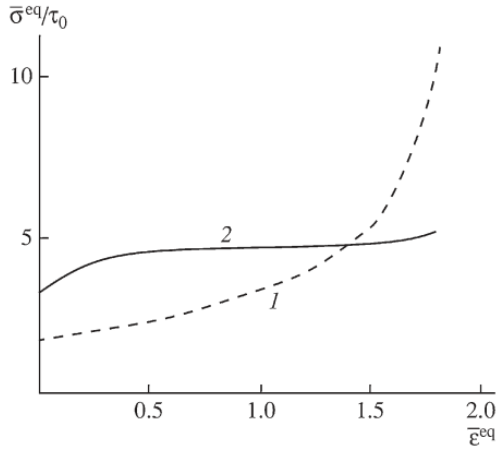

Figure 2.8.: *The dependence of normalized equivalent stresses in amorphous (1) and crystalline (2) phases of PE on equivalent strain, under uniaxial compression. Modified from* [34].

The mechanical behaviour of the isolated amorphous phase can be described by means of various thermally activated processes by assuming a number of Eyring processes [35, 36]. More current complex models are discussed by Richeton et al. [37].

2.2.3. Plasticity of the crystalline phase

The yield behaviour of semi-crystalline polymers is mainly influenced by the crystalline phase. There are three models for explanation.

- Peterlin's micronecking model [38]
- melting and recrystallisation model [39]
- crystallographic model [28]

The Peterlin model is very popular despite extensive criticism. This model shows transformation of the original chain-folded lamella morphology into the partially unfolded-chain fibrillar structure. However, cavitation is a necessary condition. But cavitation is not necessary in other deformation modes than tensile ones. Morphological transformations from initial isotropic structure into microfibrils during plastic deformation can take place also without the formation of any cavities or microvoids in the case of plane-strain or uniaxial compression. In these cavity-free modes the plasticity in lamellae develops according to crystallographic mechanisms, primarily crystallographic chain slip [19].

Recent molecular dynamics simulations [25] of a lamellae stack of polyethylene under extension, compression and shear showed different deformation types depending on the deformation rate and the strain. Crystallographic slip was observed during tensile deformation at low strains ($0 < \varepsilon < 0.08$) regardless of deformation rate. Only at high levels of strain ($\varepsilon > 0.26$) were melting and recrystallization observed. Under compressive deformation at the low deformation rates, crystallographic slip was again observed at low strains. However, no melting or recrystallization phenomena occurred, even at the highest strains simulated (ε = - 0.33). Under shear deformation, interlamellar slip was observed. However their results regarding the macroscopic stress differ markedly from experimental results. Nevertheless, it shows that in the future, in addition to the experimental investigations, simulations for the understanding of the essential micro-mechanical processes will become more important.

A comparison of calculations [40] and measurements [41] of the critical resolved shear stress (CRSS) have shown that overcoming the Van der Waals bonds requires a 10-fold higher CRSS than was measured in experiments. Comparing the enthalpies of activation of local melt processes with the generation of dislocations (in polymers regarded as a thermally activated process [18]) an estimation shows that the energy requirement for local melting is approximately 50 % higher than for the generation of dislocations [23]. This suggests that the dislocations must play the most important role in the plastic deformation of semi-crystalline polymers.

However, the CRSS for a particular slip system is not an absolute material parameter. According to the dislocation theory crystallographic slips occur via the propagation of dislocations along the slip plane. The CRSS for a crystal depends then on the number of mobile dislocations and their mobility. An increasing number of mobile dislocations decreases the CRSS. This reduces the energy necessary for generation of new mobile dislocations upon deformation [42]. Several sources for the increase of yield stress are distinguished with regard to the plasticity of metals [43].

- misorientation of crystallites
- lower purity of the crystalline phase
- change of crystal surface conditions
- change in the number of mobile dislocations

Other interesting discussions regarding the different models can be found in the reviews from Oleinik [30], Seguela [44] as well as Bartczak and Galeski [19].

In summary it can be said that the crystallographic model is the decisive model for the description of the plasticity in semi-crystalline polymers.

2.2.4. Crystallographic model

The crystallographic model is based on the clasical theory of crystal plasticity. Bowden and Young applied 1974 the classical crystallographic (nonpolymer) mechanisms of plasticity to polymer crystals [28]. They convincingly showed, that these classical concepts of nucleation of dislocations and their slip along the crystal lattice agrees well with the behaviour of semi-crystalline polymers. Young and other researchers extended this approach in the following years [18]. Numerous experimental investigations have clearly shown that the deformation of polymer crystals occurs via the crystallographic mechanisms [45, 46].

In the case of the plastic deformation of the lamellae, the crystalline structure is not changed. Only at very large tensile deformation levels, when cavitation and voiding lead to unravelling of the folded chains does a complete break down of the crystals occur. Polymer crystals can deform plastically by [19]

- crystallographic slip,
- twinning and
- martensitic transformation.

Thereby the crystallographic slip mechanism is the most important. It can accommodate plastic strains much larger than the other two mechanisms. Much larger plastic strains are possible than by the other two mechanisms.

Crystallographic slip

Crystallographic slip occurs, if two parallel crystallographic planes move relative to each other. In this respect a line-shaped defect (screw or edge dislocation) travels along the slip plane through the crystal. The slip takes place, if the critical resolved shear stress (CRSS) τ_0 of the slip system (= crystallographic plane (hkl) in which slip occurs, and a slip direction $[uvw]$) is exceeded. Single slip is a pure shear deformation. For a uniaxial deformation with the stress σ the resolved shear stress τ can be calculated using Schmid's law.

$$\tau = \sigma cos(\chi) cos(\lambda) = m\sigma \tag{2.1}$$

where χ and λ are the angles of the slip plane normal and of the slip direction with respect to the axial stress s, respectively (Figure 2.9).

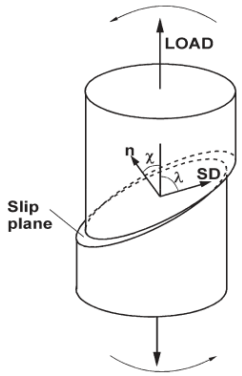

Figure 2.9.: *Definition of a slip system, slip plane and slip direction (SD). From* [19].

The factor $m = cos(\chi)cos(\lambda)$ is the Schmid factor and can vary within $0 \leq |m| \leq 0.5$. For a given stress σ is the highest resolved shear stress τ in the slip system with the highest Schmid factor. Yielding, i.e. the beginning of plastic deformation, starts when $\tau > \tau_0$ in a slip system.

In order to achieve a homogeneous deformation, more slip systems are necessary. There are a minimum number of 5 independent slip systems required [47]. In polymers the number of possible independent slip systems is generally lower, since a molecular fracture is not possible. Thus, the slip planes are limited to those that contain the chain direction, i.e. $(hk0)$-planes when [001] is the chain direction. Three main slip systems are observed in case of polyethylene and polypropylene [46, 48, 49]. Due to the soft amorphous phase the lamellae can rearrange upon deformation. This permits the compensation of the low number of slip systems and enables a homogeneous deformation.

Two basic mechanisms for crystallographic slip have been observed.

- chain slip
- transverse slip

For the chain slip, the slip direction is parallel to the chain direction. Chain slip already occurs at low plastic strains due to its low CRSS [50]. For the transverse slip the slip direction is normal to the chain axis. Commonly transverse slip appears at higher deformations due to the higher CRSS for this type of slip [16]. The slip planes lie parallel to the polymer chains for both of these slip mechanisms. Crystallographic slip with the slip plane perpendicular to the chain axis would require chain rupture which is not possible due to the strong covalent bonds in the chains (Figure 2.10).

The chain and transverse slip in lamellae can proceed in two different ways [30].

- fine (homogeneous) slip

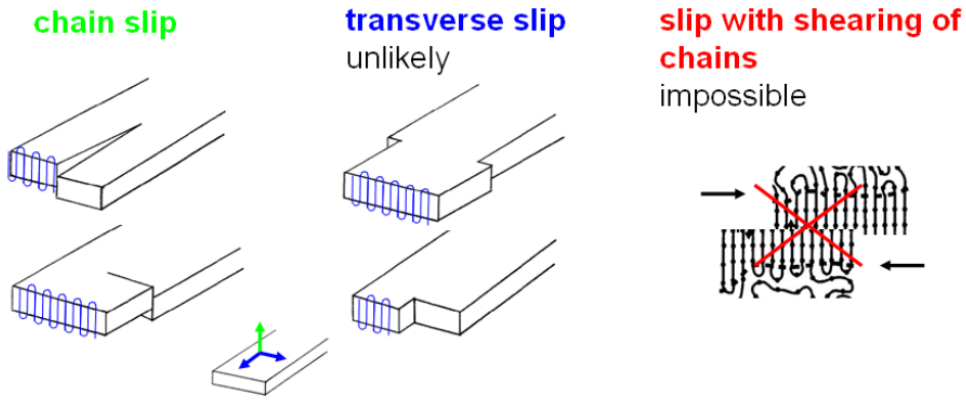

Figure 2.10.: *Schematic representation of different slip types. Slip that takes place in planes perpendicular to the chain direction is impossible do to the strong covalent bonds within the chains.*

- coarse (heterogeneous, block) slip

Figure 2.11a and b show schematically two different crystals which have deformed by single slip to the same final shear strain. Thereby fine slip is defined as a small amount of slip on a large number of planes and corresponding coarse slip by large amount of slip on fewer planes. In polymers the slip modes can be distinguished since a wide-angle X-ray diffraction pattern (WAXS) indicates the direction of the chain axis c, and a small-angle X-ray pattern (SAXS) indicates the direction of the lamella normal $\mathbf{n}$. For fine slip only $\mathbf{n}$ rotates relative to c whereas for coarse slip $\mathbf{n}$ and c rotate together but the angle between $\mathbf{n}$ and c does not change during deformation. In polymer crystals with larger unit cells such as polyamide (PA) more complex effects can arise. This can be explained by shearing of the lattice by partial dislocations with a coresponding Burgers vectors less than the lattice vector in the chain direction. The effect is illustrated schematically in Figure 2.11c [28].

WAXS and SAXS experiments showed that only fine slip occurs at small deformations [46, 51] and at higher strains fine slip is still the prevalent mechanism related to crystallographic slip [32].

Twinning

The most commonly obtained types of twinned crystals are those in which one part of the crystal is a mirror image of another part. The boundary between the two regions is called twinning plane. Deformation twins can be explained in terms of a simple shear of the crystal lattice. The type of twins that are obtained in polymers are formed in such a way that the lattice is sheared without either breaking or distorting the polymer molecules. Figure 2.12a shows a micrograph of a twin obtained by deforming a polydiacetylene single crystal. The single crystal is viewed at 90 ° to the chain direction. The striations in the crystal define the molecular axis and it can seen that the molecules kink over sharply at

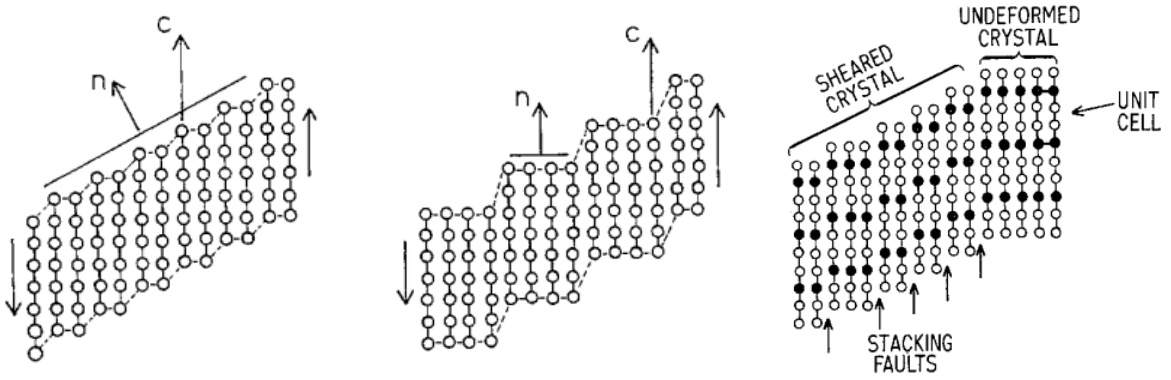

Figure 2.11.: *Schematic diagrams illustrating different degrees of fineness of slip. From* [28].
(a) Fine slip. A small displacement of one lattice vector has occurred on every lattice plane in the crystal. The direction of the normal to the surface of the crystal **n** *has rotated relative to the chain axis c during deformation.*
(b) Coarser slip. A displacement of two lattice vectors on every fourth plane results in the same total shear.
(c) Fine slip of partial dislocations.

the twin boundary. A schematic diagram of the molecular arrangements on either side of the twin boundary is given in Figure 2.12b. The result of the twinning process is that the molecules on every successive plain in the twin are displaced by one unit of *c* parallel to the chain direction. This is identical to the result of a chain direction slip [8].

Another type of twinning has been found to occur in polymer crystals involves a simple shear in directions perpendicular to the chain axis, which, in this case, does not bend the molecules. An example of this type of twinning was found in polyethylene [52]. Two particular twinning planes (110) and (310) have been found. The occurrence of twinning can be detected from measurements of the rotation of the *a* and *b* axes about the *c* axes since the twinning causes a large rotation of the crystal lattice.

Martensitic Transformation

A Martensitic transformation is a diffusionless (no long-range diffusion) phase transition which involves a change in crystal structure. Martensitic transformations have not been widely reported in polymers, but an important one occurs during deformation in polyethylene [53]. The normal crystal structure of polyethylene is orthorhombic. But after or during deformation an extra Bragg reflection are found in diffraction patterns (Figure 2.24). These could be explained in terms of the formation of a monoclinic form. The transformation takes place by means of simple two-dimensional shear of the orthorhombic

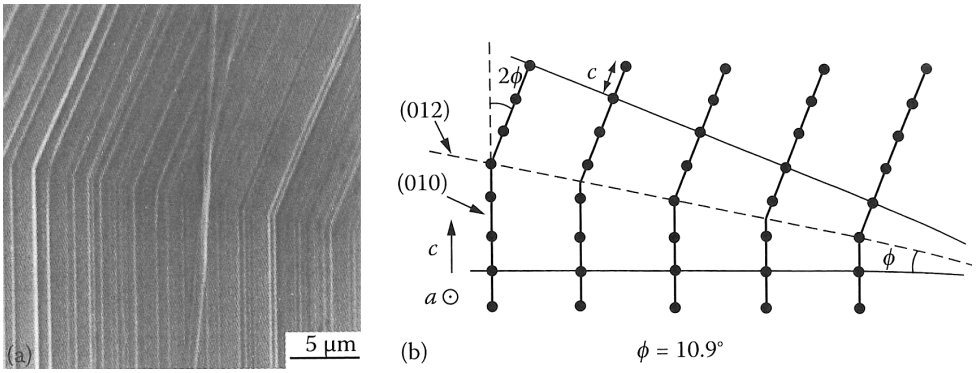

Figure 2.12.: *Large twin in a polydiacetylene single crystal. From* [8].
(a) Scanning electron micrograph of a twin.
(b) Schematic diagram of twin on molecular level. The chain direction axis c is perpendicular to the page and ϕ is the angle of rotation of the twin.

crystal structure in a direction perpendicular to c. The chain axis length remains virtually unchanged by the transformation, at about 0.254 nm, but in the monoclinic cell it is conventionally indexed as b [8].

2.3. Dislocations

If the strength of metal single crystals is investigated, it is found that this can be several orders of magnitude smaller than the theoretical value. It has been shown that the strength is strongly effected by lattice defects. Thereby the dislocations play the decisive role [47].

Dislocations are one-dimensional, line-shaped lattice defects. One differentiates between edge and screw dislocations (Figure 2.13). Edge dislocations can be considered as the transition of an extra plane of atoms to the undisturbed crystal. Screw dislocations arise if the crystal is sheared off on one side of the dislocation line by an atomic distance parallel to the dislocation line. Thereby the Burgers vector b describes the magnitude and the direction of the relative displacement of the crystal parts. The Burgers vector for edge dislocations is oriented perpendicular to the dislocation line and for screw dislocations parallel to the dislocation line.

In a real crystal there are always a combination of edge and screw dislocations. Thus the dislocation lines (lines along the defect in the crystal) are generally not straight but curved. They form closed curves within or end at the surface of the crystal. Within the crystal, dislocation lines cannot end for geometrical reasons. Since the crystal lattice is locally distorted by dislocations, a dislocation always produces an stress field around the dislocation line (Figure 2.14).

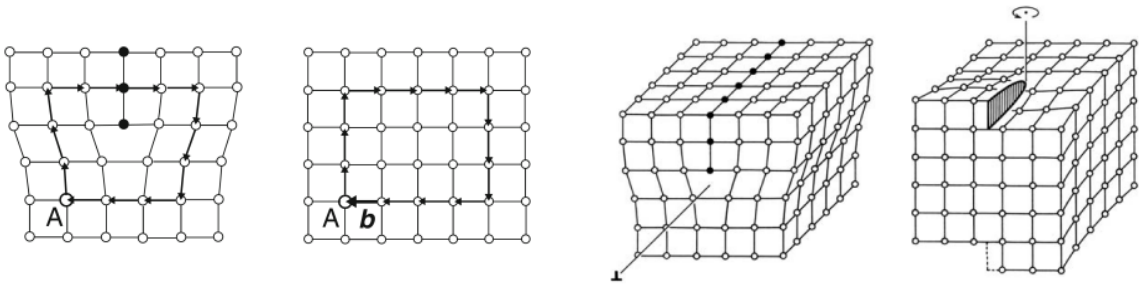

(a) (b)

Figure 2.13.: *Schematic illustration of edge and screw dislocation. From* [54].
(a) Edge dislocation - an extra half-plane of atoms in a lattice. The Burgers vector is perpendicular to the dislocation line.
(b) Screw dislocation - generated by shearing one side of a crystal with against its opposite side.

Screw and edge dislocations cause different distortions. **Screw dislocations** only have a shear stress component $\tau_{\Theta z}$ (in cylindrical coordinates) which acts in a radial plane Θ in an axial direction z [3]. According to Hook's law for the shear stress this gives

$$\tau_{\Theta z} = \mu \gamma_{\Theta z} = \frac{\mu b}{2\pi r} \tag{2.2}$$

where μ is the shear modulus, γ the shear strain, r the radial distance from the core and b the Burgers vector. This leads to the stress tensor $\sigma^{\odot}_{r\Theta z}$ for screw dislocations in cylindrical coordinates

$$\sigma^{\odot}_{r\Theta z} = \begin{bmatrix} 0 & 0 & 0 \\ 0 & 0 & \tau_{\Theta z} \\ 0 & \tau_{\Theta z} & 0 \end{bmatrix}. \tag{2.3}$$

This relation in Cartesian coordinates would read as

$$\sigma^{\odot}_{xyz} = \begin{bmatrix} 0 & 0 & \tau_{xz} \\ 0 & 0 & \tau_{yz} \\ \tau_{xz} & \tau_{yz} & 0 \end{bmatrix} \tag{2.4}$$

with

$$\tau_{xy} = \mu\gamma_{xz} = -\frac{\mu b}{2\pi}\frac{y}{x^2+y^2} \tag{2.5a}$$

$$\tau_{yz} = \mu\gamma_{yz} = \frac{\mu b}{2\pi}\frac{x}{x^2+y^2} \tag{2.5b}$$

The stress field of the **edge dislocations** is more complex. Beside the shear stress components it also contains normal stress components. In Cartesian coordinates the stress tensor $\sigma^{\perp}_{xyz}$ has the form

$$\sigma^{\perp}_{xyz} = \begin{bmatrix} \sigma_{xx} & \tau_{xy} & 0 \\ \tau_{xy} & \sigma_{yy} & 0 \\ 0 & 0 & \sigma_{zz} \end{bmatrix}. \tag{2.6}$$

The components of this tensor are

$$\sigma_{xx} = -\frac{\mu b}{2\pi(1-\nu)}\frac{y(3x^2+y^2)}{(x^2+y^2)^2} = -\frac{\mu b}{2\pi(1-\nu)}\frac{\sin\theta(2+\cos(2\theta))}{r} \tag{2.7a}$$

$$\sigma_{yy} = \frac{\mu b}{2\pi(1-\nu)}\frac{y(x^2-y^2)}{(x^2+y^2)^2} = \frac{\mu b}{2\pi(1-\nu)}\frac{\sin\theta\cos(2\theta)}{r} \tag{2.7b}$$

$$\sigma_{zz} = \nu\left(\sigma_{xx}+\sigma_{yy}\right) \tag{2.7c}$$

$$\tau_{xy} = \frac{\mu b}{2\pi(1-\nu)}\frac{x(x^2-y^2)}{(x^2+y^2)^2} = \frac{\mu b}{2\pi(1-\nu)}\frac{\cos\theta\cos(2\theta)}{r} \tag{2.7d}$$

This stress components are illustrated in Figure 2.14.

In contrast to the screw dislocation, an edge dislocation causes a change in the crystalline volume. This will be expressed by the additional Poisson ratio ν.

For the strongly anisotropic polymer crystals the displacements related to the distortions can be calculated by applying Stroh's approach [56].

In this continuum-mechanical approach the dislocation core has been ignored, since due to the large distortions Hooke's law is no longer valid in this region. To estimate the magnitude of the dislocation core (r_0 inner cut off radius), one can use the fact that the elastic stress cannot exceed the theoretical stress τ_{th}.

For screw dislocations [3] applies

$$\tau(r_0) = \frac{\mu b}{2\pi r_0} \approx \tau_{th} \approx \frac{\mu}{2\pi} \tag{2.8}$$

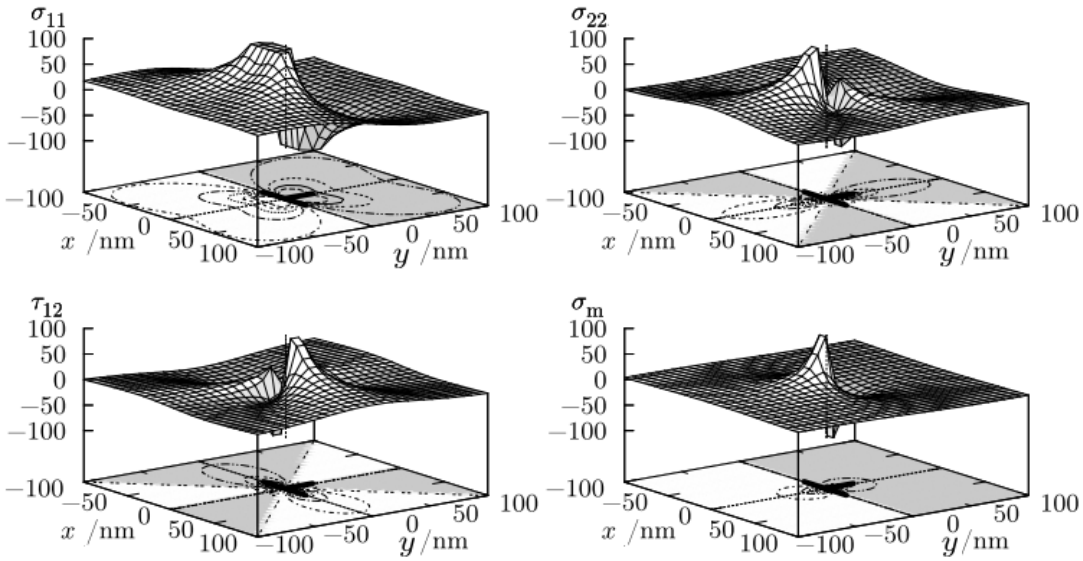

Figure 2.14.: *Scaled stress field around a in z-direction running edge dislocation. Areas with compressive stress are darkened.* Modified from [55].

with

$$r_0 \approx b \tag{2.9}$$

The elastic energy associated with a dislocation can be calculated from the elastic stress field. Thereby the elastic energy is equal to the energy necessary to create a dislocation [3, 57]. This can be done by introducing a displacement with the magnitude ξ. The stress field of an edge dislocation on the glide plane ($\Theta = 0$, Figure 2.15) at a distance x from the dislocation core is given by equation 2.7d as

$$\tau_{xy}(x) = \frac{\mu\xi}{2\pi(1-\nu)}\frac{1}{x}. \tag{2.10}$$

From the force f_x acting on a surface element $L \cdot \mathrm{d}x$ (L unit length)

$$f_x(\xi) = \tau_{xy} \cdot L \cdot \mathrm{d}x \tag{2.11}$$

one can calculate the elastic energy E_{el} which is necessary for the displacement with a magnitude of the Burgers vector $\xi = b$.

$$E_{el} = \int_{r_0}^{R_0}\left(\int_0^b f_x(\xi)\mathrm{d}\xi\right)\mathrm{d}x = L\frac{\mu b^2}{4\pi(1-\nu)}\int_{r_0}^{R_0}\frac{\mathrm{d}x}{x} = L\frac{\mu b^2}{4\pi(1-\nu)}\ln\frac{R_0}{r_0}. \tag{2.12}$$

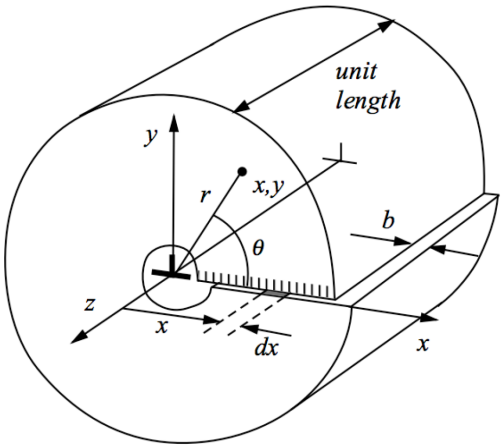

Figure 2.15.: *Geometrical correlations for the calculation of the line energy of an edge dislocation. From* [58].

By an integration from the dislocation core size r_0 (inner cut off radius) to the crystal size R_0 (outer cut off radius) one excluded the dislocation core where Hook's law is not applicable.

If one assume that the the theoretical shear stress τ_{th} acts in the core [3], the core energy can be calculated approximately with

$$E_{core} \approx L \frac{\mu b^2}{4\pi(1-\nu)}. \tag{2.13}$$

Then the total energy per unit length of an edge dislocation is found as

$$E^{\perp} = \frac{E_{el}}{L} + \frac{E_{core}}{L} = \frac{\mu b^2}{4\pi(1-\nu)} \left(\ln \frac{R_0}{r_0} + 1 \right) \tag{2.14}$$

and the corresponding line energy of the screw dislocation is

$$E^{\odot} = \frac{\mu b^2}{4\pi} \left(\ln \frac{R_0}{r_0} + 1 \right). \tag{2.15}$$

2.3.1. Dislocations in crystal plasticity

The plastic deformation of the crystalline lamellae in polymers is mainly controlled by the generation and motion of crystal dislocations. For energetic reasons screw dislocations are preferably generated [59] and therefore they are of particular importance. Apart from the screw dislocations, however, the edge dislocations also play a role in plasticity [16], especially at high strains [16, 23].

From low molecular weight substances is known, that the dislocation density increases with increasing molecular weight. But there are only rough estimations about the dislocation density of polymers [19]. Due to the weaker Van der Waals bonds, dislocations can easier generatet by thermal fluctuations. Therefore the dislocation density should be higher than in metals, where a dislocation density of about 10^{14} m^{-2} is found in undeformed polycrystals [3]. It is likely that sufficient mobile dislocations are available to initiate plastic deformation. However, in order to maintain the plastic deformation by crystallographic slip many more new screw dislocations must be generated at crystal edges and propagate through the crystal.

An interesting aspect of the plasticity of semi-crystalline polymers is that no strain hardening occurs through the interaction of the dislocations [34]. Although a strong stress increase at large strains is observed macroscopically, this is attributable to a strong stretching of the molecules in the amorphous phase and to a less extent also to the reorientation of crystals due to crystal slip (change in Schmid factor) [19]. The lack of strain hardening by dislocations can be explained by the fact that the dislocations are necessarily pushed out of the thin crystal core into the interface. They will never be trapped in the crystal [30].

2.3.2. Generation of dislocations

The standard approaches to describing the plastic behaviour of semi-crystalline polymers are the models of thermal nucleation of screw dislocations from Peterson [60, 61] and Young [62]. These models describe the plasticity of polyethylene [63, 64] and polypropylene [65] and the yield stress dependence on crystal thickness very well. These models are successful since only thermal nucleation of dislocations is crucial for the plasticity. A Frank-Read mechanism can be excluded due to the limited size of the crystallites (lamella thickness).

All these models are based on the assumption of a homogeneous nucleation of [001] screw dislocations which cause a ($hk0$) [00l] slip [63] as sketched in Figure 2.16. The necessary energy for the nucleation can be provided by

- the applied mechanical shear stress and
- by thermal activation.

In the lamellae a dislocation has a length which is equal to the lamella thickness λ. The thermal activation of 180 ° chain twist defects are assumed as the origin of the dislocation generation. Such a twist defect causes a $c/2$ compressive strain [27, 40, 67]. Thus, the Burgers vector is considered to be of the dimension of a half of the crystallographic c-axis. The orthorhombic unit cell of PE leads to a dislocation with Burgers vector [67]

$$b = \frac{c}{2} = 0.127\ nm. \tag{2.16}$$

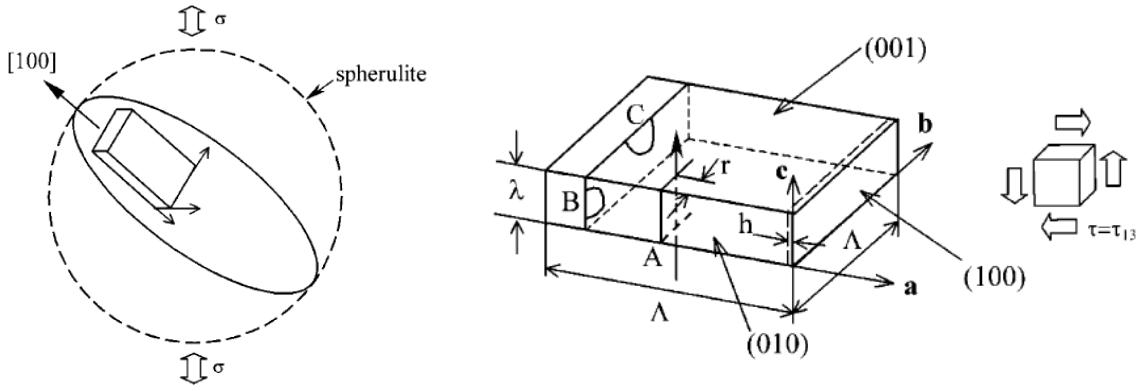

(a) (b)

Figure 2.16.: *Schematic illustration of the formation of dislocations in the crystalline lamellae of polyethylene. From* [66].
(a) A lamella with an arbitrary orientation in a spherulite.
(b) Principal slip systems of the lamella.

The elastic energy of a screw dislocation can be calculated with the dislocation line energy (equation 2.15) multiplied with its length λ. According to Figure 2.16b is $R_0 = r$ the distance from the nucleation surface. By neglecting the core energy this leads to

$$E_{el}^{\odot} = \lambda \frac{\mu b^2}{4\pi} \ln\left(\frac{r}{r_0}\right). \tag{2.17}$$

This energy is generated on the one hand by the work ΔW done by the applied shear stress τ and on the other hand by the Gibbs free energy related to the thermal fluctuations ΔG. The work applied by the shear stress is

$$\Delta W = \lambda \tau b r \tag{2.18}$$

Thus, ΔG can be written as

$$\Delta G = E_{el}^{\odot} - \Delta W = \lambda \frac{\mu b^2}{4\pi} \ln\left(\frac{r}{r_0}\right) - \lambda \tau b r. \tag{2.19}$$

The dislocation will be generated and moves (due to very low Peierls stress) when ΔG has a maximum (Figure 2.17).

$$\left(\frac{\partial \Delta G}{\partial r}\right)_{\tau} = 0 \tag{2.20}$$

From this condition we can calculate the critical value r_c for the distance r.

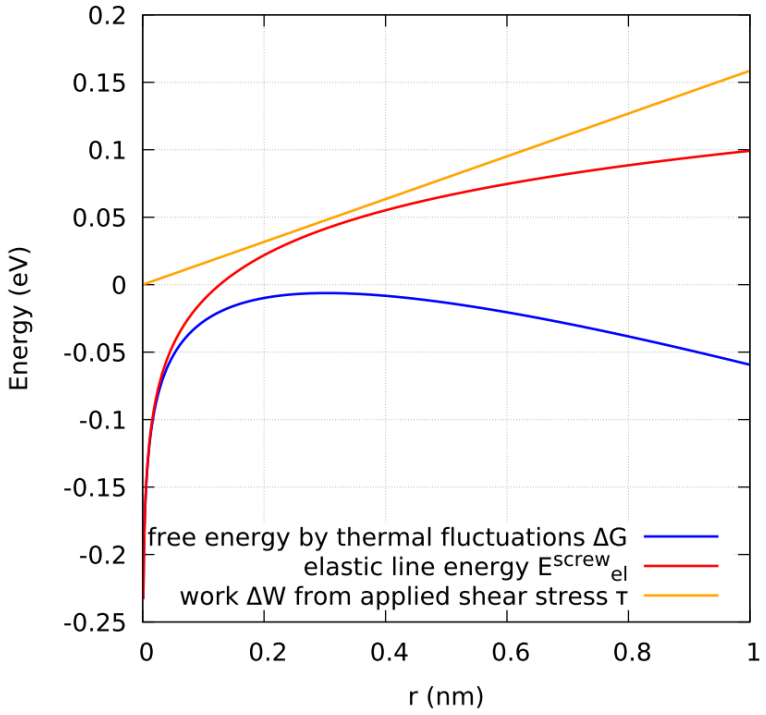

Figure 2.17.: *Different energies for the generation of a screw dislocation. Calculated with equation 2.19 for λ = 20 nm, μ = 300 MPa, b = 0.127 nm, $r_0 = b$, τ = 10 MPa.*

$$r_c = \frac{\mu b}{4\pi\tau} \tag{2.21}$$

With r_c it is possible to rewrite equation 2.19 in order to calculate the critical Gibbs free energy to generate a screw dislocation.

$$\Delta G_c = \lambda \frac{\mu b^2}{4\pi} \ln\left[\left(\frac{r_c}{r_0}\right) - 1\right] = \lambda \frac{\mu b^2}{4\pi} \ln\left(\frac{\mu b}{4\pi\tau r_0} - 1\right) \tag{2.22}$$

If we set now $r_0 = b$ [40, 68] and use equation 2.22, one get the yield stress with.

$$\tau_y = \frac{\mu}{4\pi} \exp\left(-\frac{4\pi\Delta G_c}{\lambda\mu b^2} - 1\right) \tag{2.23}$$

This formula shows that the yield stress has a pronounced dependence on the lamella thickness λ. Taking into account the Taylor factor $m \approx 3$ [3, 34, 66], the yield stress σ_y can be related to the critical (resolved) shear stress τ_y by $\sigma_y = 3\ \tau_y$.

The energy contribution by the thermal fluctuations ΔG_c is in the order of 40 to $80kT$ [40]. It's interesting that such a simple model describes well the lamella thickness dependence of the yield stress in polyethylene [69] for thicknesses up to 40 nm. As early as 1974 Young

[62] had shown that thermal activation becomes very implausible for crystals exceeding 40 nm. For such thick lamela crystals a different process for dislocation generation should be activated. A reasonable explanation is the occurrence of half loop sources at the edges (Figure 2.16b) which were discussed by Argon et al. [66] based on the experimental data of Kazcmierczak [51]. They found a good agreement with the experimental data, by combining the thermally activated process for small lamellae with the half loop mechanism (Figure 2.18) [23].

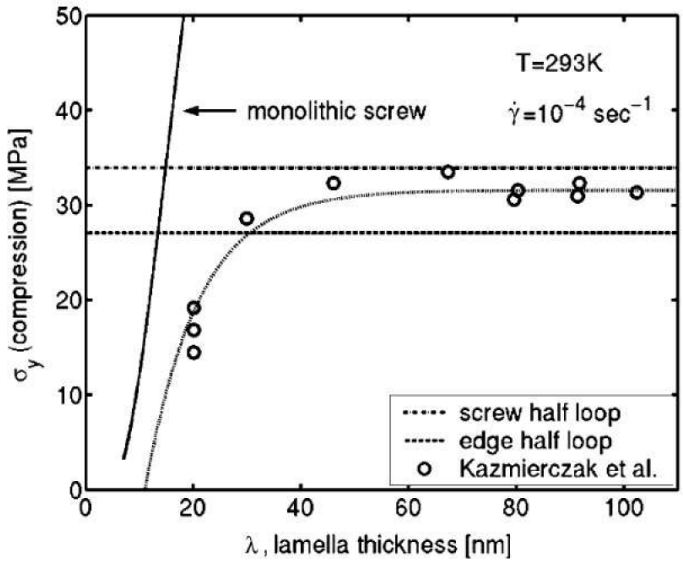

Figure 2.18.: *Dependence of compressive flow stress of polyethylene measured at 293 K and $\dot{\gamma} = 10^{-4}\ s^{-1}$ on lamella thickness (open circles) compared with dislocation models (straight lines). From* [66].

2.4. Proof of dislocations

Today the standard method for the direct proof of dislocations in metals is microscopy. Since dislocations have always a stress field, they can be visualized with metallographic methods. For this purpose, the surface of a sample is etched. The atoms in the stress field of a dislocation dissolve more quickly from the surface and leave characteristic etching pits which are easily visible using an optical microscope (OM). Furthermore, dislocations can be detected by electron microscopy. Edge and screw dislocations generate contrast by electron diffraction in the transmission electron microscope (TEM). Screw dislocations can also be detected by scanning electron microscope (SEM) images of crystal surfaces [3].

In polymers the proof of dislocations is much more difficult. Although evidence of screw dislocation was successfully proven using electron microscopy as early as 1959 in polyethylene

single crystals grown from the solution [70], there is no literature for a sample preparation method which allows to visualize the dislocations in melt-grown lamella crystals with electron microscopy.

Indirect detection methods such as the electric resistivity measurement, where the dislocation density can be determined, are only suitable for metals.

A rather universal method for the detection of dislocation and the measurement of the dislocation density is the X-ray line profile analysis (XPA). This method uses the fact that any deviation from the regular crystal structure causes a characteristic contrast which leads to a broadening of the measurable X-ray reflection peaks. Since the 1960s it has been known that point, line, surface defects and the crystal size influence the X-ray reflections differently [71, 72]. Point defects cause a homogeneous scattering and thus lead to an amplification of the diffuse scattering. Line defects (dislocations) cause an diffraction Bragg peak broadening which increases with the order of diffraction. Surface defects cause asymmetric peak broadening and/or broadening with complex order dependence. The crystal size affects the peak width independent of the order if the crystals are spherically symmetrical.

According to Warren and Averbach [71, 73] is the intensity profile of a diffraction pattern composed of two contributions. They are

- a strain effect caused by crystal defects (dislocations, twins, stacking faults) and
- a size effect which take into account the limited size of a crystal.

This two parts can be added by a convolution of the size and distortion profiles in the real space (or a multiplication of the Fourier transform)

$$A(L) = A^S(L) \otimes A^D(L) \tag{2.24}$$

where $A(L)$ are the absolute values of the Fourier coefficients of the physical profiles, $A^S(L)$ and $A^D(L)$ are the Fourier coefficients for size and distortion, respectively, L is the Fourier variable. The distortion coefficient $A^D(L)$ were calculated by Warren and Averbach [73] with statistical distortions

$$A^D(L) = exp\left(-2\pi^2 K^2 L^2 \langle \epsilon_L^2 \rangle\right) \tag{2.25}$$

where $\langle \epsilon_L^2 \rangle$ is the mean square strain and K is the length of the diffraction vector.

Krivoglaz [72] and Wilkens [74] calculated $\langle \epsilon_L^2 \rangle$ under the assumption that the peak broadening is mainly caused by the strain field of restricted random distributed dislocations.

$$A^D(L) = exp\left[-\frac{1}{2}\rho\pi b^2 L^2 f\left(\frac{L}{R_0}\right) K^2 C\right] \tag{2.26}$$

where R_0 is the outer cut of radius and $f(L/R_0)$ is a function derived explicitly by Wilkens [74].

In 1953, Williamson and Hall [75] simplified the Warren-Averbach approach to determine the particle size d (coherently scattering domain size) by plotting the peak width ΔK (full width at half mean (FWHM) or integral width) over the diffraction vector K (Figure 2.19a). Thereby ΔK depends on two influences.

$$\Delta K = \frac{0.9}{d} + \Delta K^D \tag{2.27}$$

The first term, which is independent of the diffraction order K, represents the dependence on d whereas the second, ΔK^D, includes the broadening from lattice distortions which strongly depends on K. Because of the anisotropy of this distortion, equation 2.27 usually is of limited use but, especially if the distortions arise from dislocations, the model for the strain results in a single quantity to cover the whole complicated hkl dependence [71, 74].

Applying this to texture-free polycrystals, in 1996, Ungár and Borbély [76] introduced the so-called modified Williamson–Hall analysis. Here the full width at half maximum (FWHM = $\Delta K(K)$) is plotted as a function of the diffraction vector, using the K^2C_{hkl} as independent variable, introducing an average dislocation contrast factor C_{hkl}. The average dislocation contrast factor comprises the total anisotropy of the distortion field of the dislocation ensemble. To average the contrast it was assumed that the polycrystal is texture free and all slip-systems are equally active. The average contrast factors C_{hkl} are obtained by averaging the contrast factors of the (hkl) planes by considering their permutations for different crystal structures [76].

With this modification they achieved in the so-called modified Williamson–Hall plot (Figure 2.19b) a monotonous function of $\Delta K(K)$ when K in equation 2.27 is replaced by K^2C_{hkl}.

$$\Delta K_{FWHM} = \frac{0.9}{d} + \alpha'(K\sqrt{C_{hkl}})^2 + O(K\sqrt{C_{hkl}})^4 \tag{2.28a}$$

$$\alpha' = \frac{\pi T b^2}{2}\sqrt{\rho} \tag{2.28b}$$

This allows one to determine the dislocation density ρ and the mean crystallite size d (size of the coherently scattering domains - CSD size) in separate way. A typical application is shown in Figure 2.19.

Ungár and Borbély succeeded in extending the Warren-Averbach approach with an average contrast factor by applying the same dislocation model to the full profile. Thereby not only the FWHM but also the shape of the peaks are taken into account. With their so-called Multiple Whole Profile Analysis (MXPA) [76] it is possible to determine the dislocation

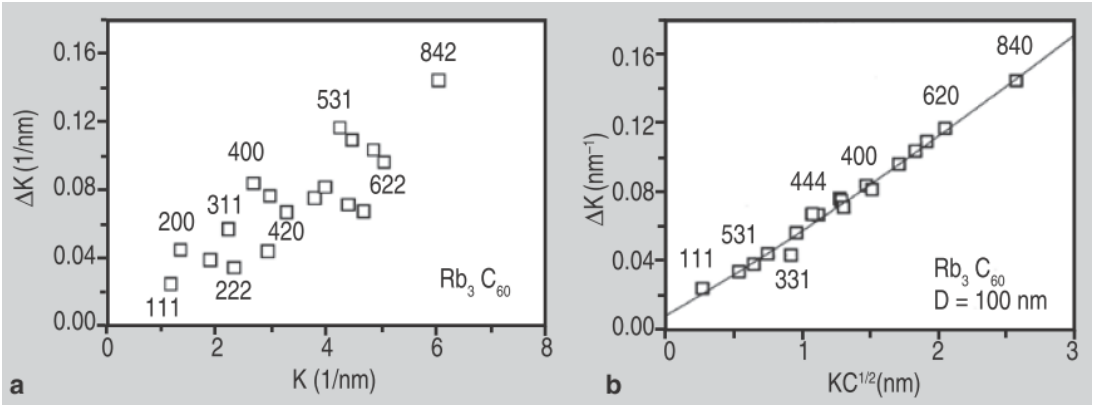

Figure 2.19.: *Modified Williamson–Hall analysis of Rb_3C_{60}. From* [77].
(a) The classical Williamson–Hall analysis shows strong anisotropy and assumes the presence of dislocations.
(b) The modified Williamson–Hall plot with the consideration of a dislocation contrast factor C shows an excellent description of the order dependence of the peak broadening. The intersection at K = 0 gives d = 100 nm for the average crystallite size.

density, the crystallite size and with some assumption the crystallite size distribution. It is based on the approach to fit the Bragg profile measured with the theoretical peak profiles.

As an X-ray method, the MXPA is also applicable to polymer crystals [78]. However, in this respect mathematical fit problems arise. Since the polymer crystals normally have a much lower symmetry there are much more fit parameters than for metals and resulting the fits may not converge. [1]

In addition to the direct methods, however, indirect detection methods for dislocations via dynamical mechanical experiments (e.g. strain rate jump experiments) are of great importance. Thus, the essential parameters for the physical dislocation models such as activation energies and activation volumes can be determined [85].

Nevertheless, in semi-crystalline polymers a two-phase model must be applied to take into account the influence of the amorphous phase. By combining the model of Young for the crystalline phase with a simple Ree-Eyring model for the amorphous phase Scogna and Register [86] could model the strain rate dependence of the yield stress $\sigma_y(T)$ for a wide temperature range,

$$\frac{\sigma_y}{T} = \frac{\sigma_a}{T} + \frac{\sigma_c}{T} \tag{2.29}$$

[1] This conclusion relates to the initial situation of the present dissertation. Within the scope of the dissertation, the method has been further developed and has already been successfully applied to different polymers [79–84].

where σ_a is the yield stress of the amorphous fraction, and σ_c is the yield stress of the crystalline fraction. The yield stress of the amorphous phase can, according to Eyring [87], be written as

$$\sigma_a = \frac{kT}{V_a} arcsinh\left[\frac{\dot{\varepsilon}}{\dot{\varepsilon}_{0a}} exp\left(\frac{\Delta H_a}{kt}\right)\right] \tag{2.30}$$

where k is the Boltzmann constant, H_a is the activation enthalpy of the related Eyring process, V_a is the corresponding activation volume and $\dot{\varepsilon}_{0a}$ is the reference strain rate in the amorphous phase. The yield stress of the crystalline fraction is given by [62, 66]

$$\sigma_c = \frac{\mu(T)b}{\pi r_0} exp\left(\frac{-2\pi\Delta G_c^*}{\mu(T)b\lambda} - 1\right) \tag{2.31}$$

where $\mu(T)$ is the temperature dependence shear modulus of the polymer crystal, b is the Burgers vector length, r_0 is the inner dislocation cut-off radius (core radius of the dislocation), and λ is the lamella thickness. The activation Gibbs free energy ΔG_c^* is strain rate sensitive and can be expressed by [88]

$$\Delta G_c^* = -kT log\left(\frac{\dot{\varepsilon}}{\dot{\varepsilon}_{0c}}\right) = -kT log\left(\frac{\dot{\varepsilon}}{b\rho_m v_0}\right) \tag{2.32}$$

where $\dot{\varepsilon}_{0c}$ is the reference strain rate in the crystalline phase. $\dot{\varepsilon}_{0c}$ is thereby related to the number of mobile dislocations by making use of the Orowan equation [57] as suggested by Argon et al. [66]. In this equation b is the Burgers vector length, ρ_m the dislocation density of mobile dislocations and v_0 the average dislocation velocity which results from the experimental frequency ν_0 multiplied by the mean free path of the dislocation L ($\sim$ lamella thickness λ). This makes it possible to describe the influence of the average dislocation velocity v_0 on the strain rate and allows one to relate the Gibbs free energy ΔG_c^* of the dislocation process to physical parameters that can be determined experimentally. Strain rate jump experiments with high density polyethylene have shown that it was possible to obtain very realistic values for $\dot{\varepsilon}_{0c}$ with this model [88].

However, a decisive disadvantage of the classical mechanical experiments is that the deformation cannot be evaluated phase-specifically. Thus, the physical models have many fit parameters (for the amorphous and crystalline phase). To obtain reasonable model parameters by the fit of the experimental data some of the physical model parameters must be estimated.

Li and Ngan [89] were able to illustrate one possible solution to this problem. They could show with nanoindentation creep experiments on high density polyethylene that the deformation in the amorphous and crystalline phase does not occur simultaneously with very small loads. They found discrete relaxation events (strain bursts) on the sub-micron

scale during constant load. Thus, macroscopic deformation can be divided into a uniform smooth amorphous and a jerky crystalline deformation (Figure 2.20).

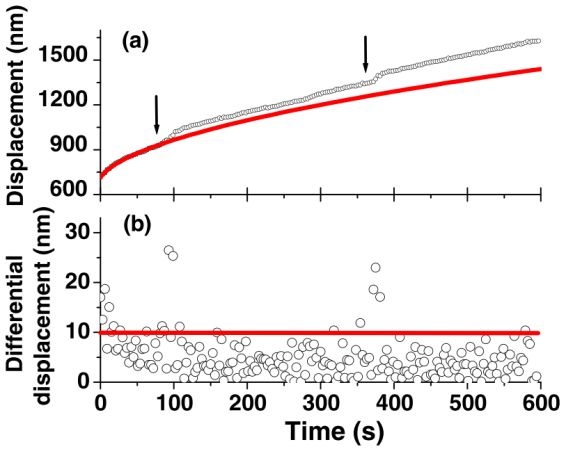

Figure 2.20.: *Nanoindentation creep experiments. From* [89].
(a) Example of a displacement–time curve of PE-HD (61.2 % crystallinity) during holding at 900 µN at 30 °C, showing two strain bursts at 97 and 372 s, respectively.
(b) Differential displacement between two successive data points, versus holding time.

They assumed dislocation avalanches as the source of the jerky deformation. From metals it is known that very small single crystals (µm range) are jerkily deformed by dislocation avalanches [90]. The interpretation that dislocation avalanches are the reason for the strain bursts was supported by Zare Ghomsheh et al. [91] with systematic nanoindentation creep experiments. They investigated the effect of variations in the loading rate and of the applied load on the number and the height of strain bursts. In a current analysis they were also able to determine the activation energy of strain bursts during nanoindentation creep on polyethylene by a statistical evaluation [92].

Although the nanoindentation creep experiments allow the separation of the deformation into the amorphous and the crystalline phase, this experimental set-up has some decisive disadvantages.

- Inhomogeneous stress field
  The stress field is strongly inhomogeneous. Figure 2.21b shows the result of a FEM simulation with the typical stress concentration at the indentor tip. The stress distribution is also dependent on the penetration depth. The deeper the indent penetrates the larger the projected area. With a constant force (= constraint of the nanoindentation creep experiment) the stress decreases with increasing penetration depth. In addition, there is also a complex three-dimensional stress field with a superposition of tensile, compressive and shear stresses. Thus, the stress can only be estimated approximately for the evaluations.

- Plastic deformation
  Since the indentor has only a very small projecting surface, there are locally large

stresses despite the small loads (some μN), especially at the indentor tip. Therefore, irrespective of the penetration depth, a plastic deformation beyond the yield point can occur locally.

- Small sample volume tested
  The sample volume tested is very small and local effects can play a role. It has also been shown that strain burst occurs very rarely [89]. In order to obtain statistically reliable results (for example, the frequency distribution of the step heights), many experiments have to be carried out.

- Complex evaluation
  Due to the above mentioned disadvantages some assumptions and estimates are required for the evaluation.

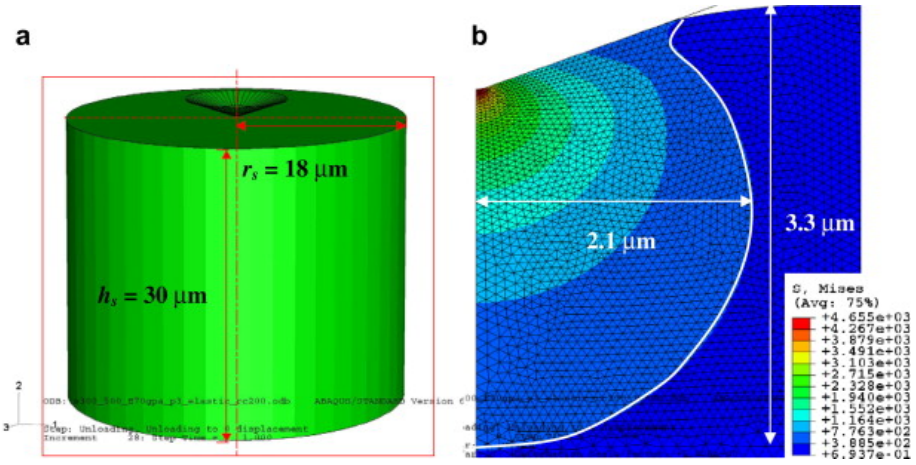

Figure 2.21.: *FEM simulation results of nanoindentation. From* [93].
(a) Geometry of indentation of a cylindrical specimen.
(b) The von Mises equivalent stress field.

2.5. Reference materials

Among the semi-crystalline polymers, polypropylene (iPP) and polyethylene (PE-LD and PE-HD) are the two most important polymers with $\sim$ 50 % of the world market share. Both materials have been extensively investigated in many scientific papers. Therefore, both were selected as reference materials for this dissertation.

Due to its regular linear molecular structure, polyethylene is the reference material for studies on the plasticity of semi-crystalline polymers. It was used for the nano-creep experiments (chapter 6). Unfortunately, polyethylene has only two prominent X-ray reflections (Figure 2.24) and is therefore not suitable for defect analysis by means of MXPA. Since polypropylene with five main peaks (Figure 5.6) has a sufficient number, it was chosen

for the X-ray investigations (chapter 4 and 5). In addition, with the gamma phase, it has an extraordinary crystal modification, which is very interesting with regard to dislocation mobility.

2.5.1. Polypropylene

Polypropylene crystallizes from the melt with a crystallinity of 60 - 70 % and has a glass transition temperature T_g = 0 °C. It is polymorphic and has three different crystal modifications [94].

The standard phase is the monoclinic **alpha phase** with the lattice parameters a = 0.665 nm, b = 2.096 nm, c = 0.65 nm and β = 99.62 °. The main peak positions are listed in Table 2.1. A special feature of the alpha phase is the formation of a branched lamella structure (lamella branching, Figure 2.22).

(a) (b)

Figure 2.22.: *Structural anomalies of polypropylene.*
(a) Lamella branching of α-PP. SEM micrograph of a thin film with profuse branching of lamellae at a constant angle of 100 ° or 80 ° and schematic diagram. This lamella branching is the root of the unusual optical properties of spherulites of the alpha phase. From [94, 95].
(b) Cross over molecular arrangement of γ-PP in the unit cell, (110) plane viewed from above. From [96].

In the case of the plastic deformation (rolling with side constraints - plain strain compression), the slip systems (010) [001], (110) [001], (100) [001] are activated in the alpha phase [97]. Bartczak et al. [42] has measured a CRSS of 22.6 MPa for the (010) [001] slip system.

The **beta phase** is metastable [98] compared to the alpha phase (T_m ∼155 °C versus 170 °C) and has a significantly higher toughness than the alpha phase approaching -10 °C. The

crystal structure is trigonal with the lattice parameters $a = b = 1.101$ nm and $c = 0.65$ nm. Isotactic polypropylene (iPP) crystallizes preferentially in the alpha phase, so that practically no beta polypropylene is formed during the crystallisation from the melt.

During crystallisation under shear [99, 100], or with addition of suitable nucleation agents [101], polypropylene can be produced with a high content of the beta phase.

The **gamma phase** is crystallographically similar to the alpha phase (isomorphism of the alpha phase [96]). The crystal structure is very complex and was be clarified by von Meille and Brückner [102]. The gamma phase is formed by crystallization under high pressure ($p > 180$ MPa) [103–105]. γ-polypropylene crystallizes in a very large area-centered orthorhombic unit cell ($a = 0.854$ nm, $b = 0.993$ nm, $c = 4.241$ nm) with a triclinic subcell. The macromolecules are arranged in bilayers (Figure 2.22b) each rotated by 80 ° or 100 °. The main peak positions for α and γ-PP are listed in Table 2.1. The typical X-ray diffraction pattern of polypropylene (alpha and gamma phase) is shown in Figure 5.6.

Gamma polypropylene is a material where the structure can be strongly influenced by the crystallisation conditions. For instance the crystallisation pressure p_c and temperature T_c change the spherolithe structure [103]. Figure 2.23 illustrated the different spherolithe morphology obtained by different crystallisation pressure at the same crystallisation temperature.

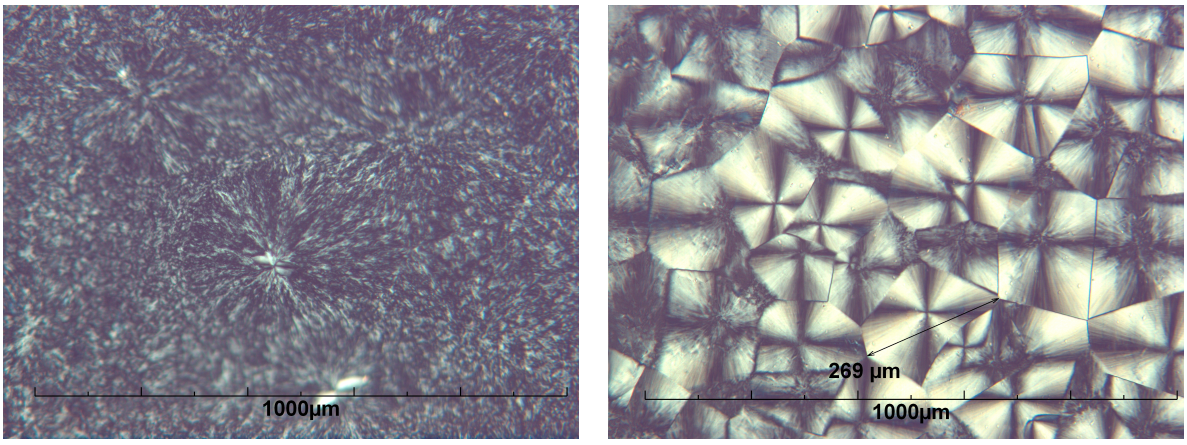

$p_c = 200$ MPa $p_c = 300$ MPa

Figure 2.23.: *Optical micrographs, viewed between crossed polarizers, from γ-PP spherulites, crystallized at different pressures and $T_c = 195$ °C.*

Interestingly, the strength of the gamma phase can be much higher than of the alpha phase [106]. Since the gamma phase is an isomorphism of the alpha phase, the chain distances are only slightly different. Although the heat of fusions are different ($H_\alpha = 207$ J/g [107], $H_\gamma = 145$ J/g [104]), this does not explain the magnitude of the strength difference, especially since $H_\gamma < H_\alpha$. Therefore, the difference in strength cannot be explained either by breaking of Van der Waals bonds or by local melting processes.

2 Theta [°]	k [1/nm]	phase	hkl
13.86	1.5649	γ	111
14.11	1.5928	α	110
15.11	1.7053	γ	113
16.86	1.9014	α	040
17.02	1.9194	γ	008
17.36	1.9574	γ	115
18.47	2.0816	α	130
20.27	2.2823	γ	117
21.19	2.3845	α	111
21.32	2.3992	γ	202
21.70	2.4413	α	13-1
21.77	2.4495	α	041
21.97	2.4715	γ	026
25.29	2.8394	α	060
25.65	2.8790	γ	00 12
27.28	3.0586	γ	1,1,11
27.58	3.0916	γ	220
27.92	3.1290	γ	222
28.80	3.2254	α	061
28.91	3.2376	γ	224
30.40	3.4006	γ	226
32.30	3.6076	α	042

Table 2.1.: *Polypropylene peak positions for alpha and gamma phase* [108]. *2 Theta for Cu K_α with λ = 0.1542 nm.*

2.5.2. Polyethylene

Polyethylene is a very versatile material. Depending on the number and length of the side chains, crystallinity, density and mechanical properties can vary widely. High density polyethylene (PE-HD, $\rho = 0.94 - 0.97$ g/cm^3) shows the highest crystallinity of about 80 %. The glass transition temperature is typically far below 0 °C.

Polyethylene crystallizes in an orthorhombic unit cell (Figure 2.3) with a = 0.742 nm, b = 0.495 and c = 0.255 nm [109]. The main peak positions are listed in Table 2.2.

Bartczak et al. [46] identified the (100) [001], (010) [001] chain slip and (100) [010] transverse slip processes as the dominant active slip systems during plastic deformation. The respective critical shear stresses were directly determined in mechanical shear tests as 7.2, 15.6, and 12.2 MPa, respectively, at room temperature. In addition 110 twinning and the Tl_2 stress-induced martensitic transformation to a monoclinic unit cell are also known to be active modes of plastic deformation for certain particular orientations of polyethylene

2 Theta [°]	k [1/nm]	hkl
21.3	2.3970	110
23.5	2.6413	200
29.6	3.3132	210
36.0	4.0080	020

Table 2.2.: *Polyethylene peak positions* [110]. *2 Theta for Cu K_α with λ = 0.1542 nm.*

crystals [26]. At room temperature these two mechanisms occur at approximately 14 MPa of resolved shear stress [53]. The typical X-ray diffraction pattern of PE-HD undeformed and deformed is shown in Figure 2.24.

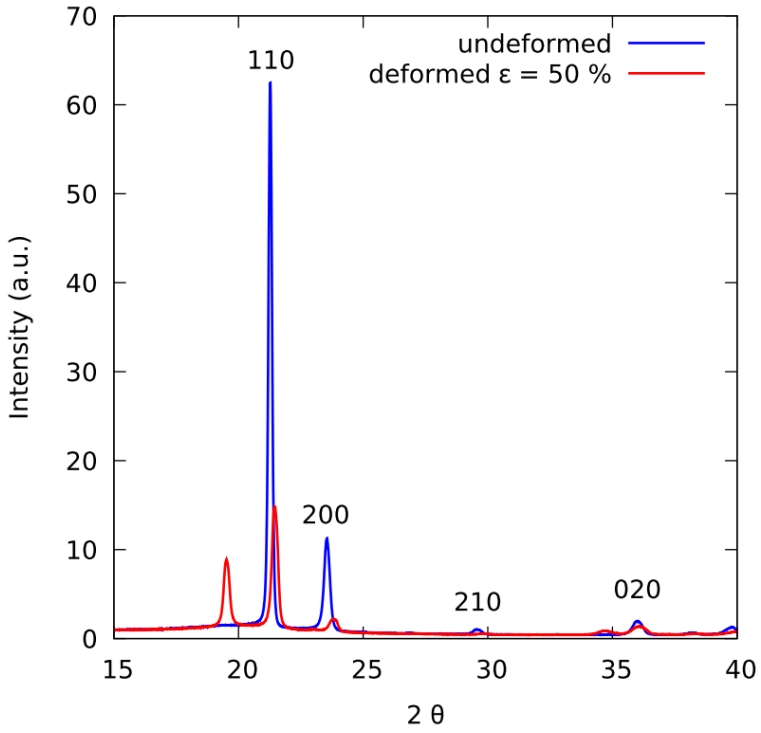

Figure 2.24.: *X-ray diffraction pattern (WAXS) of PE-HD undeformed and deformed with the typical additional peak left from the stress-induced martensitic transformation to the monoclinic crystal unit cell.*

Modern high-performance PE-HD types (PE100 and PE100 RC types respectively) used today for pressure pipes are copolymers of ethylene and hexene. As a result, the resistance to slow crack growth (SCG) can be significantly increased.

3. Aim of this work

In several semi-crystalline polymers, it was found that the deformation of the crystalline phase is governed by the generation and motion of dislocations, especially at deformations within the extended plastic regime [27, 40, 62, 65, 66]. Although the importance of dislocations for the plastic deformation in many semi-crystalline polymers is beyond dispute [32, 50, 88], the kinetic mechanisms of dislocations remains widely unclear.

In order to be able to investigate mechanisms involving dislocations for plasticity in more detail, **methods for** the

- **proof and quantification of dislocations** and
- **determination of the model parameters of the dislocation models**, such as dislocation density, activation energy, and activation volume of the dislocation generation of mobile dislocations

capable for semi-crystalline polymers are necessary.

Unfortunately, many investigation methods, which have been developed for metals, cannot be applied to semi-crystalline polymers. This is, apart from the complex structure (amorphous and crystalline phase, atomic bonding and Van der Waals bond, macromolecules which form complex superstructures and create additional constraints), an important reason why the processes responsible for the plasticity could not fully clarified yet.

Therefore, **existing methods for the investigation of dislocation should be improved and new methods for the characterization of the kinetics of dislocations should be developed** within the framework of the dissertation.

A standard method for the proof of dislocation and the determination of the dislocation density is the Multiple Whole Profile Analysis (MXPA) [76, 78]. As a X-ray diffraction method, the MXPA should be applicable to polymer crystals. However, polymer crystals normally have a substantially lower symmetry. Thus there are much more fit parameters in the evaluation, as opposed to the metals, and the fits may not converge. Thus, the evaluation process must be improved in order to allow the application of the method to polymers in a reliable way.

Nanoindentation creep experiments from Li and Ngan [89] have shown that with very small loads the deformation of the amorphous phase and that of the crystalline phase can be

analysed in separated way. This allows the direct investigation of the deformation processes in the crystalline phase with mechanical experiments and thus the determination of essential parameters of the dislocation models. However, this method has some decisive disadvantages which limits the exact determination of the model parameters. Therefore a new mechanised test method should be created which does not have these disadvantages.

Part II.

Proof of dislocations by X-ray diffraction

4. Evidence of dislocations in melt-crystallised and plastically deformed polypropylene[1]

4.1. Introduction

The direct observation of dislocations in polymer crystals is difficult. Only in solution grown single crystals it is possible to verify the existence of dislocations by means of transmission electron microscopy [111]. In melt-crystallised spherolites no preparation method is yet available to allow detection of dislocations. However, several mechanical investigations indicated that dislocations must exist in spherolites and their lamellas. The dislocation model of Peterson [60] and Young [62] suggested that the yield stress depends primarily on crystal thickness rather than crystallinity, and has been indeed confirmed by experiments of Darras et al. [69] for polyethylene (PE). Furthermore, a method developed by Brown [112], for measuring the initiation and reversibility of dislocation motion in metals by means of microstrain measurements could be realized successfully on polyethylene [113].

Recently, there has been developed a new X-ray diffraction method (multiple X-ray profile analysis, MXPA [76]) which offers now the possibility to proof the presence of dislocations in an arbitrary crystalline material and to obtain the dislocation density in absolute terms [114] on the one hand, to determine the size and size distribution of the undistorted crystallites on the other. Therefore, it was the aim of this work to adapt the MXPA for semic-rystalline polymers, i.e. to apply it for the first time to variously deformed samples of isotactic polypropylene.

4.2. Experiments

The polypropylene used in this work was BE 50 produced by Borealis. This material type includes a nucleation agent, which affects the crystallisation in the monoclinic α-phase. Thereby a uniform structure with small spherolites across the whole cross-section is achieved with approximately 70 % crystallinity.

[1] published in Materials Science and Engineering A 387–389 (2004) p1018–1022

The polymer was processed by injection moulding to shouldered test bars (DIN 53455, type 3). From these test bars the highly oriented surface layer of 0.5 mm has been mechanically removed in order to avoid surface texture effects. The resulting thickness amounted to 3 mm. Specimens were plastically deformed by rolling to different amounts. The maximum deformation achieved was $\varepsilon_{true} = \ln(d_o/d) = 0.5$ (50 %).

The rolling deformation was performed by several passes; the magnitude of passes has been adapted to the actual sample thickness in order to achieve roughly constant true strain per pass being within 0.02 – 0.03. The rolling direction was chosen identical with the injection moulding direction at sample preparation (Figure 4.1a).

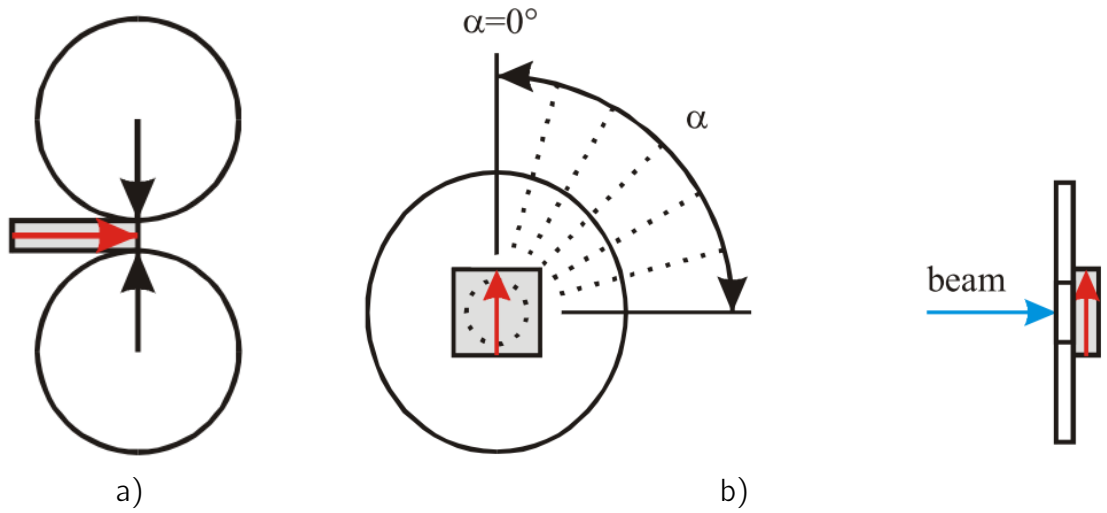

Figure 4.1.: *Deformation modes.*
(a) rolling. The broken line arrows indicate the injection direction by the sample preparation, the full line arrows the deformation direction.
(b) Sample adjustment during measuring. α is the rotation angle for texture reduction.

For the X-ray diffraction investigations, samples revealing 10 mm in square were cutted from the parallel section of tensile specimens. The X-ray measurements were performed at the small-angle X-ray scattering (SAXS) beamline of the Synchrotron ELETTRA in Trieste. The energy was 8 keV which corresponds to a wave length of Cu K_α radiation of 0.154 nm. The incident beam was focused to a spot with size 1 mm x 1 mm. The photon flux amounted to $5 \cdot 10^{11}$ photons $mm^{-2}s^{-1}$. The measurements were made with a linear position-sensitive detector (1024 channels, type PSD 50 of Braun, Munich, Germany). The distance of the detector to the specimen was 370 mm. As a condition for reliable evaluation of wide-angle X-ray scattering (WAXS) profiles, at least 10^4 counts were registered in the maximum of the diffraction peaks. In order to minimize the inluence of the texture an average WAXS profile has been determined; for this purpose the specimens were rotated perpendicularly to their square plane to different sample orientations (0 – 90 ° in 10 ° steps, Figure 4.1b) at which individual WAXS profiles have been taken and averaged. From the resulting WAXS profile the (110), (040), (130), (050) and (041) peaks were considered for evaluation.

4.3. Evaluation procedure

4.3.1. The modified Williamson–Hall analysis

In 1953, Williamson and Hall [75] suggested to determine the particle size d (coherently scattering domain size) by plotting the peak width ΔK (full width at half mean (FWHM) or integral width) over the diffraction vector K (Figure 4.2), with ΔK depending on two influences:

$$\Delta K = \frac{0.9}{d} + \Delta K^D \tag{4.1}$$

The first term which is independent of diffraction order K represents the dependence on d whereas the second, ΔK^D, includes the broadening from lattice distortions which is strongly depending on K.

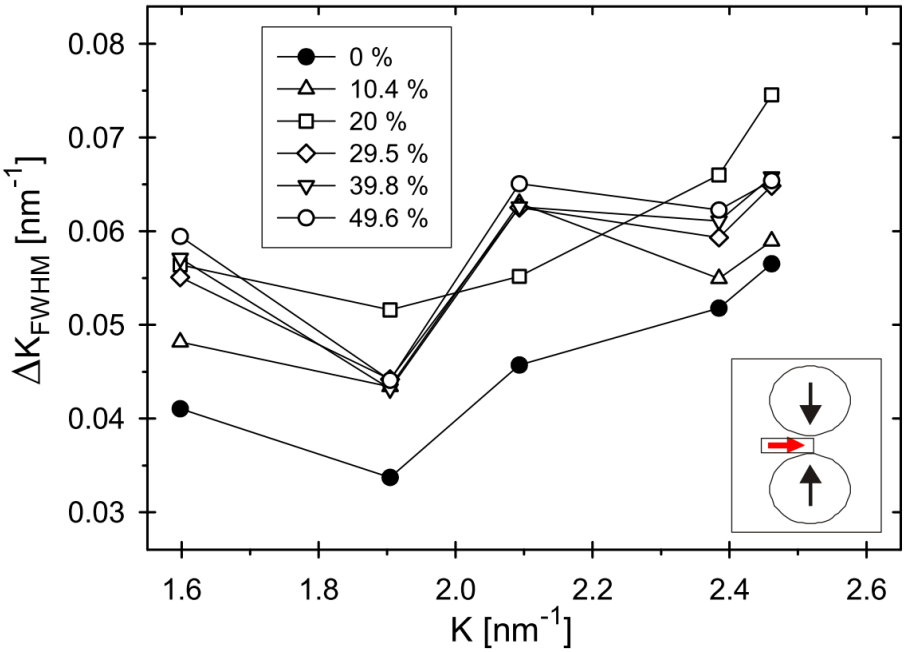

Figure 4.2.: *Classical Williamson–Hall plot for polypropylene peaks (110), (040), (130), (050) and (041) deformed by rolling up to ε_{true} = 49.6 %.*

Because of the anisotropy of this distortion, equation 4.1 is usually not satisfied. However, in case when the distortions arise from dislocations it is possible to quantify this contribution in terms of dislocation contrast theory [74], equation 4.2. In 1996, Ungár and Borbély [76] introduced the so called modified Williamson–Hall plot (Figure 4.3), which achieves a monotonous function $\Delta K(K)$ when K in equation 4.1 is replaced by K^2C as

$$\Delta K_{FWHM} = \frac{0.9}{d} + \alpha'(K\sqrt{C_{hkl}})^2 + O(K\sqrt{C})^4 \tag{4.2a}$$

$$\alpha' = \frac{\pi T b^2}{2}\sqrt{\rho} \tag{4.2b}$$

where C is the dislocation contrast factor which, e.g. depends on the orientation of its Burgers vector b relative to the diffraction vector K. The coefficient α' also contains the dislocation density ρ, and the constant T, which itself depends on the effective outer cut-off radius of dislocations R_0.

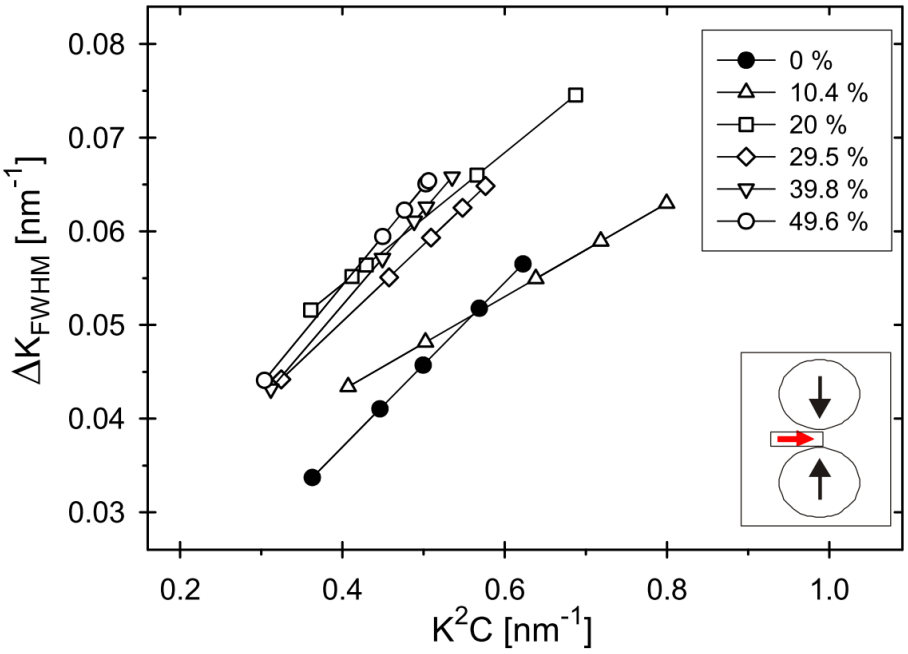

Figure 4.3.: *Modified Williamson–Hall plot for polypropylene peaks (110), (040), (130), (050) and (041) deformed by rolling up to ε_{true} = 49.6 %.*

Now, as a proof of the existence of dislocations, the measured peak width ΔK must linearly increase in CK^2 [76, 115]. In order to fully calculate the dislocation contrast factor C it is necessary to know the atom lattice and the elastic constants (equation 4.3). Unfortunately, in the literature no equation for the contrast factor of the monoclinic lattice is available. In this situation it has been decided to use the equation for the orthorhombic lattice for the determination of the dislocation contrast factor [115, 116]

$$CK^4 = h^4 + a_1k^4 + a_2l^4 + a_3h^2k^2 + a_4k^2l^2 + a_5h^2l^2 \tag{4.3a}$$

$$K^4 = \left(\frac{h^2}{a^2} + \frac{k^2}{b^2} + \frac{l^2}{c^2}\right)^2 \tag{4.3b}$$

where the coefficients a_1, ... , a_5 include the elastic constants of the material, and a, b, c are the lattice parameters. The error due to this approximation should be small, because for α-PP, the β-angle amounts to 99.33 ° which is only slightly different from β = 90 ° as being true for the orthorhombic unit cell.

4.3.2. Multiple whole X-ray profile analysis (MXPA)

In contrast to the modified Williamson–Hall plot which only provides an estimation of the dislocation density, the MXPA provides an accurate analysis of the defects in a crystal. This is possible because of the consideration of the whole peak profile instead of the peak width by the Williamson–Hall analysis. From the kinematical theory of X-ray diffraction it is well known that a physical profile of a Bragg's reflection is given by a convolution of the size and distortion profiles [73, 75]. With the assumption that the lattice distortions are caused by dislocations, the Fourier transform reads as [72, 74, 117]

$$A(L) = A^S(L) \otimes A^D(L) = A^S(L) exp(-\frac{1}{2}\rho\pi b^2 L^2 f(\eta) K^2 C) \tag{4.4}$$

where $A(L)$ are the absolute values of the Fourier coefficients of the physical profiles, $A^S(L)$ and $A^D(L)$ are the Fourier coefficients for size and distortion, respectively, L is the Fourier variable, and η stands for $\eta = L/R_0$ (for the meaning of other quantities, see above). C is the average dislocation contrast factor, and $f(\eta)$ is a function derived explicitly by Wilkens [74]. With the MXPA the Fourier transform of the whole profile will be fitted by theoretically derived functions.

In the first evaluations it turned out that the standard version of the program MWP for the MXPA for metals [118] is not suitable for the presently studied polymer. Because of the complex lattice (monoclinic), 10 parameters had to be fitted simultaneously: five parameters a_1, ... , a_5 of the dislocation contrast factor (equation 4.3), three parameters of the theoretical distortion function, and two parameters of a size function. Moreover, only five peaks were available for the evaluation. A careful analysis showed that only four fitting parameters can be independently chosen in order to account for a convergent fit with small errors. One possibility to reduce the parameters of the MXPA is the precalculation of the dislocation contrast factor, i.e. of the coefficients a_1, ... , a_5. They were precalculated by non-linear fitting of the a_i with the condition of linearisation of $\Delta K(K^2C)$ in the modified Williamson–Hall plot. A further and reasonable reduction of the fitting parameter was achieved by fixing the dislocation arrangement parameter as M = 1 [119]. This means that the effective outer cut-off radius of dislocations R_0 equals the average dislocation distance $(1/\rho)^{1/2}$. Other simplifications concern the assumptions that: (i) all slip systems have the same dislocation density, and that (ii) screw type dislocations prevail because of the low dislocation line energy in polyolefins [40].

4.4. Results

In Figure 4.2 for the case of rolled PP specimens, the classical Williamson–Hall plot is demonstrating the typically irregular slope of the peak width with K. The peak width of the undeformed sample was remarkable lower than that of the plastically deformed samples. Already the sample deformed with ε_{true} = 10 % exhibited a clear peak broadening. Further deformation led to only small increases of the peak width. Nevertheless, it was possible to obtain an almost perfectly monotonous slope of FWHM over K^2C (Figure 4.3) by suitably adapting the dislocation contrast factor C (i.e. by proper choice of coefficients a_1, ... , a_5 in equation 4.3). Thereby the calculation of the dislocation contrast factor occurred independently for each undeformed and deformed sample.

The convergence of the final fit with small errors, by the use of theoretical functions of distortions caused by dislocation, can be regarded as proof that dislocations are present in melt-crystallised polypropylene being the predominant crystal defects.

Figure 4.4 shows the dislocation density resulting for different degrees of true deformation for the rolled specimens, as it has been calculated by MXPA. It increases from $2 \cdot 10^{16}$ to $2.2 \cdot 10^{17}$ m^{-2} with increasing plastic deformation. The increase can be explained by the deformation induced formation of new dislocations which is consistent with the experience in other materials [114]. In general, the generation of dislocation density in PP is remarkable higher than in metals and alloys where typical dislocation densities span 10^{10} to 10^{16} m^{-2} [3].

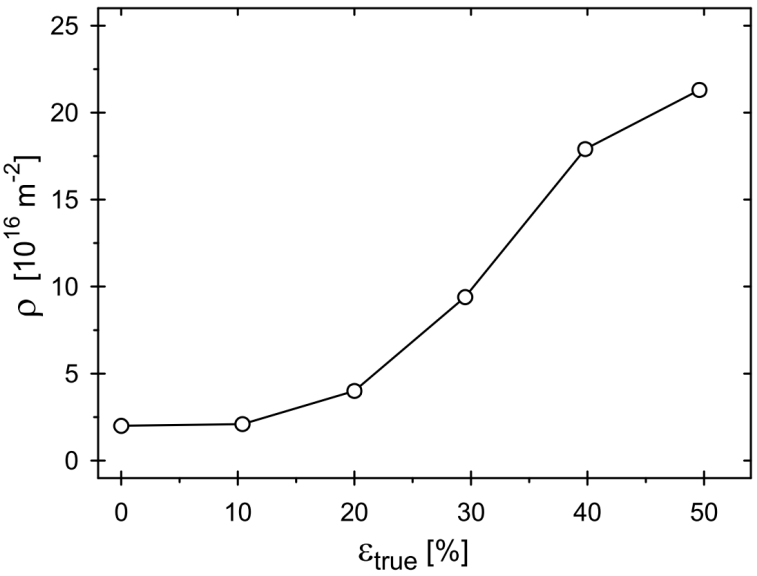

Figure 4.4.: *Dislocation density depending on the true deformation for the rolled specimens. The dislocation density was calculated by MXPA.*

The value of the dislocation arrangement parameter M gives the extent of the dipole character of dislocations (i.e. of their strain field) and does not directly reflect either the

distance between dislocations or the coherently scattering crystallite size [120]. In this work the MXPA has been performed for a series of reasonable values of M. It turned out that the best fit convergence was achieved by taking $M = 1$ although other M values up to 2 yielded similar dislocation densities.

For the coherently scattering crystallite size (apparent particle size) the evaluation yielded a continuous decrease with increasing plastic deformation. The resulting domain sizes lie between 20 nm (undeformed) and 15 nm ($\varepsilon_{true} = 50$ %). This value well agrees with the known lamella thickness [107].

4.5. Discussion

The reported dislocation densities in polypropylene are considerably higher than the values for common metals. An explanation is the long-chain nature of the macromolecules which cause additional constraints when polymer crystals develop. This, in some natural way, leads to a considerable generation of dislocations already in the undeformed material [16].

However, it must be noted that only correlated defects have been considered in the evaluation, i.e. such with long range strain fields ruling the position of adjacent atoms and/or molecules and thus the position of other crystal defects. Particularly at the interface with the amorphous phase, also uncorrelated defects may exist which can cause peak broadening, too. As a consequence, the dislocation density will be overestimated when the presence of uncorrelated defects will not be taken into account.

Nevertheless, two basic estimates for the dislocations density can be done:

(i) The amount of dislocations necessary for plastic shear in terms of Burgers vector b, and the mean free path of the dislocations L is as follows [57]:

$$\rho_m = \frac{\varepsilon}{bL} \tag{4.5}$$

Using $b = 0.65$ nm for polypropylene [65], a mean free path of the dislocations of the order of the lamella thickness (20 nm) and a deformation of $\varepsilon = 50$ %, the density of mobile dislocations is obtained as $3.8 \cdot 10^{16}$ m^{-2}. This assumption suggests that almost all dislocations contribute to plastic deformation and predominantly move across the lamellas.

(ii) The other estimation is based on theoretical considerations by Peterson [60]. He showed that the lamellas are too thin to act as a Frank-Read source. This suggests that plastic slip is mainly controlled by the nucleation of screw dislocations at the

edge of lamellas caused by local shear and thermal fluctuations. By this assumption is it possible to estimate an upper limit of the dislocation density [67]:

$$\rho_m = \frac{1}{ab} \tag{4.6}$$

With the crystallographic parameters a and b (a = 0.66 nm, b = 2.08 nm) an upper limit of $7.3 \cdot 10^{17}$ m^{-2} for the dislocation density is derived.

As mentioned, in polymer crystals already the density of grown-in dislocations is much higher than those in metals. Accordingly, the dislocation density of samples amounted to about 10^{16} m^{-2} before any deformation occurred, and has been increased through deformation to $2 \cdot 10^{17}$ m^{-2}. These values exceed estimation (i) but satisfy estimation (ii). Together with some possible overestimation because of the restriction to correlated defects, the conclusion might be that both processes (i, ii) account for the resulting values of the dislocation density. The increase of dislocation density by a factor of 10 with respect to the initial dislocation density during a deformation of 50 % is higher than that occurring in metals where, however, the initial dislocation density is much lower yielding fewer sources for dislocation generation. As a matter of fact, the results of our measurements seem reasonable and can be consistently understood which encourages to further investigations.

4.6. Conclusions

The combination of the multiple X-ray Bragg profile analysis (MXPA) and the modified Williamson–Hall procedure yields evidence for the massive presence of dislocations in melt-crystallised and plastically deformed polypropylene. The application of MXPA further allows for the determination of the dislocation density which increases with the deformation degree applied. Although the dislocation densities of plastically deformed PP exceed that of metals by two orders of magnitude, two independent theoretical estimations for dislocation activity in polypropylene provide values 10^{16} to 10^{17} m^{-2} similar to the experimental results.

5. In situ measurements of dislocation density during cyclic deformation of polypropylene

5.1. Introduction

Dislocations play a decisive role in the plasticity of semi-crystalline polymers [16, 19, 50, 62]. For energetic reasons, there are mainly screw dislocations in undeformed specimens [59]. The dislocation density is typically considerably larger in comparison to metals and is in the order of 10^{15} - 10^{16} m^{-2} (chapter 4) [83]. Dislocation density measurements on deformed polypropylene samples have shown that with progressive plastic deformation, the dislocation density increases by an order of magnitude (chapter 4). While at the beginning of the deformation only screw dislocations are present, the amount of edge dislocations increases during compression experiments with increasing plastic deformation to approximately 20 %. At the same time, the slipping mechanism changes. At the beginning of the deformation exclusively chain slip occurs which is increasingly accompanied by transvers slip. From a deformation of about ε = 50 % a balance of 60 % chain slip and 40 % transverse slip is achieved [23]. If the dislocation density is measured on deformed polypropylene samples (which were immediatly cooled in liquid nitrogen after deformation) during heating, a significant decrease of the dislocation density occures at about 10 °C and 85 °C. These distinct changes in the dislocation density could be identified as the mechanisms of β (= glass transition) and α-relaxation [54, 84]. This shows that the dislocations in semi-crystalline polymers can also recover. In order to measure the actual dislocation density during the plastic deformation, dislocation density measurements have to be carried out in situ during the deformation.

For the determination of the dislocation density in semi-crystalline polymers, it was possible to combine the modified Williamson-Hall analysis and the Multiple Whole Profile Analysis (MXPA) [76] successfully for various semi-crystalline polymers [79–84]. Thereby the number of fit parameters for the MXPA, carried out using the CMWP-fit program [118], can be reduced by a modified Williamson-Hall analysis (chapter 4). This is necessary because the semi-crystalline polymers have a more complex crystal structure (lower symmetry crystal systems such as monoclinic in isotactic polypropylene (iPP) and nylon (PA6), orthorombic in polyethylene (PE) and poly(3-hydroxybutyrate) (B3HB) [121]). This results in a large

number of fit parameters for the MXPA and the fits may not converge. The modified Williamson-Hall analysis can be used to determine the coefficients of the average dislocation contrast factor C_{hkl} [76]. This significantly reduces the number of fit parameters of the MXPA and a successful application is possible. However, there are some limitations and problems with the modified Williamson-Hall analysis. Mathematically, the fits always converge. However, depending on the starting values, there are very different results for the coefficients of the average dislocation contrast factor. Since these are used as starting values for the MXPA, they also influence the result of the MXPA. If the coefficients of the average dislocation contrast factor not determined correctly in the modified Williamson-Hall analysis, the MXPA usually does not converge or only with very large residuals. This means that a large number of fit tests are always necessary to determine the correct starting values for the MXPA. This greatly increases the time and effort required for a successful MXPA application. In order to optimize the evaluation process, an improvement of the fit procedure for the modified Williamson-Hall analysis is necessary. Thus, an important aim of the present work was to optimize the modified Williamson-Hall analysis by reducing the degree of freedom with additional physically reasonable assumptions. That allows to find the best start parameter sets for the MXPA and is an distinct improvement compared to the first application of the MXPA in polymers described in chapter 4.

5.2. Methods

5.2.1. Advanced modified Williamson-Hall analysis

As described in section 4.3.1, the modified Williamson-Hall analysis will be used to investigate the dependence of the peak width at half peak height ΔK (full width at half mean (FWHM) or integral width) on the diffraction vector K. If a linearization can be achieved by introducing an average dislocation contrast factor C_{hkl}, this can be regarded as an evidence of dislocations, since the half-width with the diffraction order only increases linearly in the case of dislocation like lattice distortions [115]. Thereby the average dislocation contrast factor considers the complex anisotropy of the distortion field of a dislocation. If the ratio of edge to screw dislocations, the crystal orientations (texture) and the elastic constants of the material are known, an average dislocation contrast factor can also be calculated theoretically. However, in practice this is almost never the case. Therefore the average dislocation contrast factor must be determined by fitting the measured data (FWHM depending on K). Thereby, C_{hkl} is determined so that a linearization of the FWHM of all peaks as a function of $K\sqrt{C_{hkl}}$ is obtained (Figure 5.15).

Most semi-crystalline polymers have relatively few X-ray diffraction (XRD) peaks which originates from a complex crystal structure with low symmetry. This leads to the unfavorable situation that the contrast factors have many fittable parameters with simultaneously

few measuring points (half-widths). Therefore, a fit for linearization has many local minima and no pronounced global minimum. This means that the physical meaning gets lost and the desired reduction of the degrees of freedom for the determination of the contrast factor coefficients cannot be fulfilled completely. Thus the contrast factor coefficients can only be restricted in their range of values and the fit parameters for the MXPA can only be reduced to a limited extent.

In order to improve the modified Williamson-Hall analysis further boundary conditions had to be added. Since the typical lamella thickness of semi-crystalline polymers is known from differential scanning calorimetry (DSC) measurements, the crystallite size can be limited to $5 - 50$ nm. Furthermore, complex valued contrast factors can be excluded. If we fix the crystallite size at 5 to 50 nm in 1 nm steps, 46 solutions are obtained. It has been shown that for small crystallite sizes only complex valued contrast factors are found and thus are eliminated. As a whole, this approach makes it possible to limit the number of solutions.

The average contrast factor C_{hkl} represents the anisotropy of the distortion field. C_{hkl} can be considered as a scaling factor of the displacement field. Therefore, a small average dislocation contrast factor or a small shift on the x-axis is more favourable. Large contrast factors are not reasonable, since these increases the degrees of freedom of the modified Williamson-Hall analysis. Based on the modified Williamson-Hall plot, this means that the peak shift should be minimal for the contrast factors. Therefore, the shift on the x-axis ($K\sqrt{C_{hkl}}$) of the modified Williamson-Hall plot relative to the position on the Williamson-Hall (x-axis = K) plot was used to reduce the degrees of freedom. It was chosen as criteria for the best fit selection. The one with the smallest shift was chosen as the best fit. The shift is proportional to $|1 - \sqrt{C_{hkl}}|$ because a $\sqrt{C_{hkl}}$ of 1 means no shift. If the sum of $|1-\sqrt{C_{hkl}}|$ for all peaks is plotted versus the crystallite size, a unique minimum is obtained (Figure 5.1).

This minimum means that the linearization is realized with the smallest possible shift of the peaks. This can be seen as the most physically reasonable solution. An alternative option would be to evaluate only the minimum for the largest contrast factor. However, this always leads to larger crystallite sizes and is therefore in disagreement to the crystallite sizes measured by DSC.

With this additional criterion, the crystallite size and the dislocation density can be estimated more reliably from the modified Williamson-Hall plot. The resulting contrast factor coefficients are better starting values for the MXPA and allow the reduction of the fit parameters in the MXPA.

5.2.2. Multiple Whole Profile Analysis (MXPA)

In the case of the MXPA, the whole XRD profile is fitted with theoretical functions, which are composed of the undisturbed scattering function and contributions of the different

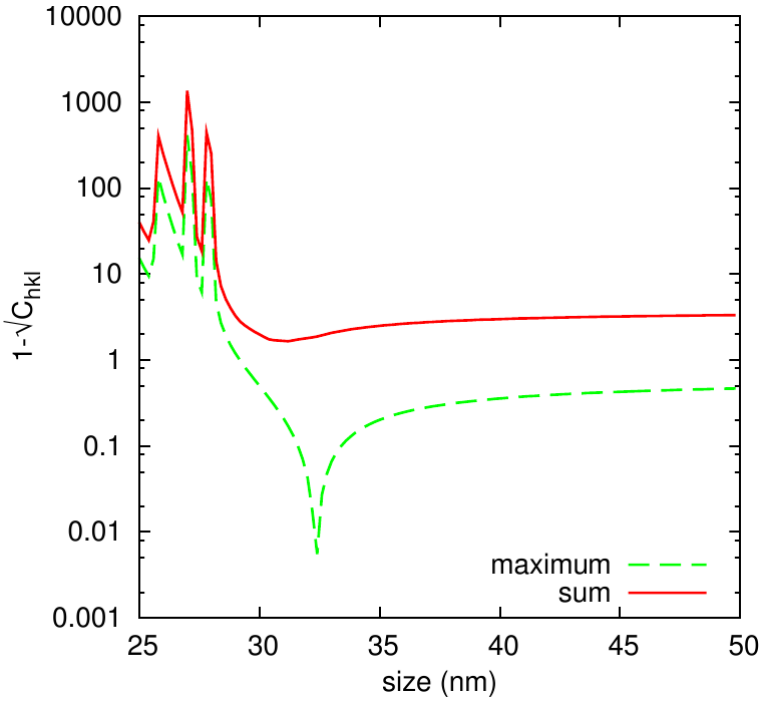

Figure 5.1.: *Shift factors from Williamson-Hall Plot depending on given crystallite size for an undeformed iPP sample. Red line sum over $|1-\sqrt{C_{hkl}}|$ of all five peaks, green dashed line only $|1-\sqrt{C_{hkl}}|$ of maximum contrast factor. Fit results for crystallite sizes < 25 nm were neglected, since they had partly complex valued contrast factors.*

defect types [76, 118]. In contrast to the modified Williamson-Hall analysis, where only the half-width of the peaks is taken into account, with the MXPA the whole peak shape is considered. Since each defect has a specific order dependence and effects the peak shape on the X-ray profile, the various defects can be separated from others and described separately. Of particular importance are the tails of the peak profiles since they are strongly influenced by the long range displacements. For an accurate analysis a good peak to background ratio as well as a good peak to noise ratio is crucial.

The MXPA has proven, particularly in the analysis of dislocations, mainly in metals but also in nonmetals [78, 122]. For the MXPA should be available at least 5 independent reflections with a good signal to background ratio. Of the commercially most important semi-crystalline polymers, only polypropylene has a sufficient number of reflections. Furthermore, the biopolymer polyhydroxybutyrate (PHB), polyamide (PA), polyethylene terephthalate (PET), polytrimethylene terephthalate (PTT), polybutylene terephthalate (PBT) and isotactic polystyrene (iPS) are suitable for the MXPA.

The analysis of dislocations by using the MXPA is possible due to the characteristic distortion field of dislocations [57] (see section 2.3). Especially, the drop in the distortion field around a dislocation is unique and thus is cannot arise from other lattice defects. This particular distortion field causes an order dependent peak broadening and a characteristic

change in the profile shape in the peak tails. The contrast also takes into account the position of the dislocation (Burgers vector b) with respect to the incident X-ray beam. The contrast and therefore the contribution to the peak broadening is maximal if b is parallel to the diffraction vector K and 0 if b is perpendicular K. This means, e.g. if the Burgers vector is perpendicular to the incident x-ray, the dislocation does not contribute to peak broadening.

Through the use of an average conrast factor, it is not necessary to know the fraction of the dislocations (edge or screw) and their distribution. In semi-crystalline polymers are mainly screw dislocations and it can be expected that a maximum of 20 % edge dislocations are formed during plastic deformation [23]. Thus the edge dislocations may be neglected. The distortion field around a dislocation is usually anisotropic and depends on the elastic constants of the crystal system and the material respectively. This anisotropy and a preferential orientation of the crystals (texture) are also taken into account with the average dislocation contrast factor C_{hkl}. The lower the symmetry, the more complex is C_{hkl}. For an orthorhombic crystal system the average dislocation contrast factor has 5 coefficients a_1 ... a_5 [123], which depend on the elastic constants (Figure 5.2).

$$\text{orthorhombic: } C_{hkl} = C_{hk0}(H_0^2 + a_1 H_1^2 + a_2 H_2^2 + a_3 H_3^2 + a_4 H_4^2 + a_5 H_5^2)$$

with

$$H_0^2 = \frac{\frac{h^4}{a^4}}{(\frac{h^2}{a^2}+\frac{k^2}{b^2}+\frac{l^2}{c^2})^2} \qquad H_1^2 = \frac{\frac{k^4}{b^4}}{(\frac{h^2}{a^2}+\frac{k^2}{b^2}+\frac{l^2}{c^2})^2} \qquad H_2^2 = \frac{\frac{l^4}{c^4}}{(\frac{h^2}{a^2}+\frac{k^2}{b^2}+\frac{l^2}{c^2})^2}$$

$$H_3^2 = \frac{\frac{h^2k^2}{a^2b^4}}{(\frac{h^2}{a^2}+\frac{k^2}{b^2}+\frac{l^2}{c^2})^2} \qquad H_4^2 = \frac{\frac{l^2h^2}{c^2a^4}}{(\frac{h^2}{a^2}+\frac{k^2}{b^2}+\frac{l^2}{c^2})^2} \qquad H_5^2 = \frac{\frac{k^2l^2}{b^2c^4}}{(\frac{h^2}{a^2}+\frac{k^2}{b^2}+\frac{l^2}{c^2})^2}$$

Figure 5.2.: *Average dislocation contrast factor C_{hkl} for orthorhombic crystal system (h, k, l Miller indizes and a, b, c latice constants).*

It turned out that for the successful application of the MXPA for polypropylene is a pre-fit of the wide-angle X-ray scattering (WAXS) profile, in which overlapping peaks, the scattering parts from different crystalline phases (alpha and gamma) and the amorphous phase will be separated. Additionally a modified Williamson-Hall analysis is necessary in order to reduce the degrees of freedom for the fit. Thereby reliable start values for the contrast factor coefficients are determined.

For the fit, the theoretical XRD profile is composed of three parts,

- the undisturbed instrumental profile function,
- the theoretical Wilkens functions describing the distortion field of dislocations and
- a size component.

These are combined by a convolution operation in the Fourier space. For a convergent fit, the dislocation density ρ , the outer cut off radius R_0 (the measure of the drop in the stress field around the dislocation line), the mean crystal size d (CSD size), and the crystal shape (deviation from the spherical symmetry) can be determined.

Lamella crystals shape in polymers are extremely asymmetric. Due to the non-planar arrangement in the spherulite, the lamella is divided into relatively symmetrical subregions (coherently scattering domains, CSD). A mutual tilting of this subregions by a few degrees causes the X-rays no longer to be coherently scattered. For X-ray measurements, this is equivalent to a crystal boundary (Figure 5.3).

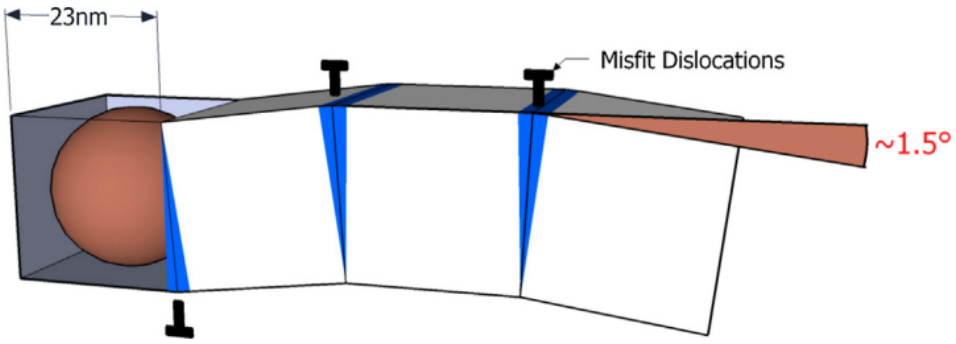

Figure 5.3.: *Schematic representation of a lamella. The lamella is divided in sub-blocks (= CSD for X-rays). Misfit dislocations are located between this blocks (highlighted blue areas). In a first approximation a single block can be considerd as approximately spherically symmetric (fitted sphere with an ellipticity of 1). From* [124].

The reliability of the MXPA method for polymers was already demonstrated impressively by Spieckermann et al. [81]. The lamella thickness distribution on undeformed and plastically deformed polypropylene samples was determined using DSC and MXPA. These two methods are based on entirely different physical principles. It was found that, with increasing deformation, the lamella thickness distribution from the MXPA agrees with the DSC measurements but only if an increase in the dislocation density is considered. If the dislocation density is fixed at the level of the undeformed sample, the MXPA provides too large lamella thicknesses compared to the DSC measurements. If the dislocation density is a fit parameter of the MXPA the lamella thickness distribution obtained is in very good agreement with DSC measurements. This is a clear evidence for the fundamental validity of the MXPA method for polymers. Furthermore it confirms the increase in the dislocation density by plastic deformation of polypropylene.

However, the experiments have also shown that the resolution limit for the dislocation density is 1 to 2 orders of magnitude worse than for metals ecause of the much worse signal to nois ratio. If, in the case of the undeformed specimens, the dislocation density is intentionally reduced and fixed during the fit, the lamella size distribution is still correctly calculated by the MXPA. It was found that a dislocation density in the order of 10^{14} m^{-2}

causes no significant broadening, compared to the size effect. Due to the small crystallite size of approximately 10 – 30 nm, a distinctive peak broadening already occurs. An additional measurable peak broadening only results for relatively large dislocation densities. Therefore, dislocation densities less than 10^{14} m^{-2} cannot be reliable determined with MXPA in semi-crystalline polymers [81].

5.3. Experiments

5.3.1. Sample preparation

For the experiments, polypropylene BE50-7032 from Borealis was used. This is an extrusion type with a density of 905 kg/m^3, a Melt Flow Rate (MFR 230 °C/2.16 kg) of 0.30 g/10 min and a tensile modulus (measured at 1 mm/min) of 1650 MPa. This type contains a nucleating agent for the alpha phase. To obtain non-textured test specimens, extruded 10 mm thick sheets were stored in a furnace for 3 h at 190 °C, followed by 2 h at 160 °C, and then slowly cooled in the furnace once switched off. Cylindrical test specimens (diameter 6 mm, height 10 mm) were machined from the pretreated sheets.

5.3.2. Mechanical cyclic experiments

The deformation was carried out cyclically with an average deformation speed of $d\varepsilon/dt$ = 0.0035 s^{-1} in compression to prevent crazing. At each cycle, the maximum strain was gradually increased (nominal engineering strain ε = 1, 2, 3, 5, 10, 15, 20, 25, 30, 35, 45, 55 %). XRD measurements were carried out under load and fully unloaded (relaxed) (Figure 5.4) respectively.

In order to calculate the true stress, images were taken from the sample during the deformation and the sample diameter was evaluated. Due to the friction between the sample and the pressure plate, the sample deforms inhomogeneously during compression experiments. This can be seen by a bulging of the sample during deformation. In order to keep this effect as low as possible, a Teflon film was inserted between the sample and the pressure plate.

5.3.3. FEM simulation

FEM simulations were performed to determine the true (inhomogeneous) deformation in the sample. The coefficient of friction between the sample and the punch was set to 0.2. With this coefficient of friction a good agreement between the simulation and the experiment was obtained for the sample diameter. Thus the mean true strain over the

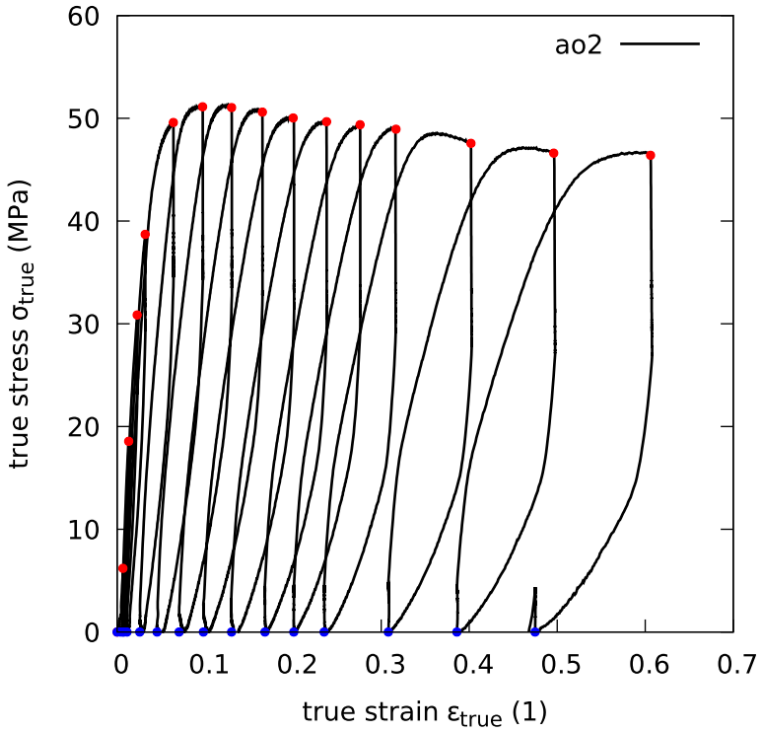

Figure 5.4.: *Cyclic deformation, red points – measurements under load, blue points – measurements in a fully relaxed state.*

sample cross-section, which was penetrated by the X-ray beam, could be calculated from the simulation results. Ansys Workbench 17.1 was used for the FEM calculations. A true stress-strain diagram from a standard compression experiment [125] was used as material data. The material behaviour was considered as multilinear without softening.

5.3.4. DSC

DSC measurements were performed to determine the lamella thickness distribution and the degree of crystallinity. For this purpose, disks with a thickness of 1 mm were cut from the cylindrical compression samples from the center of the sample by means of a diamond saw. A sample with a mass of about 20 mg was then punched out from these disks for the DSC measurements. The measurements were carried out using a Netzsch DSC 204 calorimeter. 10 K/min was chosen as the heating rate in order to minimize a change in the lamella thickness by postcrystallization during the measurement.

5.3.5. X-ray measurements

Polypropylene with a glass transition temperature of $T_g \sim 0$ °C shows a pronounced relaxation behaviour at room temperature, like all semi-crystalline thermoplastics above the

glass transition temperature. The relaxation processes take place mainly in the soft amorphous phase. This also results in a back deformation of the lamellae despite the load being maintained. These (back) deformations can lead to recovery processes in the crystals and thus they are accompanied by a decrease in the dislocation density [54, 84]. In order to suppress these relaxation processes as far as possible, in situ XRD measurements were performed with synchrotron radiation during the cyclic compression experiments. Thus, despite the high demands of the MXPA on the signal-to-noise ratio, the measurement time could be limited to 10 minutes. The in situ X-ray measurements were performed on the SAXS Beamline of the ELETTRA synchrotron in Trieste. The energy was 8 keV, which corresponds to the wavelength of the Cu K_α radiation of λ = 0.154 nm. The incident X-ray beam was focused to 1 x 1 mm^2 and the sample was always penetrated in the center perpendicular to the compression direction, independent of the deformation. The measurements were carried out in transmission with a linear position-sensitive detector (1024 channels, type PSD 50 of Braun, Munich, Germany). The distance between the sample and the detector was approximately 380 mm. Between the sample and the detector there was a vacuum chamber to prevent air scattering. It was possible to take evaluable XRD measurements up to a deformation of ε = 0.55. The X-ray profiles for larger deformations could not be acceptably evaluated because of the large backgrounds and the associated bad peak to background ratio.

5.4. Evaluation

5.4.1. Mechanical cyclic experiments

From the cyclic deformation curves the characteristic points A, B and C were determined by using the method of Hiss et al. [20]. Thereby A correlates with the start of isolated gliding processes, B with the activation of massive gliding processes (corresponds to the yield point) and C with the beginning of the crystallite fragmentation. For this evaluation, the strain at the load maximum of each cycle is separated in a relaxing $\varepsilon_{recoverable}$ and an elastic $\varepsilon_{residual}$ part (Figure 5.5).

$$\varepsilon_{total} = \varepsilon_{residual} + \varepsilon_{recoverable} \tag{5.1}$$

If we plot for all cycles the relaxed strain $\varepsilon_{recoverable}$ against the maximum stress of the cycle, the characteristic points B and C can be evaluated (Figure 5.7b) [125].

5.4.2. DSC measurements

The DSC measurements were performed to determine the lamella thickness distribution. For plate-shaped lamellas with a uniform lamella thickness, the Gibbs-Thomson formula

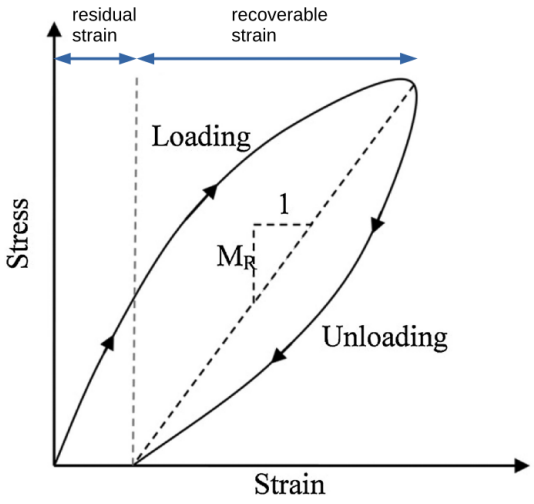

Figure 5.5.: *Strain definitions. Modified from* [126].

$$T_m = T_m^0 \left(1 - \frac{2\sigma_e}{\Delta h_c \lambda}\right) \tag{5.2}$$

can be used to determine the lamella thickness λ from the melting temperature T_m of the sample. For iPP the free fold surface energy is σ_e = 0.07 J/m^2 and the melting temperature of the 100 % crystalline material T_m^0 = 187.5 °C (= 460.6 K). The enthalpy of fusion per unit volume $\Delta h_c = \Delta H^0/\rho_c$ can be calculated with the enthalpy of fusion ΔH^0 = 207 J/g and the density ρ_c = 0.936 g/cm^3 of the ideal crystalline sample [107, 127]. In polymer crystals of homopolymers, the distribution of the lamella thickness λ has usually a log-normal form [23, 128]

$$f(\lambda) = \frac{1}{\lambda\sigma\sqrt{2\pi}}\, exp\left(-\frac{(ln\,\lambda - ln\,m)^2}{2\sigma^2}\right) \tag{5.3}$$

with the paramter σ and m. Thereby $\mu = ln(m)$ is the median and σ the variance of the distribution. Such a distribution is typical of nucleation-controlled crystallization processes.

In order to determine a correct lamella thickness distribution from a DSC measurement, a differential approach must be used [128, 129]. This is necessary since the DSC signal $P(T)$ is proportional to the molten volume and therefore cannot be directly used as a lamella thickness distribution function.

$$P(T) = \alpha_m \Delta H^0 m \beta f(T) \tag{5.4}$$

With α_m mass fraction crystallinity, ΔH^0 heat of fusion per unit mass, m sample mass, $\beta = \mathrm{d}T/\mathrm{d}t$ heating rate and $f(T)$ the volume fraction which melts at a certain temperature. The resulting lamella size distribution function $g(\lambda)$ for a constant heating rate β is given by

$$g(\lambda) = f(T)\frac{\mathrm{d}T}{\mathrm{d}\lambda} = \frac{P(T)}{\alpha_m \Delta H^0 m \beta}\frac{\mathrm{d}T}{\mathrm{d}\lambda} \tag{5.5}$$

Setting $T_m = T$ and assuming Δh_c to be temperature independent we can substitute equation 5.2 in 5.5. This leads to an equation for the lamella size distribution function $g(\lambda)$ depending on the DSC signal $P(T)$.

$$g(\lambda) = aP(T)(T_m^0 - T_m)^2 \tag{5.6}$$

The normalisation constant a can be considered as temperature independent and is therefore determined by the numerical integration of $P(T)(T_m^0 - T_m)^2$ [128].

In order to calculate an average lamella thickness from the lamella thickness distribution, the distribution function must be multiplied by the lamella thickness. This takes into account that thicker lamellae occupy a larger volume.

Due to the tilt of the molecular axis (c axis in the crystal) against the surface normal n of the lamella crystal (Figure 2.11a) small differences between the lamella thicknesses, determined from DSC measurements and XRD measurements respectively, can occur. For the XRD method, the stem length (= crystal thickness measured parallel to the c axis) is decisive since only crystal parameters parallel to the crystal axes a, b and c can be determined. The chain axis is tilted by 10 ° against the lamella normal in polypropylene. Therefore, the XRD method usually provides larger lamella thicknesses than the DSC method.

5.4.3. WAXS measurements

Although the iPP materials tested contains a α-nucleating agent, the WAXS profile measured shows a significant amount of γ-phase. This can be seen in the distinct additional peak between the α-peaks 130 and 111 as well as the pronounced anisotropy of the first reflection (Figure 5.6).

This anisotropy results from the overlap of the α 110 reflection with the γ 111 and γ 113 reflections. For an accurate analysis, the WAXS profile has to be separated into the phase-specific fractions. Therefore, a special fit program has been developed in scope of this dissertation which reproducibly performs the separation in several steps according to objective criteria. In a first step, the background is fitted by means of interpolation points between non-overlapping peaks with a polynomial of 5^{th} degree. Afterwards, a Pearson VII

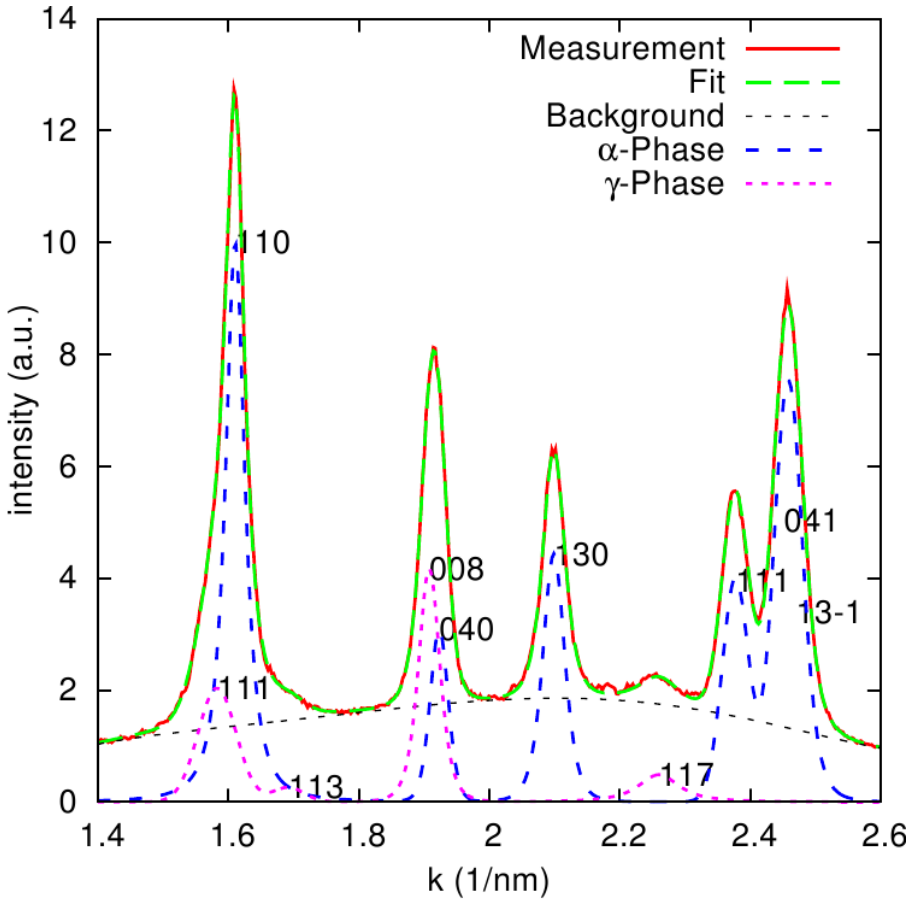

Figure 5.6.: *Phase specific WAXS profil of undeformed sample.*

function is fitted at a fixed background for each distinct peak (single peak or superimposed peaks). As a result, the WAXS profile can be decomposed into individual profiles for each pronounced peak by subtracting the residual profile (background + n-1 peaks). If these individual peaks are still composed of overlapping peaks, they are separated in a further step. The starting values for the two separated peaks are calculated from the amplitude, the peak position and the half-width of the single peak. The separation fit is robust (i.e., it has a clear solution even with slightly modified starting values) if there is a clear distance between the maximum of the individual peaks. This procedure can be applied to separate the α 040 and γ 008 reflections. The separation of the 041 and 13-1 α-reflections is much more difficult since both reflections appear at the same angular position. In order to obtain a stable fit result, one peak position had to be fixed. This leads to a small peak distance. With this special fit algorithm it was now possible to separate the measured WAXS profile into a WAXS profile of the α and γ-phase as well as the background. This allows the different phases to be analysed independently.

5.4.4. Modified Williamson-Hall Analysis

For the modified Williamson-Hall analysis, the FWHM of the fitted Pearson VII functions were used. An orthorhombic contrast factor (Figure 5.2) with 5 coefficients a_1 ... a_5 was used for the fits because the MXPA software currently supports only one orthorhombic lattice. Since the monoclinic α-phase with β = 99.62 ° is only slightly different from orthorhombic geometry (β = 90 °), the error is small.

If all the parameters (d, a_1 ... a_5) are freely fitted, the fit usually converges with negative crystallite sizes. In order to obtain physically reasonable values, the crystallite size was specified for the fit in the range from 5 to 50 nm and the resulting average dislocation contrast factors C_{hkl} were evaluated. Results with complex contrast factors or negative slopes in the modified Williamson-Hall plot were rejected. For the remaining fits, the shift on the x-axis ($K\sqrt{C_{hkl}}$) of the modified Williamson-Hall plot was judged against the Williamson-Hall plot (x-axis = K). As best fit that one with the smallest shift was selected.

5.4.5. Multiple Whole Profile Analysis (MXPA)

For the MXPA, the program *CMWP-fit*[1] [118, 130] with the extension *Multi-Eval extension to CMWP-fit* from Kerber [131] was used. The Multi-Eval extension varies the different starting values of each parameter over the whole parameter range and all possible permutations and uses the *CMWP-fit* program for the fit. This procedure ensures that the global minimum which represents the best physical solution can be determined with a high degree of reliability. This allows one to calculate a value for the reliability of the fit results. If many different starting values lead to the same fit result, this results in a high degree of reliability. In the result plots, this is expressed by error bars. The smaller the error bars the more robust the fits are. The error bars do not represent a confidence interval, but are a measure of the mathematical robustness of the fits.

In order to reduce the parameters to be fitted, the fit was performed in two steps. For the first step, the contrast factor coefficients were taken from the modified Williamson-Hall analysis and fixed. In a second step further parameters were released by a semi-automated procedure.

5.4.6. Determination of degree of crystallinity

The degree of crystallinity from the XRD profiles was additionally determined by the method of Ruland and Vonk [132, 133]. This method expands the standard formula for calculating the crystallinity degree

[1] CMWP-fit is freely available at `http://www.renyi.hu/cmwp/`

$$X_c = \frac{I_c}{I_t} = \frac{\int i_c \mathrm{d}V}{\int i_t \mathrm{d}V} = \frac{\int i_c s^2 \mathrm{d}s}{\int i_t s^2 \mathrm{d}s} \tag{5.7}$$

by the following factor.

$$K = \frac{\int \overline{f}^2 s^2 \mathrm{d}s}{\int \overline{f}^2 s^2 D(s) \mathrm{d}s} > 1 \tag{5.8}$$

With the factor K the disturbances in the crystalline phase, such as thermal fluctuations and local lattice defects, can be considered. For the calculation of the degree of crystallinity according to the variant of Vonk [133], only the linear approach was used because the WAXS measurements were only made in an angle range from $2\Theta = 12 - 23.5$ °.

The crystallinity degree from the DSC measurements was calculated from the melt peak area with a enthalpy of fusion of $H = 207$ J/g (100 % crystalline α-iPP [107]).

In contrast to the lamella thickness distribution, where for polymers with a log-normal distribution a very good agreement between DSC and X-ray method can be found [81], the crystallinity degree typically shows a difference between DSC and X-ray measurements. The order of magnitude depends on the assumed enthalpy of fusion for the DSC evaluation, which is very different in the literature [107].

5.5. Results and Discussion

5.5.1. Mechanical cyclic experiments

The residual and recoverable strains determined from the cyclic compression experiments show the typical characteristics for semi-crystalline polymers (Figure 5.7a) [20, 125]. The huge slip within lamellae and the lamellae rotation begins at the macroscopic yield point (Point B in Figure 5.7b). Therefore, from this point the mobile dislocation density should increase. Since the MXPA cannot distinguish between fixed and mobile dislocations, this means that the dislocation density (= total dislocation density) measured does not have to increase automatically. In semi-crystalline polymers, the dislocation density in undeformed samples is relatively high (chapter 4), and therefore it is not unlikely that many of them can be mobilized and new dislocations need not be formed immediately at the beginning of the plastic deformation.

These results also show that the point C is just reached at the maximum deformation. Until this point no fragmentation of the lamellas should be occur [20]. The lamella thickness and the degree of crystallinity thus remain almost unchanged up to the point C.

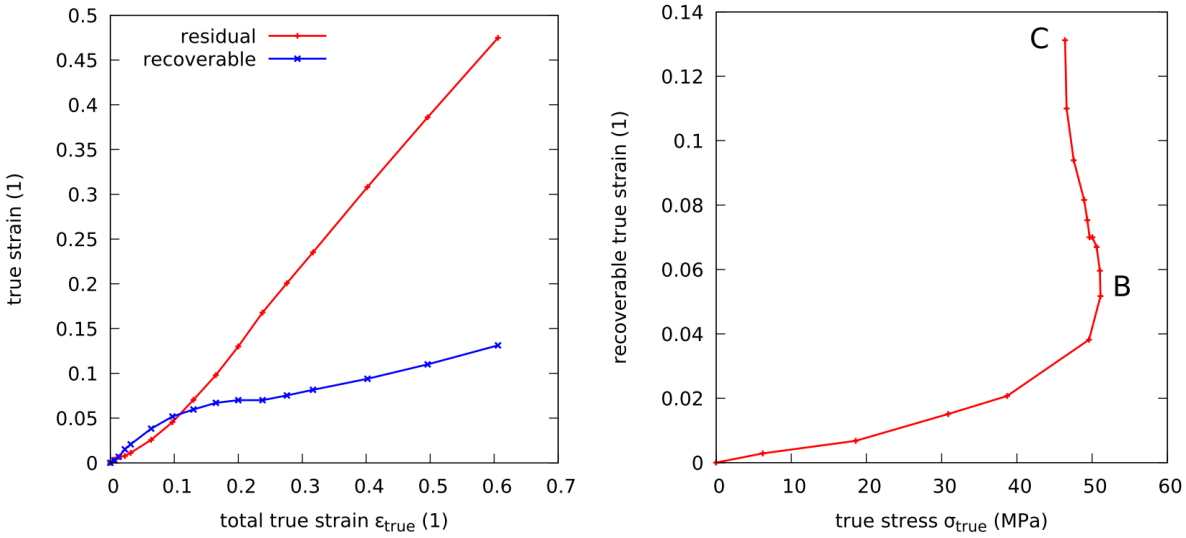

Figure 5.7.: *Evaluations of the cyclic experiment.*
(a) Residual and recoverable strains for each cycle as a function of the total true strain.
(b) Characteristic points B and C from cyclic compression experiments.

5.5.2. FEM Simulation

The FEM simulation results clearly show that the deformation in the compression experiment is inhomogeneous (Figure 5.8a).

The forging cross typical of this type of deformation is formed [134]. The largest plastic deformation (equivalent plastic strain) occurs in the sample center and decreases towards the edge. The local deviation of the actual plastic strain from the mean value increases strongly with the deformation. Figure 5.9 shows the von Mises equivalent plastic strain over the cross section for different deformation paths s.

(a)

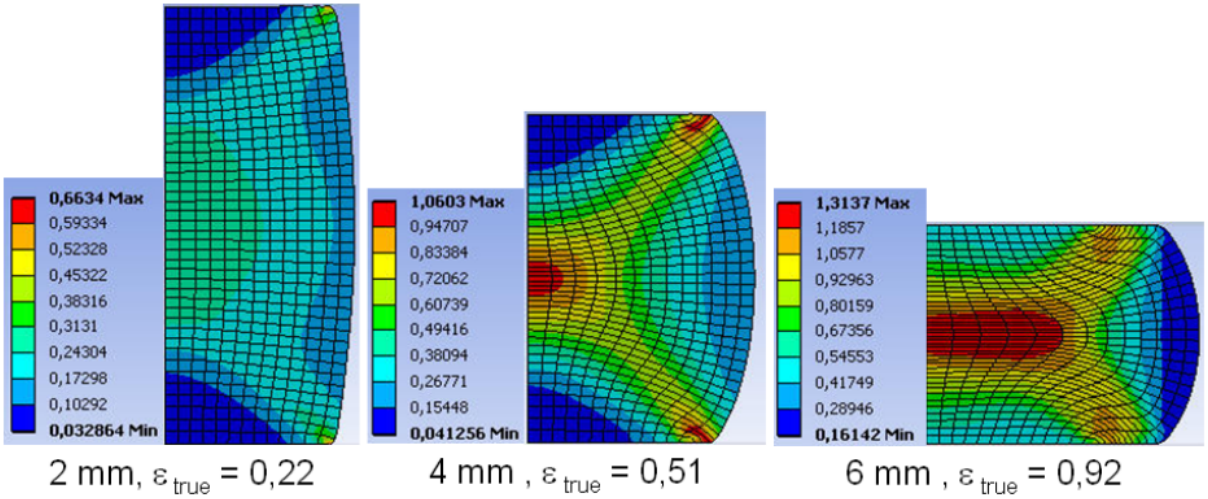

(b)

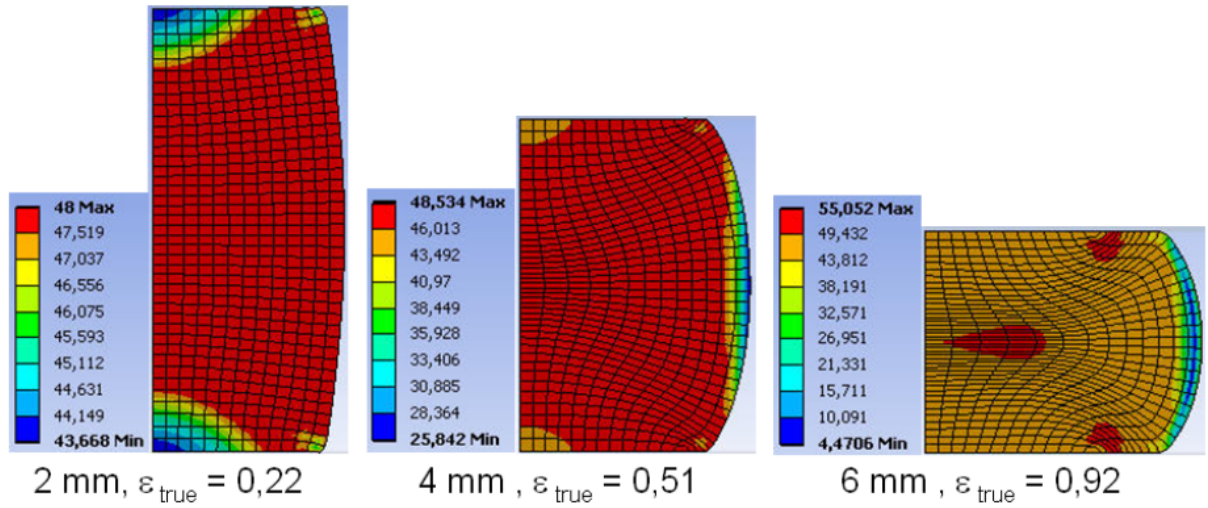

Figure 5.8.: *Results from FEM calculation.*
(a) Von Mises equivalent plastic strain for different deformations $\varepsilon_t rue$, elastic strain 0.042.
(b) Von Mises stress for different deformations ε_{true}.

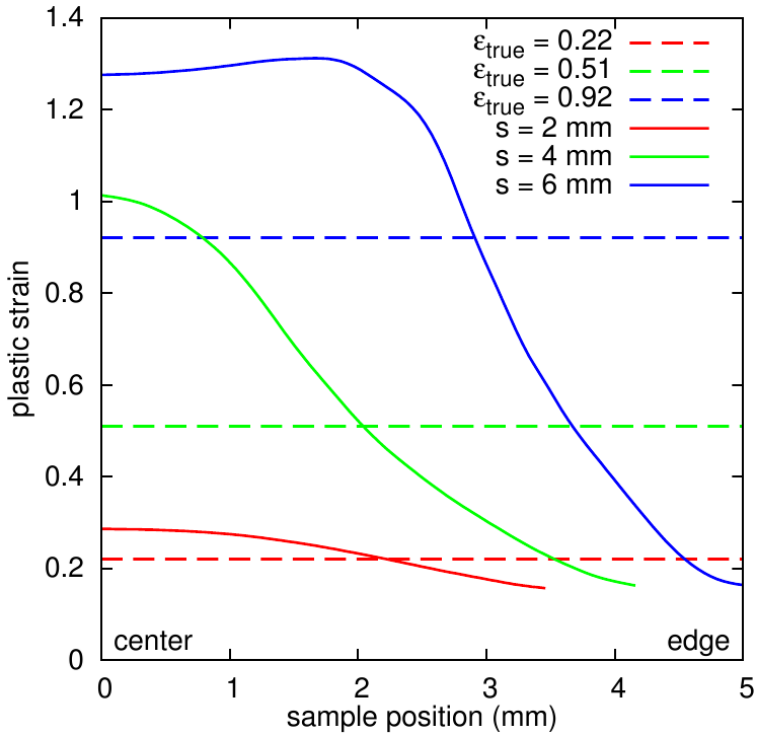

Figure 5.9.: *Von Mises equivalent plastic strain from FEM calculations depending on the sample position (left - sample center, right sample edge) for different deformation paths s.*

However, it is noteable that the average plastic deformation over the sample volume (average of Mises equivalent plastic strain) calculated from the FEM simulation agrees very well with the true strain $\varepsilon_{true} = -ln(l/l_0)$ from the compression experiment. The deviation is at maximum 4 % (Table 5.1).

deformation path	ε_{true}	$\overline{\varepsilon}_{FEM}$	difference
[mm]	[1]	[1]	[%]
2	0.22	0.24	-2
4	0.51	0.55	-4
6	0.92	0.91	1

Table 5.1.: *Comparison of true stain ε_{true} with average von Mises equivalent plastic strain from FEM $\overline{\varepsilon}_{FEM}$.*

In contrast, the stress distribution (Figure 5.8b) is relatively homogeneous. This is relevant as the generation of the dislocations and the dislocation movement is stress-controlled.

5.5.3. DSC

The lamella thickness distribution from the DSC measurements has in principle the typical log-normal distribution shape for polypropylene. However, the samples investigated show in detail a superimposition of two log-normal distributions. (Figure 5.10).

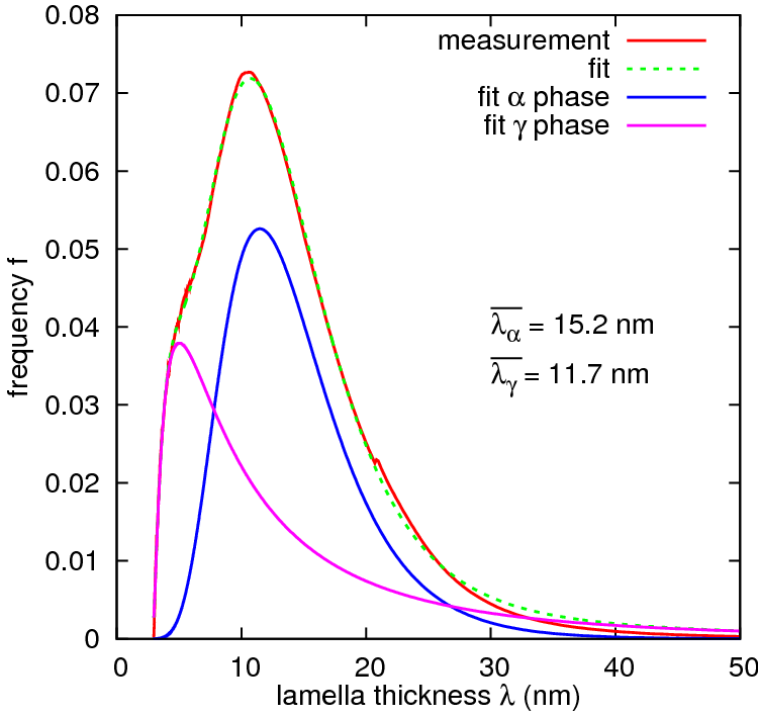

Figure 5.10.: *Lamella thickness distribution for an undeformed sample measured with DSC.*

From the WAXS measurements it is clear that the sample examined consists of approximately 40 % α-phase and 10 % γ-phase (Figure 5.12). This suggests to assign the two log-normal distributions to the different crystalline phases. However, the lamella thickness distribution does not give a volume fraction. Therefore, a direct identification of the phases over the volume fraction is not possible. The evaluation of the WAXS measurements with respect to the half-widths of the peaks (FWHM) shows that the crystallite size (lamella thickness) of the γ-phase is less than that of the α-phase, thus making an identification possible. This results in the average lamella thicknesses of the undeformed sample $\overline{\lambda_\gamma}(\varepsilon = 0) = 11.7$ nm in the γ-phase and $\overline{\lambda_\alpha}(\varepsilon = 0) = 15.2$ nm in the α-phase. The lamella thickness distribution of the γ-phase is strongly asymmetric and has its maximum at a lamella thickness of 5 nm. Thus, the lamella thickness of the γ-phase is comparable to the results of Lezak et al. [106] which found an average lamella thickness of 8.5 nm for pure γ-PP by means of SAXS measurements. With increasing deformation the characteristics of the distribution changes only slightly (Figure 5.11).

Also, the bimodal log-normal character remains. Up to a deformation of $\varepsilon = 0.7$, there

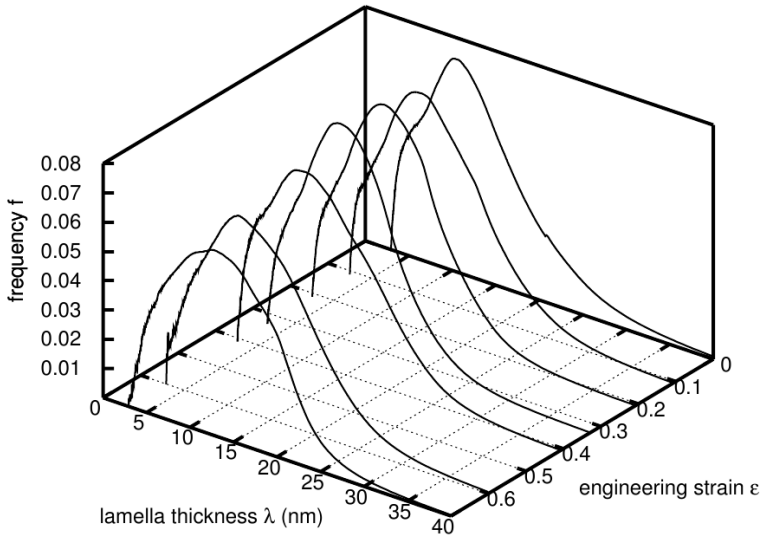

Figure 5.11.: *Lamella thickness distribution from DSC depending from deformation. From* [23].

is also no significant change in the average lamella thickness. The degree of crystallinity is constant at $X_c^{DSC} = 0.5$ and agrees well with the degree of crystallinity from the X-ray measurements for the undeformed and slightly deformed samples (Figure 5.12). Larger deviations are only in the case of larger deformations ($\varepsilon > 15$ %), since the degree of crystallinity from the WAXS measurements decreases continuously.

The mechanical evaluations have shown that the point C (Figure 5.7b) is not significantly exceeded. Therefore, only a small fragmentation of the lamellae should take place up to the maximum deformation, and the crystallinity should not change significantly. However, it must be noted that the deformation in compression is relatively inhomogeneous. The FEM simulations have shown that the plastic deformation in the core of the sample is significantly larger (Figure 5.9). This means that the point C is also clearly exceeded, and fragmentation of the lamellae can take place locally. This can explain the decrease in the degree of crystallinity by X-ray measurements, since the measurement was carried out in transmission through the sample center.

5.5.4. WAXS measurements

Phase selection

The WAXS profile measured (Figure 5.6) shows a pronounced asymmetry for the α 110 reflection, and there is an additional peak between the α 130 and α 111 reflection. These are clear indications of the existence of a γ-phase. The 111, 113, 008 and 117 reflections of the γ-phase could be separated relatively reliably using the procedure described in section 5.4.3. A reliable separation of the γ 115 reflection is not possible because the

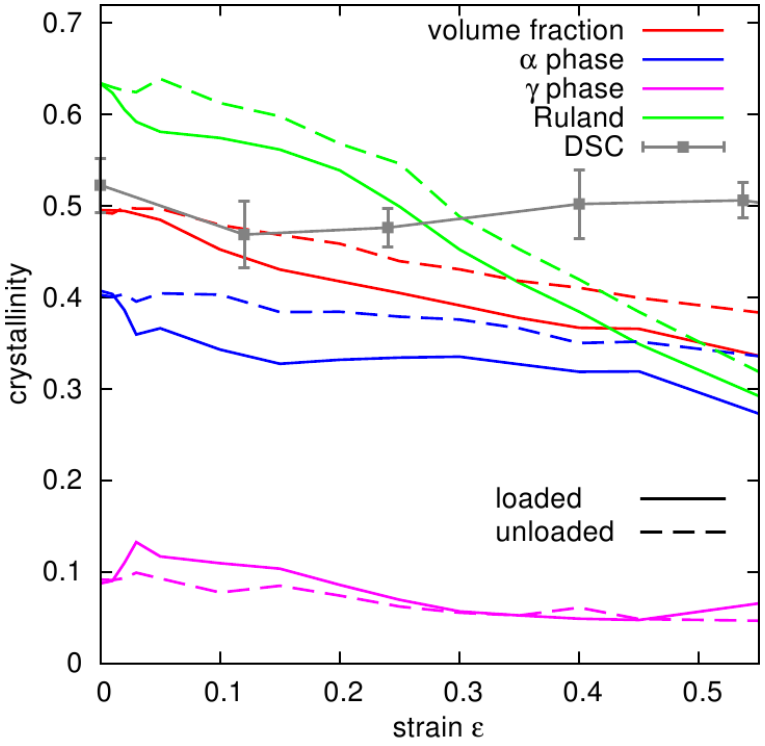

Figure 5.12.: *Normalised phase specific X-ray scattering intensities X_c compared with cristallinity from DSC X_c^{DSC}.*

intensity is too low. The γ 202 and 026 reflections could not be separated, since they are too close to the α 041 and 13-1 reflections.

Phase fractions, crystallinity

The phase-specific WAXS evaluations have been shown a very high γ-phase content. With absolute 10 % γ-phase content and 20 % γ-phase content in the total crystalline phase, respectively, the investigated material shows a significantly higher γ-content than in polypropylene without alpha nucleation agents where the γ-phase content is typically 6 % [135]. For high-pressure crystallization (p = 200 MPa), a α-nucleating agent also acts as a γ-nucleating agent [136]. Obviously, this effect is also present under atmospheric pressure, although not so strongly pronounced. This is rather a disadvantage for phase-specific defect analysis, since the α-phase separation of the XRD profile is more difficult.

While the α-phase fraction decreases continuously, for the γ-phase a slight decrease occurs only in case of deformations $\varepsilon > 15$ % (Figure 5.12). The ratio of the phase fractions hardly changes with the deformation and is α:γ = 4:1.

If we compare the phase-specific scattering intensities measured under load (loaded) and relaxed (unloaded), a significant constant increase is already shown for the α-phase at

small deformations. There are the following possible explanations.

- Due to the unloading, the defects (dislocations) recover and this leads to an increase in crystallinity. Although the dislocation density decreases markedly at unloading, because many deformation-induced dislocations recover above the glass transition temperature [54, 84], this effect should be small.
- Above the glass transition temperature, the amorphous phase is much softer than the crystalline phase. The Young's modulus of the crystalline phase is larger by about 3 orders of magnitude. Therefore, the amorphous phase is compressed more significantly and thus its volume fraction under load is clearly reduced. This assumption is supported by the fact that the difference is smaller for small loads.

It is remarkable that this effect does not occur in the stronger γ-phase until a deformation of ε = 55 %. Comparing the yield stress of α and γ-phase (σ^{α}_{yield} = 48 MPa [125], σ^{γ}_{yield} = 68 MPa [106, 124]) the γ-phase is 42 % stronger. This means that there is only too little plastic deformation in the γ-phase. Furthermore, the plastic deformation in γ-PP occurs mainly by interlamella amorphous shear [106] and not by dislocation generation and dislocation mobilization. Thus, there is only a slight reduction of the absolute γ-phase fraction.

The crystallinity determined by the method of Ruland [132] and Vonk [133] is higher than the crystallinity determined from the phase-specific scattering intensities. The reason therefore is that this method also extrapolates into the WAXS region with large angles outside the measurement range. The larger decrease at larger deformations $\varepsilon > 25$ % is due to the evaluation method, the selected limits and the relatively small angular range of the measurement.

Peak shift

The peak shift during compression deformation occurs for all peaks to larger angles, which corresponds to a reduction in the lattice plane spacings (Figure 5.13).

A strong linear increase in the peak shift is observed for small deformations ($\varepsilon < 2$ %, elastic deformation range), which is for all peaks equal within the precision of measurements. The deformation in the crystalline phase can be calculated from the change in the lattice plane spacings l compared to the unloaded state l_0. Thus, a modulus of elasticity for the crystalline phase can be determined with the macroscopic stress measured. For the α 130 reflection, a modulus of elasticity of 2700 MPa is obtained. From the propagation of longitudinal sound the modulus of the crystalline phase can be calculated theoretically [137]. With this approach Menyhárd et al. [138] calculated = 6600 MPa for polypropylene, which clearly differs from the experimentally determined value. In order to be able to determine a more accurate value for E_c, one would have to measure the peak shift

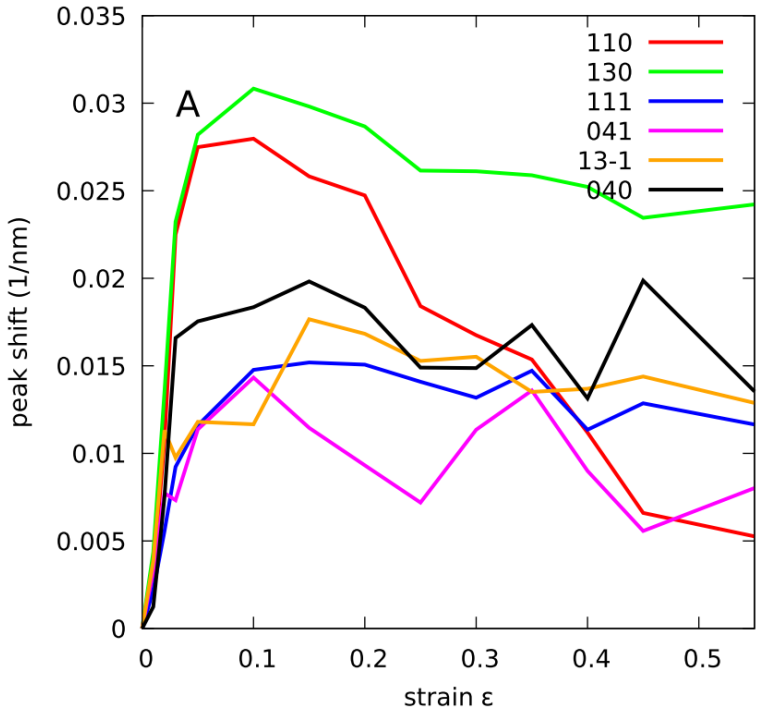

Figure 5.13.: *Peak shift during deformation for different α-PP peaks. It can be assumed that the beginning of the plateau region in the peak shift correlates with the point A which can be determined by mechanical experiments.*

continuously during deformation. But a direct determination of the modulus of elasticity of the crystalline phase from the peak shift should be possible principally.

After the range with a linear increase in the peak shift, a direct transition occurs into a plateau region with a constant or slightly falling peak shift. This transition takes place between $\varepsilon = 2 - 5$ % depending on the peak type. This means that, despite the increasing macroscopic stress, the lattice planes are not being further pressed together. This could mean that from this point

1. the deformation occurs mainly in the amorphous phase or
2. in the crystalline phase slip processes are activated, i.e. plastic deformation occurs

Since this transition does not take place at the same time for all peaks types, variant 2 is the most likely. The different strain values (and thus stress values) for the beginning of the plateau range can be explained by different CRSS in the different slip systems. In polypropylene, the (010)[001] slip system is activated before the (110)[001] slip system [97]. This is confirmed by our measurements, since the peak shift for the 040 peak is already at $\varepsilon = 3$ % and that of the 110 peak at $\varepsilon = 5$ % is on a constant level. Assuming that the beginning of the plateau level corresponds to the activation of the corresponding slip system, the critically resolved shear stress (CRSS) can be estimated by taking into account a Taylor factor $m = 3$ [3, 34, 66]. For the (010)[001] slip system a CRSS of 10

MPa and for the (110)[001] slip system a CRSS of 13 MPa are obtained. These values are significantly lower than those measured by Bartczak et al. [42] of 22.6 MPa for the (010) [001] sliding system. However, the Coulomb yield criterion was used, which does not take into account crystallographic slip before the yield point. The nano-creep experiments with polyethylene (chapter 6), have shown that plastic deformations in the crystalline phase can be detected even at stresses < 1 % of yield stress. First preliminary tests with polypropylene have shown similar results as for polyethylene. However, from which load the plastic deformation in the crystalline phase reaches a significant level is difficult to determine. One possibility to detect the beginning of relevant plastic deformation in the crystalline phase is the method presented by Hiss et al. [20] using cyclic deformation experiments. With this method a characteristic point A can be determined, which is assigned to the beginning of the plastic deformation in the crystalline phase. This point is clearly before the yield point. Due to too low resolution the point A could not be determined with the cyclic compression experiments performed. However, it can be assumed that the beginning of the plateau region in the peak shift correlates with the point A (Figure 5.13).

Peak broadening

Comparing the peak widths (full width at half mean, FWHM) of the best separable peaks of α and γ-phase with increasing deformation (Figure 5.14), it is noticeable that the FWHM of the α-peaks is about half of that of the γ-peaks.

Since the two phases crystallize under very similar conditions, it can be assumed in a first approximation that the defect density is comparable in both phases. It was possible to confirm this by dislocation density measurement [124]. Thus the different peak width has to be caused by the crystallite size (lamella thickness). Since the crystal size is proportional to 1/FWHM, one can assume that the γ-lamella is about half as thick as the α-lamella. However, one has to take into account that the broadening comes mainly from the small crystals (thin lamellae) and is not proportional to the average lamella thickness. The lamella thickness distribution from the DSC measurements (Figure 5.10) shows two superimposed log-normal distributions whose lamella thickness ratio is approximately 1:2 for the smallest lamellae (smallest 30 %). This confirms the results from the FWHM evaluations and is a further evidence for the assignment of the lamella thickness distribution to the phases.

With increasing deformation, the FWHM increases continuously for the α-peaks, while the FWHM of the γ-peaks only changes slightly. The DSC measurements show that although the lamella thickness distribution changes slightly with increasing deformation (Figure 5.11), the average crystallite size remains nearly constant for both phases. An increase in the peak width in the α-phase can therefore only be caused by an increase in the defect density (dislocation density). Measurements of the dislocation density for gamma polypropylene as a function of the deformation [124] show that the dislocation

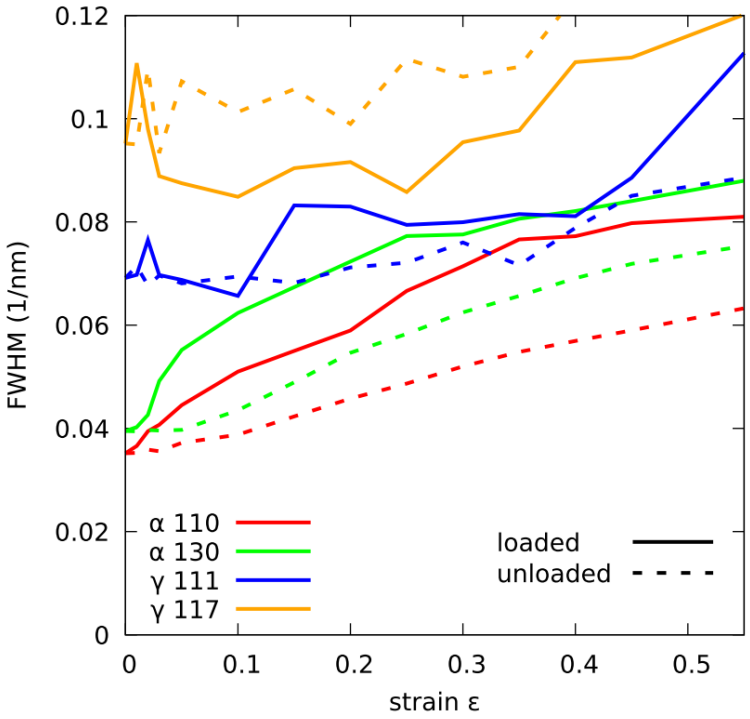

Figure 5.14.: *Peak width (full width at half mean, FWHM) of α-PP peaks during deformation.*

density in gamma polypropylene does not increase. This explains why the peak width of the γ-peaks does not change.

The FWHM in the relaxed, unloaded state is typically smaller regardless of the deformation. The difference increases with the deformation in the α-phase. During unloading the crystalline phase is also deformed back by restoring forces coming from the oriententation of the amorphous phase. Thereby defects (dislocations) can recover [84] and this leads to a decrease in the defect density (dislocation density), which is expressed by a reduction in FWHM. This is also confirmed by the modified Williamson-Hall analysis and the MXPA, where the dislocation density in the higher-deformed samples decreases markedly with unloading (Figure 5.18).

Modified Williamson-Hall analysis

In the classical Williamson-Hall Plot (Figure 5.15) the peak width (FWHM) is plotted against the peak position (diffraction vector K).

For the α-phase of the undeformed sample, a linear increase with an increasing order is seen (Figure 5.15a). If the peak width increases with the order, the broadening is caused by a strain field. The linearity means that the distortion field of the defects has only a

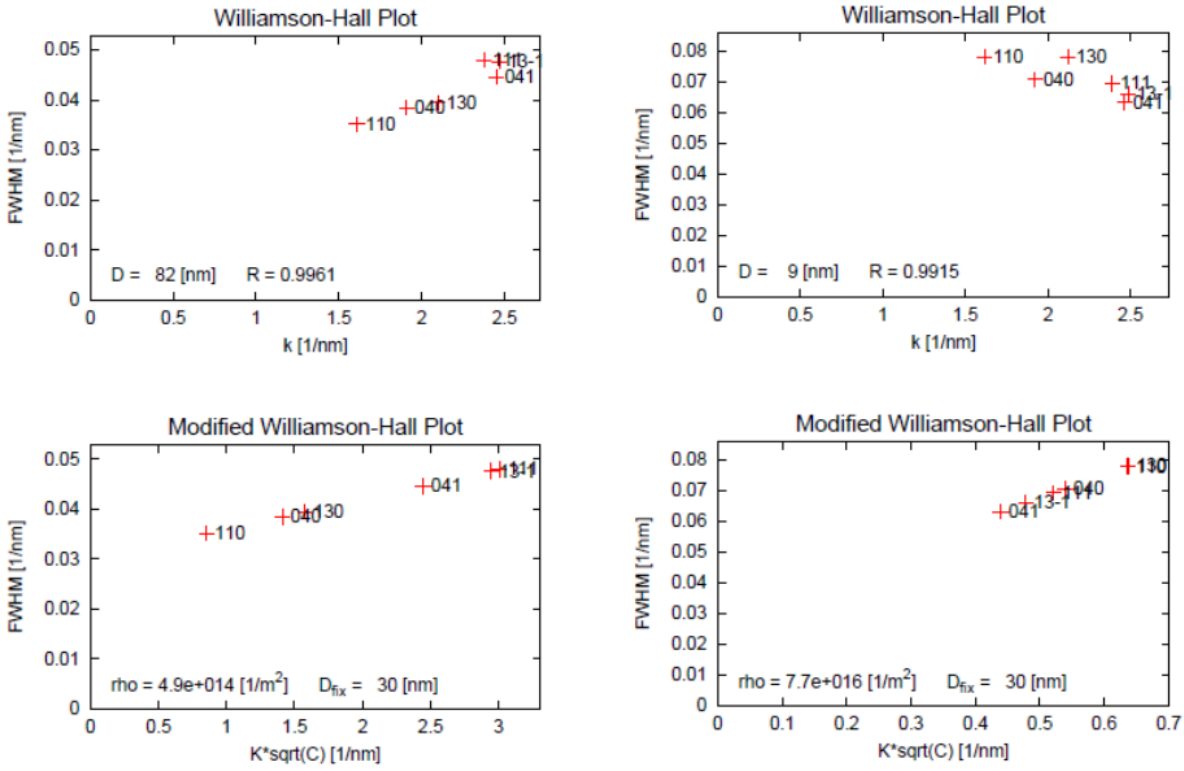

a) undeformed b) deformed

Figure 5.15.: *Williamson-Hall and modified Williamson-Hall analyses for undeformed and deformed (ε = 0.45) samples of iPP.*

small anisotropy or the stress field is not of long range [76]. This linear increase is lost with growing deformation (Figure 5.15b), which can be caused by

- an increase of the defect density or
- a decrease of the crystallite size.

Since the crystallite size, determined by DSC measurements, remains almost unchanged, a pronounced increase of the defect density (dislocation density) is likely.

For all α-PP WAXS profiles, a linearisation in the modified Williamson-Hall plot is possible by a fit of the average dislocation contrast factor coefficients a_1 ... a_5 (Figure 5.15). This is evidence of the dislocation character of the lattice imperfections [76]. It has been shown however, that a linearization for α-PP is always possible numerically, since only 6 peaks are available for the evaluation and 5 parameters of the contrast factor are fitted. Therefore, successful linearisation cannot be used as a direct proof of the dislocation characteristics of the defects. Since the linearity is present in the undeformed sample without taking into account a contrast, it can basically be assumed that the present defects have a relatively small contrast which applies e.g. to screw dislocations.

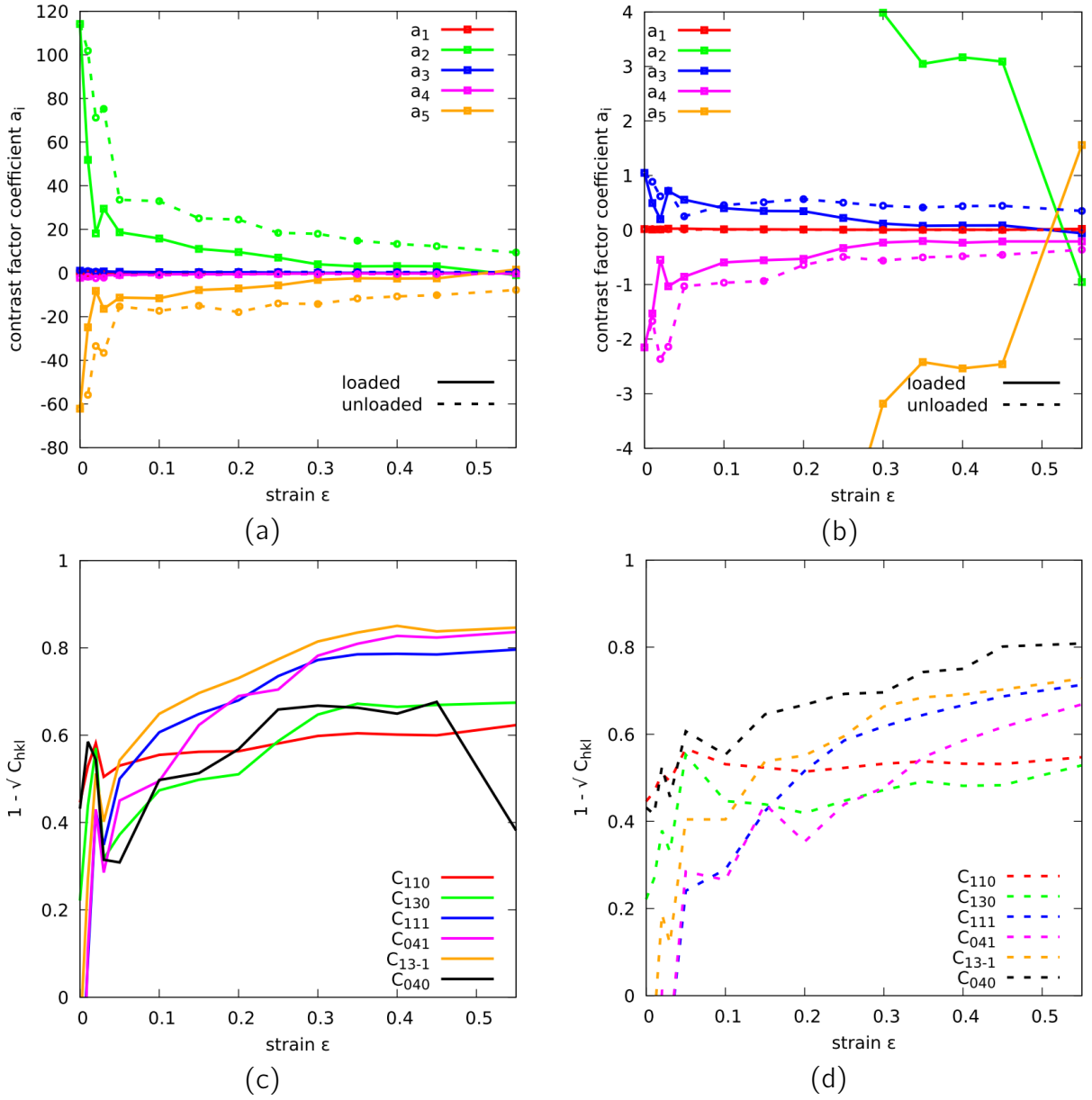

Figure 5.16.: *Average dislocation contrast factor coefficients a_1 ... a_5 (a overview, b zoom), and shift factors $1 - \sqrt{C_{hkl}}$ from average dislocation contrast factors (c loaded, d unloaded samples) determined with modified Williamson-Hall analysis.*

The contrast factor coefficients show a pronounced coupling and symmetry respectively (Figure 5.16a and b).

$$a_2 = -k \cdot a_5 \tag{5.9a}$$

$$a_3 = -k \cdot a_4 \tag{5.9b}$$

This can be explained by the fact that only three sliping systems are activated [97] and these have almost the same contrast [23].

The contrast factor coefficients decrease with increasing deformation. However, large values for a_2 and a_5 of the undeformed samples do not mean that the contrast factors and therefore the shift factors in the modified Williamson-Hall plot $1 - \sqrt{C_{hkl}}$ are also large. From the formula for the contrast factors (Figure 5.2) can be seen that, due to different sign, for large a_i the resulting contrast factor can be still small.

The shift factors (Figure 5.16c) have relatively small values up to a deformation of ε = 10 % and then a continuous increase to approximately twice the initial values.

This may mean that the dislocation characteristics up to these particular deformations do not substantially change, and thereafter also a different type of dislocation can be generated. For energetic reasons in the undeformed and slightly deformed sample there are mainly screw dislocations and the deformation in the lamellae occures by chain slip. Investigations by Spieckermann [23] with theoretical contrast factors have shown that from a deformation of about ε = 10 %, additional edge dislocations are generated and increasingly transverse slip occurs. This can explain why the shift factors increase after a certain deformation, especially since the contrast factors for the edge dislocations are larger.

The shift factor behaves similarly for unloaded samples (Figure 5.16d). Generally, the shift factor for the unloaded samples is always smaller than for the deformed samples. This can be explained on the one hand by the reduction of texture during unloading and on the other hand with a reduction in the defect density by annealing of dislocations. At temperatures above the glass transition temperature, a relatively large number of dislocations can anneal [84].

Comparing the crystallite size from the modified Williamson-Hall analysis with that from DSC measurements (Figure 5.17), it is shown that for small deformation, the average crystallite size is over-estimated by the X-ray method.

However, compared to earlier measurements (chapter 4), the determination of the lamella thickness could be improved by the additional criterion that the shift factor $1 - \sqrt{C_{hkl}}$ is a minimum. Nevertheless, for deformations up to $\varepsilon < 30$ %, there is still a quite larger difference to the DSC measurements. A much better match can be obtained by the MXPA [81]. There are only minor differences, which can be explained by the different methods.

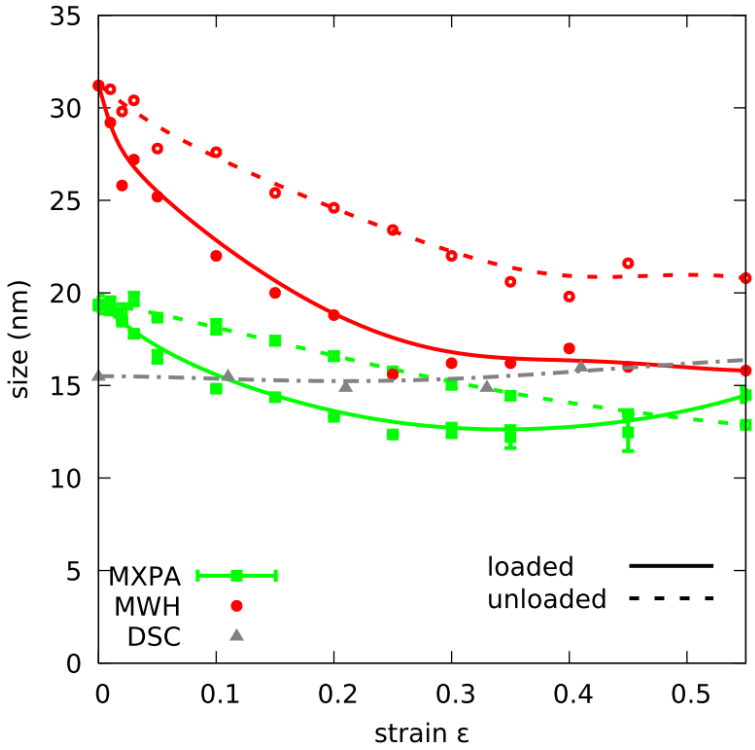

Figure 5.17.: *Lamella thickness from loaded (solid lines) and unloaded (dashed lines) samples determined with different methods.*
MXPA (green), average lamella thickness from calculated log-normal lamella thickness distribution. The error bars are a measure of the convergence of the fits at different start values.
Modified Williamson-Hall analysis (red).
DSC (gray), average lamella thickness from lamella thickness distribution (with lamella thickness weighted 50 % value).

If one assumes a lamella model consisting of several subblocks in the order of magnitude of the lamella thickness, this difference can be interpreted as a cluster of lamella blocks in a coherent position. It is likely that several adjacent sub-blocks scatter the X-ray beam coherently in the undeformed sample and even at small degrees of deformation [124].

As a result, especially the modified modified Williamson-Hall analysis provides larger crystallite sizes. As the deformation increases, the clusters disappear and thus the CSD size decreases. In addition, it must be taken into account that only a log-normal distribution of the crystallite size can be considered at the MXPA. The evaluation of the lamella thickness distribution from the DSC measurements (Figure5.10) have shown that the examined samples do not have an exact log-normal distribution of the lamella thickness.

Dislocation density

In the dislocation density from the modified Williamson-Hall analysis there can be recognized a clear difference between loaded and relaxed (unloaded) samples (Figure 5.18a). The dislocation density of the unloaded samples is clearly (almost factor 10) smaller than under load. Already at small deformations, a large increase in the dislocation density can be observed.

The MXPA was executed in two steps. In the first step, the contrast factor coefficients were taken from the modified Williamson-Hall analysis and fixed. At this fully automatic run with the Multi-Eval extension to CMWP-fit [131], the results of the MXPA scatter relatively strongly depending on the starting values (error bars in Figure 5.18b). In a second step, the MXPA parameters were adapted manually and further parameters were released for the fitting process. As a result, in the determination of the dislocation density much more stable and reliable results were obtained (Figure 5.18c and d) than of the first step which one described in the following. Up to a deformation of ε = 20 %, the dislocation density increases only slightly. This shows that there are sufficient dislocations up to far above the point B (= beginning of massive plastic deformation in the crystals) and these have only to be mobilized. Only at relatively large deformations the dislocation density increases significantly. During unloading the dislocations annihilate and the dislocation density decreases to the initial value. Measurements on pre-deformed samples have shown that beyond a residual deformation of $\varepsilon_{residual} \sim 30$ %, the dislocation density remain increased and not all additionally generated dislocations annihilate (Figure 4.4).

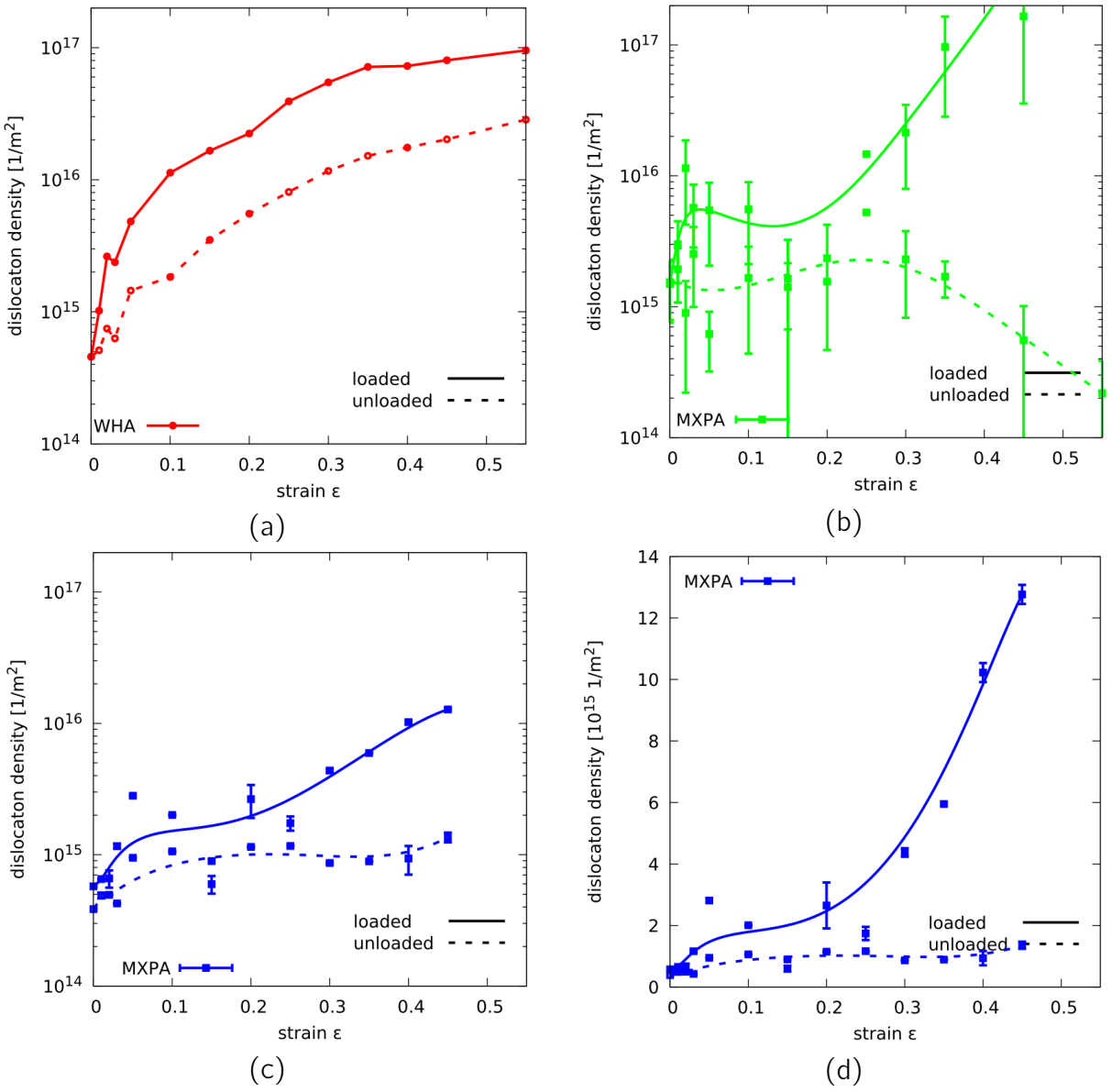

Figure 5.18.: *Dislocation density from (a) modified Williamson-Hall analysis, (b) MXPA after first step, (c) and (d) MXPA after second semi-automatic step, (d) linearly scaled plot.*

5.6. Conclusions and summary

The MXPA is a powerful method for the determination of the dislocation density and the crystallite size (CSD size) of semi-crystalline polymers. But after a first successful application on polypropylene (chapter 4) there remained some challenges. Semi-crystalline polymers have typically complex crystal systems with low symmetry. Thus, the MXPA has a lot of fit parameters and for the evaluation process many manual corrections are necessary. The aim of this second work of the dissertation was to improve the modified Williamson-Hall analysis in order to get an automatised evaluation procedure which results in reliable start values for the contrast factor coefficients and the MXPA, respectively. This goal could be achieved by an additional boundary condition for the modified Williamson-Hall analysis thus reducing the degree of freedom for the fit. This led to much better start values and convergent fits in the multieval variant of the MXPA [131]. However, the results (Figure 5.18b) were still not fully satisfactory. Good results could only be achieved with a second semi-automatic evaluation step, where the MXPA parameters were adapted manually and further parameters were released for the fitting process. Thus the evaluation process could be considerably shortened and the reliability of the results significantly improved.

By applying this improved approach, the MXPA for a undeformed polypropylene sample has shown a dislocation density of 10^{15} m^{-2}. Thus, the measured dislocation density was lower by an order of magnitude relatively to the first application of the MXPA to polypropylene (chapter 4). Recent studies on polypropylene [84, 124] have confirmed a dislocation density of 10^{15} m^{-2} in undeformed polypropylene.

In contrast to the first application of the MXPA (chapter 4), the measurements were carried out in situ during cyclic deformation at a synchrotron. Thus relaxation phenomena could be taken into account. It has been shown that with increasing plastic deformation ($\varepsilon > 10$ %), the dislocation density does not increase strongly (Figure 5.18d). This means that there are sufficient dislocations available and these are mobilized thermally. Any additionally necessary mechanical stresses are small. This is confirmed by the novel nano-creep experiments developed also in scope of this dissertation (chapter 6), where in polyethylene the dislocation movement occurs in the form of dislocation avalanches even at stresses lower than 1 % of the yield stress.

The dislocations annihilate during unloading and the dislocation density decreases to the level of the undeformed sample. This clearly shows that for the determination of the dislocation density as a function of the deformation, in situ experiments are indispensible. The first experiments for the determination of the development of the dislocation density during plastic deformation were performed on predeformed polypropylene specimens (chapter 4). Thus, these results correspond to the measurements from the unloaded sampels. For these relaxed (unloaded) predeformed samples an increase in the dislocation density not before approximately 30 % deformation occurred (Figure 4.4). However, this deformation corresponds to the permanent deformation $\varepsilon_{residual}$ (Figure 5.7a), whereas in the current

evaluations the total deformation ε_{total} was used. In order to compare the results, it is necessary to correct the strain values by the relaxing deformation $\varepsilon_{recoverable}$. This means that the strain values from the earlier measurements must be increased by approximately 10 % and therefore an increase in the dislocation density in the unloaded samples from $\varepsilon_{total} > 40$ % is expected. Unfortunately, the XRD profiles for a strain of $\varepsilon_{total} > 45$ % could not be evaluated. However, a small increase in the dislocation density of the unloaded samples appears in the measurement for $\varepsilon_{total} = 45$ % (Figure 5.18c and d). Therefore, from a deformation of $\varepsilon_{total} > 45$ %, an increase in the dislocation density in the unloaded samples is expected. This means that the dislocation density decreases by about one order of magnitude during unloading and corresponds roughly to twice the value of the data reported by Spieckermann et al. [84]. In these experiments, PP specimens were stored in liquid nitrogen immediately after deformation to $\varepsilon = 120$ % in order to prevent annihilation of dislocations. Subsequently, the dislocation density during heating was determined. It was found that at the glass transition temperature the dislocation density drops sharply. Despite the much larger deformation, the initial value of the dislocation density was lower than the value determined for $\varepsilon = 45$ % in this work. Therefore, it must be assumed that shock freezing in liquid nitrogen is not suitable to stabilize all dislocations and a large portion of dislocations already annihilate during cooling respectively. This explains the different decrease in the dislocation density and shows that the annihilation process above the glass transition temperature is significant.

With the results from the XRD measurements, the lamellar thickness distribution from the DSC measurements could be clearly assigned to the α and γ-phase. It has been found that the lamellar thickness in the γ-phase is distinctly smaller than in the α-phase. This agrees with recent lamella thickness distribution measurements of pure alpha and gamma polypropylene determined by DSC [139]. Regarding Young's dislocation model [62], where the yield stress linearly increases with the lamellar thickness (equation 2.23), the strength of the γ-phase should be much smaller than that of the α-phase. However, exactly the contrary is the case. Significantly higher strengths were found for γ-PP than in α-PP [106, 124]. Reasons could be the special cross-molecular arrangement in γ-PP which restricts the dislocation movement or a modified rigid amorphous phase which influences the generation of dislocations. Recent investigations by von Baeckmann [140] have shown that the γ-phase is not always stronger. Under standard high-pressure crystallization conditions, the γ-phase has the same strength as the α-phase. Only with special crystallization conditions, γ-PP samples with up to 40 % higher strength are obtained [139, 140].

Part III.

Investigation of the dislocation kinetics by a novel nano-creep test

6. Characterization of strain bursts in polyethylene by means of a novel nano-creep test

6.1. Introduction

In several semi-crystalline polymers, as already mentioned, it was found that the deformation of the crystalline phase is governed by the generation and motion of crystal defects - namely dislocations - especially at deformations within the extended plastic regime [27, 40, 62, 65, 66]. Although the importance of dislocations for the plastic deformation in many semi-crystalline polymers is beyond dispute [19, 32, 50], the kinetic mechanisms of dislocations remains widely unclear.

While diffraction methods like the Multi-Reflection X-Ray Profile Analysis (MXPA) [76, 78], can be considered as highly phase selective, the situation is more complex for mechanical experiments as they register an overlap of effects originating from the crystalline as well the amorphous phase. Nevertheless, for analysing the nature, mobility and annihilation of defects, the determination of activation volumes and energies from mechanical tests seems indispensable for the understanding and identification of the molecular processes controlling elastic properties, strength and ductility.

The first attempts to investigate the deformation behaviour of the crystalline phase independent of the amorphous phase were made by Rabinowitz and Brown 1967 [141]. They observed the onset of plastic deformation in the crystalline phase of high density polyethylene (PE-HD) at a stress of 0.18 MPa by cyclic tension experiments in the micro-strain region with high-resolution strain measurement (strain sensitivity of 10^{-6}).

From metals it is known that under certain conditions the flow of deformation can be jerky, which means that the macroscopic deformation curve exhibits significant jumps (strain bursts). Uchic [90] showed that the deformation of small cylindrical nickel single crystals, with a diameter of some μm, occurs almost exclusively through strain bursts. The jumps become smaller with increasing sample size and they disappear for macroscopic specimens.

The cause of strain bursts in metals are usually dislocation avalanches [142]. In metallic glasses, shear banding and martensitic transformations can also cause strain bursts [143].

Since the deformation of the crystalline phase in many semi-crystalline polymers is dislocation controlled [19, 50], strain bursts should also emerge. The first evidence for strain bursts in a polymer was found by Li and Ngan [89] with nanoindentation creep experiments on PE-HD. With some estimations they could determine an activation energy of 0.22 eV for the plastic deformation of the crystalline phase. Further comprehensive experiments were performed by Zare Ghomsheh et al. [91, 92].

However, nanoindentation creep experiments have several limitations.

- The stress field is strongly inhomogeneous, which requires some assumptions and estimations for the evaluation of the activation energy.
- The tested sample volume is very small, and local effects can play a role.

Therefore, an alternative test method would be desirable, which is not affected by these disadvantages.

In semi-crystalline, the path length is limited by the lamella thickness and therefore strain bursts can only be in the order of the lamella thickness. In order to verify single strain bursts in polymers the resolution of the deformation measurement had to be in the nm scale. In addition, the deformation rate in the amorphous phase should be not too large, so that single strain bursts can be detected. A possibility would be a creep experiment above the glass transition temperature T_g with very small loadings in the micro-strain region (finite strain near the origin). Thereby the soft amorphous phase deforms continuously with very little creep rates (few nm/s), while the deformation in the crystalline phase is may be jerky over strain bursts (some nm in typically 0.1 s). This would give the possibility to separate the deformation in the amorphous phase from that of the crystalline phase and to study independently the mechanisms of plastic deformation in the crystalline phase.

An important aspect is the constant application of a homogeneous stress field over a large specimen volume. Thus the occurrence of strain bursts becomes more likely. The separation of deformations in the amorphous and crystalline phase is only possible at very low stresses. If the stress exceeds a critical value, strain bursts do not occur as a single event. So they cannot be separated from the deformation of the amorphous phase. In addition, a too high deformation rate in the amorphous phase can make the detection of individual strain bursts impossible. Since strain burst in semi-crystalline polymers cause deformations of several nm, a nm resolution in the deformation measurement is required. The demand on the temperature stability during a measurement is very high. On the one hand temperature fluctuations can influence the strength of the amorphous phase. Otherwise the deformation caused by low thermal fluctuations is, due to the large thermal expansion coefficient of polymers, much higher as the required deformation resolution. For instance in PE-HD (linear expansion coefficient $\alpha = 2 \cdot 10^{-4}$ 1/K) causes a temperature increase of 0.1 °C at a length of 10 mm, a length change of 200 nm. Therefore, a very good temperature stability during the measurement is required. In order to avoid this problem a torsional loading with a pure shear deformation is preferred. In this load case volume changes from

temperature fluctuations do not play a crucial role, since a volume change does not cause torsional deformations. Furthermore a pure shear stress enables the determination of the stress in the sliding plane without additional assumptions/estimations.

6.2. Description of the novel nano-creep test

Many of the required criteria are fulfilled by a torsion measurement with a rheometer. This was the reason for the decision to develop the novel test method for strain bursts on the basis of a torsional rheometer tests. For the development and evaluation of the testing method an Anton Paar rheometer MCR 301 with temperature chamber CCD 600 was available. This rheometer has a torque resolution < 1 μNm and an angular resolution $<$ 1 μrad. Data acquisition with 10 Hz is possible.

6.2.1. Stress distribution

A torsional stress causes a linear stress gradient over the cross section of the sample, zero stress in the center of rotation and maximum stress at the sample surface. In order to obtain a uniform, homogeneous stress distribution within the sample the measurements were carried out with a hollow cylindrical specimen (diameter 5 mm), with a wall thickness of 1 mm (Figure 6.1). Because of the used temperature chamber the total sample height was limited to 50 mm.

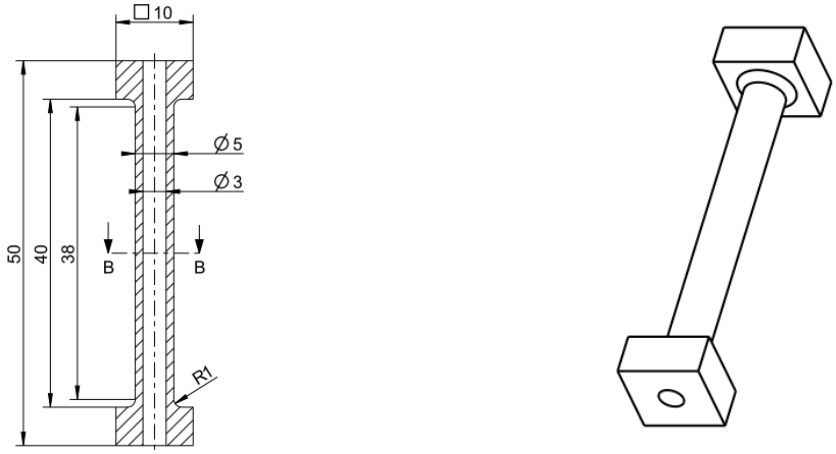

Figure 6.1.: *Sample geometry.*

For a torque of 1 mNm this results in an average shear stress in the cross section of 0.0375 MPa (inner surface 0.0281 MPa, outer surface 0.0468 MPa, Figure 6.2). This stress is significantly smaller than 1 % of yield stress (typical of PE-HD σ_{yield} = 22 - 25 MPa [144]) even if we consider the von Mises yield criterion for pure sheer [47], which is

$$\tau_{yield} = \frac{\sigma_{yield}}{\sqrt{3}} = 12.7 - 14.4\ MPa \tag{6.1}$$

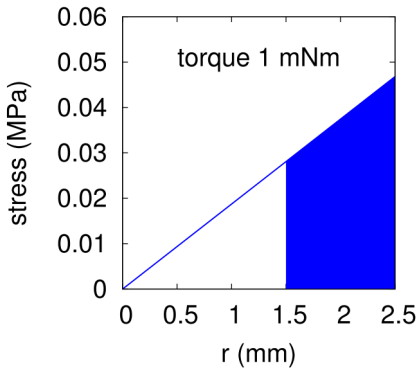

Figure 6.2.: *Stress distribution in the sample cross section (blue area) for a torque of 1 mNm.*

6.2.2. Angular resolution - deformation resolution

The Anton Paar rheometer MCR 301 has an optical incremental encoder for the angle measurement with an internal digital resolution of 0.012 μrad. The current angle position is determined by oversampling (averaging over several measurements).

The measurements have shown that the actual angular resolution φ_{res} is 0.2 μrad. This results in a shear strain resolution γ_{res} (R = 2.5 mm, l = 38 mm) of

$$\gamma_{res} = \frac{R\varphi}{l} = 1.32 \cdot 10^{-8} \tag{6.2}$$

which can be converted to a von Mises equivalent strain ε_{res}^{vM}

$$\varepsilon_{res}^{vM} = \frac{\gamma_{res}}{\sqrt{3}} = 7.62 \cdot 10^{-9} \tag{6.3}$$

With the outer sample diameter D = 5 mm this leads to an absolute deformation resolution b_{res} on the sample surface of

$$b_{res} = D\pi\frac{\varphi}{2\pi} = 0.5\ nm \tag{6.4}$$

This deformation resolution is about three orders of magnitude higher than the best extensometers for tensile tests. The latter have an absolute resolution of about 100 nm

and therefore they are not suitable for the measurement of dislocation mediated strain bursts.

6.2.3. Stability of temperature

In a torsional experiment the temperature control is not so critical, since volume changes caused by temperature fluctuation do not result torsional deformations. At the current measurements the temperature could be kept constant within several 1/100 °C. A control experiment with a temperature oscillation of $\pm$ 2 °C has only influenced the creep rate. No additional strain bursts could be observed. Therefore, the required temperature constancy was set to $\pm$ 0.1 °C, which could be fulfilled without difficulty by the temperature chamber used.

6.2.4. Measuring method - cycling

The measurements of Li and Ngan [89] showed that strain bursts occur relatively rarely. For a reliable evaluation many and long-time measurements are necessary. The mechanical sample preparation of the special rheometer specimens is complicated and thus limits the specimen number. Since the nano-creep experiments were carried out with very low stresses ($<$ 1 % of yield stress), the occurring small deformation is reversible [125] and takes place almost exclusively in the softer amorphous phase, especially for tests above the glass transition temperature. The few strain bursts do not lead to relevant plastic deformation in the crystalline phase. To keep the maximum sample deformation small even in long-time experiments, the measurements were carried out as nano cycling creep experiments. A complete cycle consists of four parts (Figure 6.3). In the first part a constant loading is applied for 33 min in one direction, followed by a 33 min relaxation phase without stress. Then the sample is creep deformed 33 min in the opposite direction and then again relaxed 33 min without loading. With this cyclic procedure the maximum deformation of the sample is limited. Thus, a sample can pass through many cycles without experiencing relevant structural changes.

For a typical test a loading of 1 mNm is applied to a PE-HD sample (Figure 6.4), which leads to a maximum deformation of about 3 mrad. This corresponds to an absolute deformation at the sample surface of b = 7.5 μm or a relative deformation of $\gamma = 1.97 \cdot 10^{-4}$ and $\varepsilon^{vM} = 1.14 \cdot 10^{-4}$, respectively. So numerous and longtime measurements can be carried out with a single sample. This also allows fully automated measurements without any manipulation of the samples. To determine whether the sample gets changes by the measurements, the loading can be varied after each cycle. A non-destructive measurement can be assumed when this randomized loading has no impact on the results.

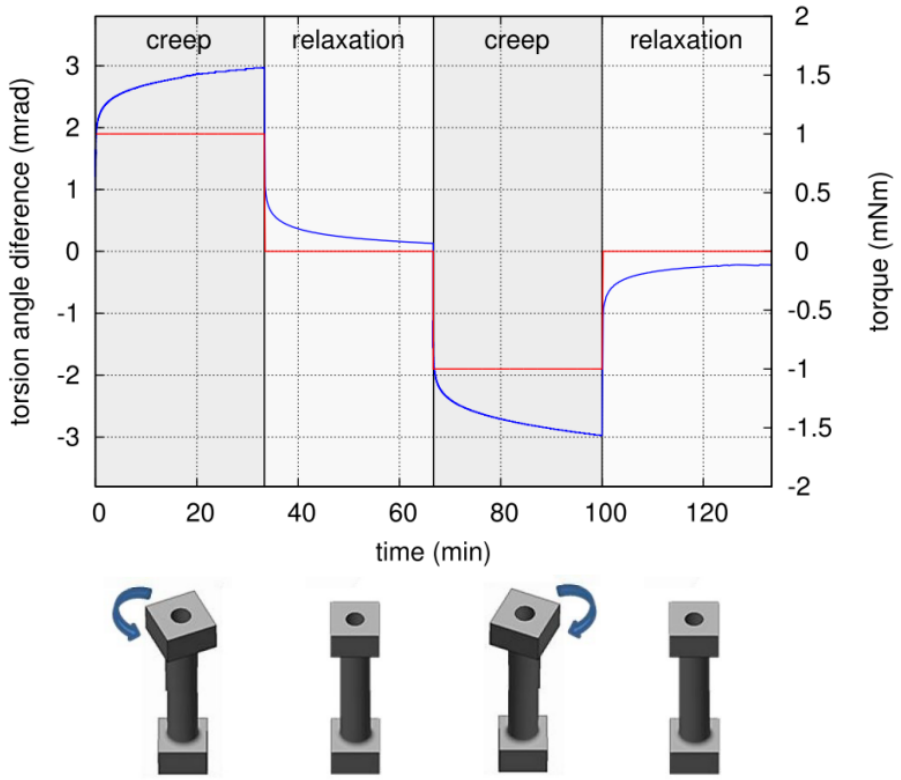

Figure 6.3.: *Torque/Stress (red) and deformation (blue) behaviour during a nano-creep cycle. PEHD sample, torque 1 mNm, temperature 30 °C.*

6.3. Experimental details

The specimens were produced by machining of a compression molded sheet of high density polyethylene Borealis HE 3492 LS-H. This material is classified as a MRS 10.0 material (PE100) with a Young's modulus E = 1100 MPa and a tensile yield stress σ_{yield} = 25 MPa. The crystallinity of the samples was 61 % determined by differential scanning calorimetry (DSC) measurements. To avoid influences due to the mechanical processing, the specimens were annealed after preparation for 4 hours in a furnace at 120 °C.

Preliminary tests have been performed to determine the optimal test conditions. It has been shown that there exists a minimum stress for reasonable experiments. Too little stress results in a very noisy signal that cannot be evaluated. Similar results were also found for nanoindentation creep experiments [91]. In principle, the lower the temperature the larger the necessary minimum stress. On the other hand, higher stress increases the risk for irreversible changes in the micro-structure of the sample. In this undesirable case, a test specimen could be used only for a single measurement. Furthermore, a higher loading results in a larger average creep rate in the amorphous phase, which makes a reliable detection of a strain burst difficult.

Table 6.1 shows the test conditions for the performed isothermal measurements.

temperature	torque	
[°C]	1 mNm	2 mNm
30	x	x
35	x	
40	x	x
45	x	
50	x	x

temperature	torque
[°C]	[mNm]
30	1
	1,5
	2
	2,5
	3
	4

Table 6.1.: *Overview of test conditions.*

In order to detect changes in the specimen caused by the experiments, the measurements were carried out in randomized way. The loading was varied after 5 cycles (10 individual creep measurements). In addition, the measurements were carried out at 30 °C with different specimens. The preliminary tests have shown that for a reasonable, statistically significant analysis at least 80 individual experiments must be carried out. There was also evidence that the clamping of the specimen is critical. Despite of a careful clamping procedure, the results of the first 5 - 10 experiments after clamping were unusual (modified strain burst number and altered creep rate in the amorphous phase). Even with the greatest care a plastic deformation of the specimens (much larger than the actual experiment) could not be prevented. Therefore, the first 10 experiments after a specimen change were not considered for the evaluation.

6.4. Results

For all evaluations only measurement data > 1.5 min after the beginning of the experiment were considered. This ensures a very small average creep rate. Thus the jump height from the creep in the amorous phase is much smaller than the expected jump height of the strain bursts. Figure 6.4 shows the result of a nano-creep experiment (red curve) with a relative high number of strain bursts.

Besides the positive strain bursts (in the direction of the loading), there are also back jumps (negative strain bursts). The green curve shows the torsion angle difference between two measuring points. Potential strain bursts are torsion angle differences between two measuring points which are larger than $\pm$ 0.0015 mrad. This corresponds to approximately $\pm$ 6 times the standard deviation of the normal distribution of the torsion angle differences caused by the creep process in the amorphous phase.

All experiments were analyzed with a self-developed octave evaluation program [145]. The evaluation program determines automatically the occurrence time of the strain burst, the

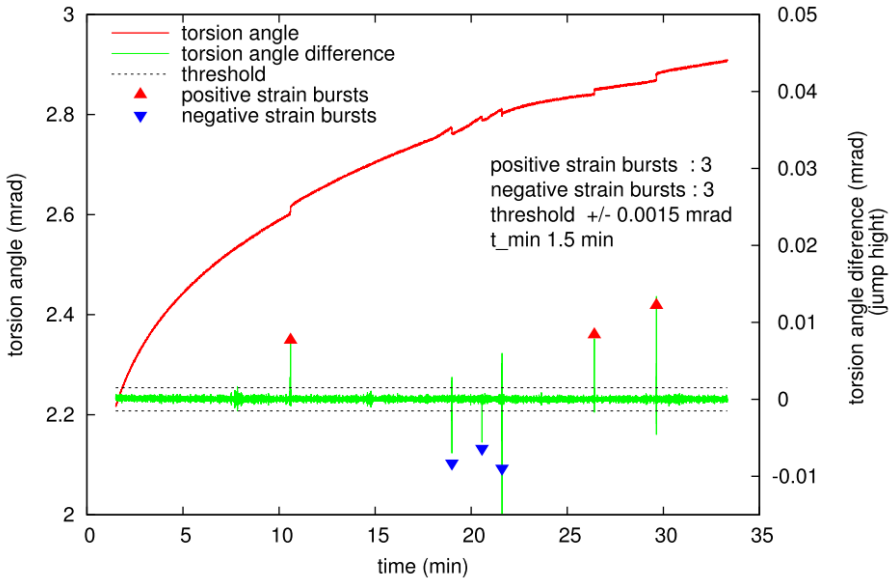

Figure 6.4.: *Nano-creep curve of PE-HD with a static loading of 1 mNm (0.05 MPa on the sample surface, i.e < 1 % of the yield stress) and 30 °C.*

strain burst height (red and blue triangles in Figure 6.4) and the average creep rate of the amorphous phase (= average torsion angle difference between two measuring points).

A key question was whether the specimens are changed by the nano-creep experiments and these results in an impact on the number of strain burst. Therefore, the experiments were carried out randomized (different test conditions for a specimen). To check whether the experiment changes the structure of the specimen (and influences the number of strain bursts), all experiments for a test condition were evaluated separately. This evaluation shows that neither the number of positive nor the number of negative strain bursts changes with multiple use of the specimen (= experiment number, Figure 6.5).

An evaluation of the number of strain bursts depending of their occurring time shows slight tendencies. The number of positive strain bursts decreases slightly with time while the number of negative strain burst increases slightly. However, the decrease/increase is not statistically significant, also due to the strong scattering. But these results were the reason to limit the time for a cycle (= single experiment) to 33 min (Figure 6.6).

For the negative strain bursts it seems that there is a slight increase after about 7 min. This can be explained by the fact that for the back jumps (negative strain bursts) a back stress is necessary witch must be built up in the amorphous phase.

Nevertheless, the results clearly show that the performed nano-creep cycling experiments are a non-destructive test method. Therefore, a specimen can be used for more than one measurements.

Looking at a single strain burst in detail (Figure 6.7a and b), it can be seen that the strain

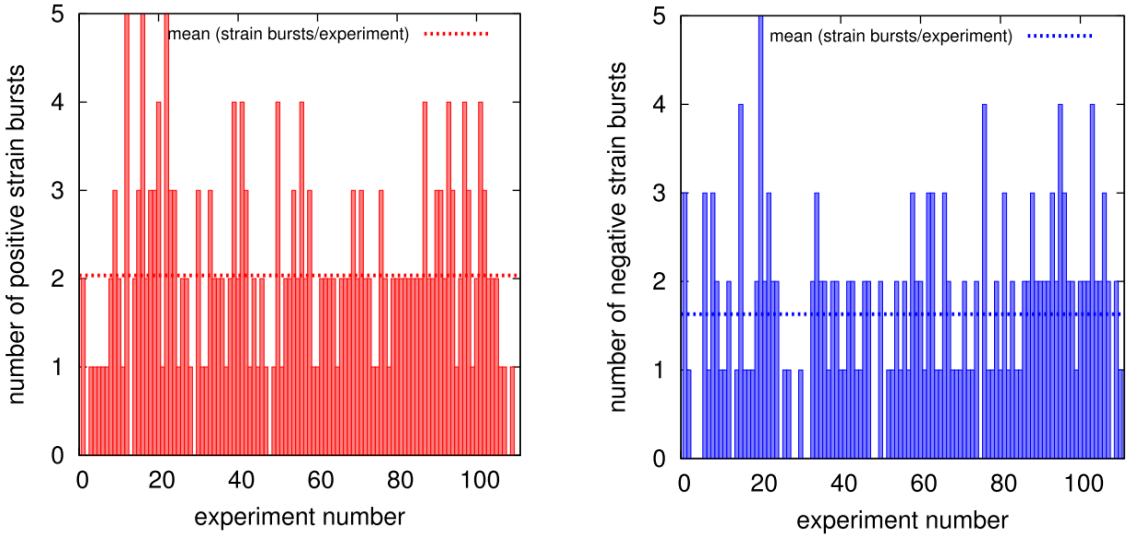

Figure 6.5.: *Distribution of positive (a) and negative (b) strain bursts depending on experiment for torque 1.5 mNm and temperature 30 °C.*

burst height is significantly larger than the angular resolution of the rheometer and the jumps caused by the creep of the amorphous phase. The time for a strain burst is within the time resolution of the measurement (0.1 s).

After a strain burst we observe temporarily a larger scattering of the measuring values as before (= post-oscillation). For some strain bursts this unstable phase lasts for several seconds, and the scattering amplitude of the measurement values is in the order of the strain burst height (Figure 66.7b, strong post-oscillation). Thereby the first 2 - 3 vibrations with the highest amplitude are with a frequency of 2 Hz. Thereafter, the amplitude decreases and the frequency increases to about 5 Hz and is then comparable to the amplitude and frequency of the low post-oscillations (Figure 6.7a).

A finite element modal analysis has revealed that the resonance frequency of a rotational vibration of the specimen is bejond 1000 Hz. Therefore, a self-oscillation of the specimen as origin of the post-oscillations is unlikely. Also as known from strain bursts in metals, emission of sound waves [146] cannot be the cause due to the extremely small frequency. One possible explanation for the post-oscillations is that dislocation avalanches cause large local deformations in a crystal lamella. The surrounding amorphous phase or the interface (rigid amorphous phase) would thereby limit the rate of deformation. Since dislocations move by the order of the speed of sound [3] the local deformation rate is high which leads to relatively stiff amorphous phase even over the glass transition temperature. This may cause strong local restoring forces (back stresses) which finally effects the post-oscillations. A strong indication of the fundamental possibility of local back deformations are the negative strain bursts.

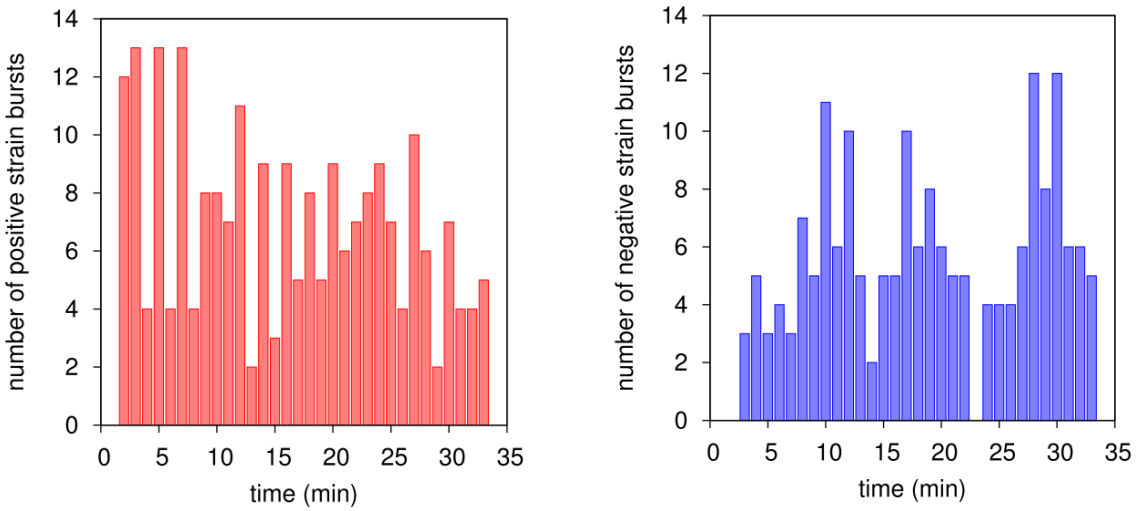

Figure 6.6.: *Distribution of positive (a) and negative (b) strain bursts depending on time, torque 1.5 mNm, temperature 30 °C.*

In order to evaluate the height of a strain bursts the measuring points prior and after the strain burst were fitted by a straight line (blue lines in Figure 6.7). The jump height of the strain bursts was then evaluated as the difference of the lines at the first major torsion angle difference (black arrows in Figure 6.7).

Over several experiments, the number of negative strain bursts is always lower than the number of positive strain bursts. Their characteristics is a mirror image of the positive strain bursts. Before some negative strain bursts there a significant increase of the creep rate of the amorphous phase is observed (Figure 6.8). It is noteworthy that the macroscopic creep of the amorphous phase (green doted line in Figure 6.8) is not affected through this short-term increase in the creep rate, therefore it is probably a local effect.

To ensure that the strain bursts are not an artefact of the rheometer, measurements with a metal (silver steel wire, diameter 3 mm) and with an amorphous rigid polyvinyl chloride (PVC) sample were carried out. Neither with the metal sample nor with the PVC sample strain bursts could be detected.

In order to get statistically valid results for each test condition (temperature, stress) at least 80 nano-creep experiments were performed. In Figure 6.9, the results of such statistical analysis for all experiments with 1.5 mNm at a temperature of 30 °C are plotted as a frequency distribution.

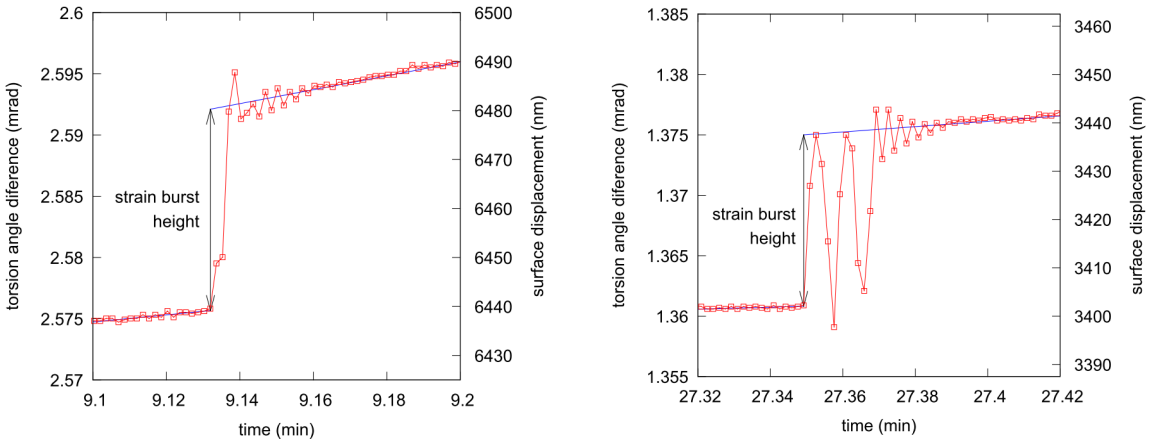

(a) (b)

Figure 6.7.: *Different types of strain bursts.*
(a) Strain burst with low post-oscillation (PE-HD, static loading 1mNm, 0.05 MPa on the sample surface and 30 °C).
(b) Strain burst with strong post-oscillation (PE-HD, static loading 0.5 mNm, 0.025 MPa on the sample surface and 30 °C).

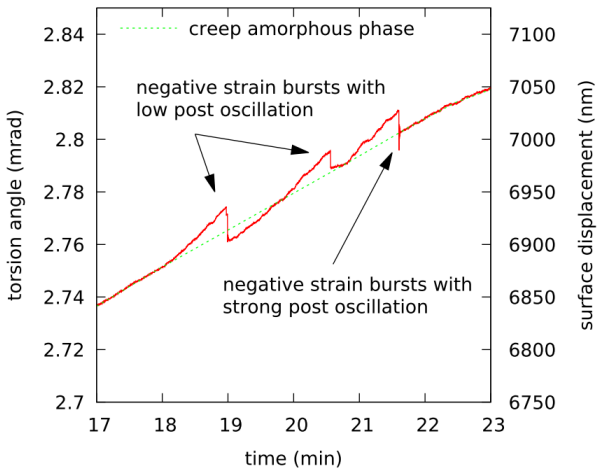

Figure 6.8.: *Negative strain bursts with increased creep rate before the strain burst (PE-HD, static loading 1 mNm, 0.05 MPa on the sample surface and 30 °C.*

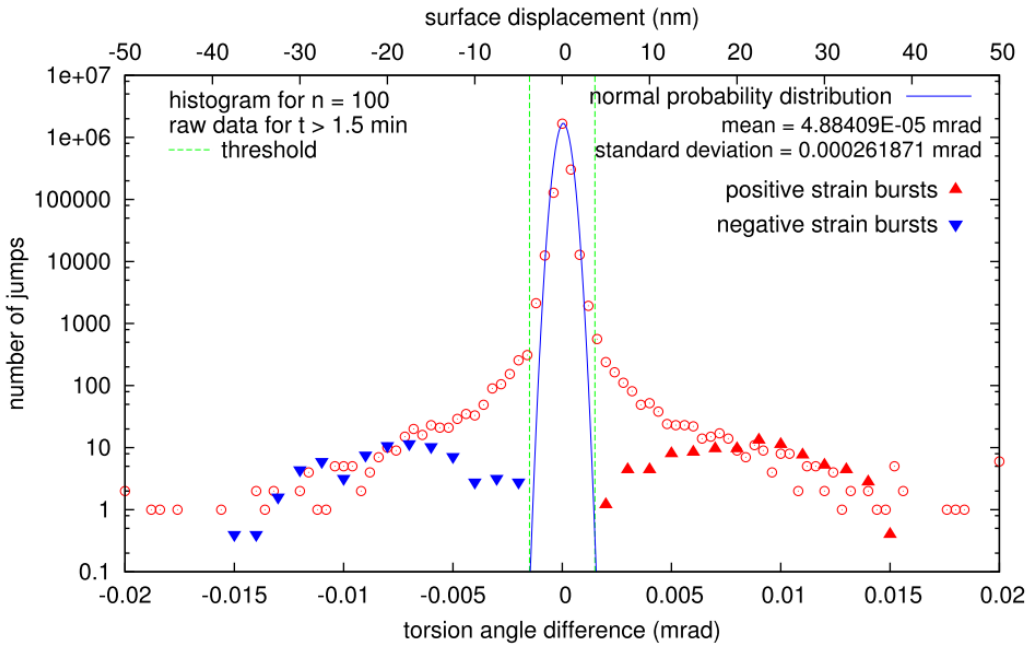

Figure 6.9.: *Frequency distribution of all torsion angle differences between 2 measuring points, torque 1.5 mNm, temperature 30 °C. The red circles correspond to all measured torsion angle differences (raw data) and the triangles to the separately evaluated strain bursts.*

One has to distinguish between the torsion angle differences between two measuring points (red circles in Figure 6.9) and the actual strain bursts (red and blue triangles in Figure 6.9). A major part of the torsion angle differences (approximately $2 \cdot 10^6$) are a consequence of the continuous creep process in the amorphous phase. This torsion angle differences show a normal distribution (blue curve in Figure 6.9) and scatter around 0 with a very small positive average value corresponding to the average creep rate of the amorphous phase. The unusual shape of the normal distribution curve results from the the logarithmic scaled y-axis. The green dotted line corresponds to $\pm$ 6 times the standard deviation of the calculated normal distribution. Values outside this limit are highly significant for another deformation process and thus allow the proper separation of the creep deformation of the amorphous phase. These much larger torsion angle differences can be separated into two groups. On the one hand into the strain bursts (red and blue triangles) and into an other part which originates from the post-oscillations after a strain burst (= range between red and blue triangles and red circles).

The creep rate in the amorphous phase increases linearly with the loading (torque proportional to stress) (Figure 6.10) and is consistent with literature values of short time creep experiments with PE-HD at higher stresses [147].

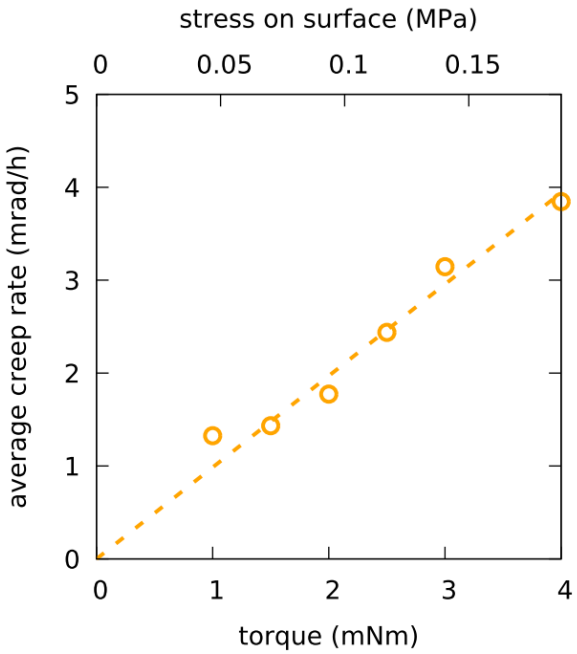

Figure 6.10.: *Dependence of the average creep rate of the amorphous phase on loading (torque).*

6.5. Discussion

So far mechanical experiments in the micro-strain region were hardly performed on polymers [148]. Reasons are that commercially available strain gauge systems do not have the required high resolution and there are very high demands on the temperature control during the experiment due to the large thermal expansion coefficient. One exception are the cyclic tensile tests of Brown and Rabinowitz [113] on PE-HD with constant strain rate. They could separate the deformation in 3 parts

- elastic strain associated with stretching of van der Waals bonds
- amorphous flow that varies as σ^2 and is activated at zero stress
- dislocation motion that varies as $\sigma^{3/2}$ and is activated at 0.18 MPa

Since the current nano-creep experiments were performed at a constant stress and not a constant strain rate, the results are not directly comparable. But it turns out that the amorphous flow in the nano-creep experiments is also activated with practically zero stress. However, the stress dependence of the amorphous flow is linear (Figure 6.10). Furthermore, strain bursts (= dislocation motion and plastic deformation in the crystalline phase) could be identified in the nano-creep experiments already at stresses of 0.05 MPa (Figure 6.4) which is 1/3 of the stress measured by Brown and Rabinowitz.

The deformation takes place mainly in the amorphous phase at small loadings, since the stiffness of the amorphous and crystalline phases above T_g is extremely different. Due to the experimental setup, a reliable detection of any strain burst in the first 1.5 min after after applying the loading is not possible. In this range of the experiment a relatively high creep rate in the amorphous phase is observed and a proof of strain bursts is therefore difficult. During these first 1.5 min locally significantly higher stresses in the interface (rigid amorphous phase) and in the crystalline phase can be build up through molecular entanglement in the amorphous phase and tie molecules. Therefore, when the first strain bursts are detected, it must be assumed that the stress distribution is no longer homogeneous, and locally higher stresses can act in the crystalline phase. Nevertheless it is remarkable that the plastic deformation can occur in the crystalline phase at macroscopic stresses lower than 1 % of the yield stress.

6.5.1. Strain bursts characteristics: jump height and deformed volume

If we consider the frequency distribution of the strain bursts, it is remarkable that the jump height of the strain bursts (maximum deformation of the sample surface) is of the order of the lamella thickness. In Figure 6.11, the frequency distribution of the strain bursts is compared with the lamella thickness distribution determined from DSC measurements (dashed red line). This lamella thickness distribution shows an average lamella thickness of 18 nm. The frequency distribution of the evaluated strain bursts has a maximum at a corresponding deformation angle of 0.009 mrad (equivalent to 22.5 nm deformation at the sample surface) of the positive strain bursts and 0.007 mrad (equivalent to 17.5 nm at the sample surface) of the negative strain bursts. Thus it seems that the majority of strain bursts have a height in the range of the average lamella thickness. But one has to consider that the shear strain and the absolute deformation increases with the radius. The deformation at the inner surface of the sample is about 40 % smaller than at the outer surface. Therefore, the deformation at the outer sample surface is an upper limit for the actual deformation in the sample.

Since only the crystalline phase is deformed in case of a strain burst, the question arises how large is the volume actually deformed by a single strain burst. The measured deformation is always the total deformation of the sample. A single strain bust leads to an overall deformation of about 20 nm on the sample surface. This corresponds to a deformation of $\gamma = 5.26 \cdot 10^{-7}$ or $\gamma^{vM} = 3.04 \cdot 10^{-7}$. With the Burgers vector b = 0.254 nm and an average lamella thickness λ = 18 nm (as an estimation for the path length) the apparent mobile dislocation density $\rho_{mobile}^{apparent}$ for a single strain burst results to [57]

$$\rho_{mobile}^{apparent} = \frac{\gamma^{vM}}{b\lambda} = 6.64 \cdot 10^{10}\ m^{-2} \tag{6.5}$$

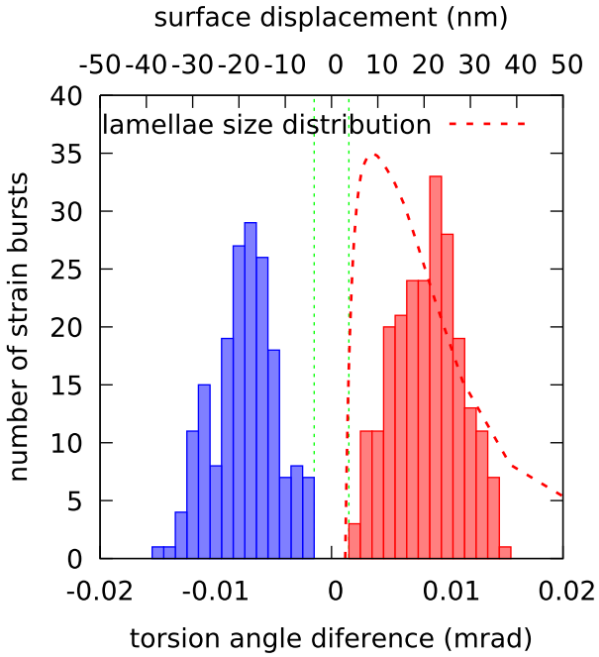

Figure 6.11.: *Histogram of evaluated strain bursts, torque 1.5 mNm, temperature 30 °C.*

This dislocation density is very small compared to the measured dislocation densities in polypropylene (chapter 4 and 5). However, one must be aware that in the present measurements the strain bursts are caused by dislocation avalanches which are limited to very small sample areas (only lamellae). Therefore, the local deformation in the area where dislocation avalanches occur, is substantially larger than the measured macroscopic one. Knowing the necessary mobile dislocation density of plastic deformation, the locally deformed volume by a strain burst can be estimated. The plastic deformation of a macroscopic PE-HD sample typically starts in the order of $\varepsilon_{yield} = 0.1$ [144], so the necessary mobile dislocation density can be estimated with equation 6.5 to $\rho_{mobile}^{plasticdeformation} = 2.2 \cdot 10^{16}$ m^{-2}.

A further possibility is the estimation of the total dislocation density for plastic deformation with the equation of Taylor [149]

$$\tau = \alpha G b \sqrt{\rho_{total}} \tag{6.6}$$

$$\rho_{total} = \left(\frac{\tau}{\alpha G b}\right)^2 = 3.3 \cdot 10^{16}\ m^{-2} \tag{6.7}$$

Here, for τ the critical resolved shear stress $\tau_{crss} = 7.5$ MPa for PE-HD with the preferred (100)[001] chain slip system at room temperature [46] have been inserted. Since the bonding in polymer crystals is highly anisotropic, the shear modulus G must be replaced by an effective crystal shear modulus. The shear modulus for slip in chain direction will be either $c_{44} = 3.19$ GPa or $c_{55} = 1.62$ GPa [150] depending upon whether the slip plane is

(010) or (100). Therefore G = 1.62 GPa was chosen. α is a parameter that varies between 0.1 and 1.0 depending on the type of dislocations involved [57]. Since the nucleation of screw dislocations is dominant in polyethylene during plastic deformation [23, 62] and a screw dislocation pile up is unlikely, a value of 0.1 was chosen for the present estimation.

This confirms the above estimation that for the plastic deformation of PE-HD a mobile dislocation density $\rho_{mobile}^{plasticdeformation} = 2.2 \cdot 10^{16}$ m^{-2} is necessary. However, this value is by a factor of 10 higher than dislocation densities measured in polypropylene during plastic deformation (chapter 5).

So the deformed volume by dislocation avalanches $V_{avalanches}$ ($V_{spesimen}^{deformed}$ = 477 mm^3) can be estimated with

$$V_{avalanches} = V_{spesimen}^{deformed} \frac{\rho_{mobile}^{apparent}}{\rho_{mobile}^{plasticdeformation}} = 0.00144\ mm^3 \tag{6.8}$$

This corresponds to a cube with an edge length of about 113 μm.

6.5.2. Activation energy

The number of strain bursts depends on the loading and temperature. The loading dependence has a pronounced maximum with a linear increase before and a linear decrease after the maximum (Figure 6.12a). A similar dependence was already proven by extensive nanoindentation creep experiments [91].

Regarding the temperature dependence of the strain bursts, it is interesting that the typical behaviour of a thermally activated process (Figure 6.12 b) was only observed for very small loadings (1 mNm, 0.05 MPa) and temperatures below 50 °C. At high temperatures and/or high loadings (but still $<$ 1 % of yield stress), the behaviour changes dramatically. The number of strain burst decreases with increasing temperature.

The creep rate in the amorphous phase according to Eyring [87] is

$$\frac{\mathrm{d}\varepsilon}{\mathrm{d}t} = \dot{\varepsilon} = \dot{\varepsilon_0} e^{-\frac{\Delta H}{k_B T}} sinh\left(\frac{\nu\sigma}{RT}\right) \tag{6.9}$$

with $\dot{\varepsilon_0}$ being the constant pre-exponential factor, ΔH the potential energy barrier, T the temperature, k_B the Boltzmann constant, ν the activation volume for the molecular event, σ the stress and R the ideal gas constant.

With the measured average creep rates in the amorphous phase (Figure 6.13a) and equation 6.9, one obtains for the creep process in the amorphous phase an activation energy ΔH = 0.31 eV and an activation volume ν = 1 nm^3. Literature values range from 0.23

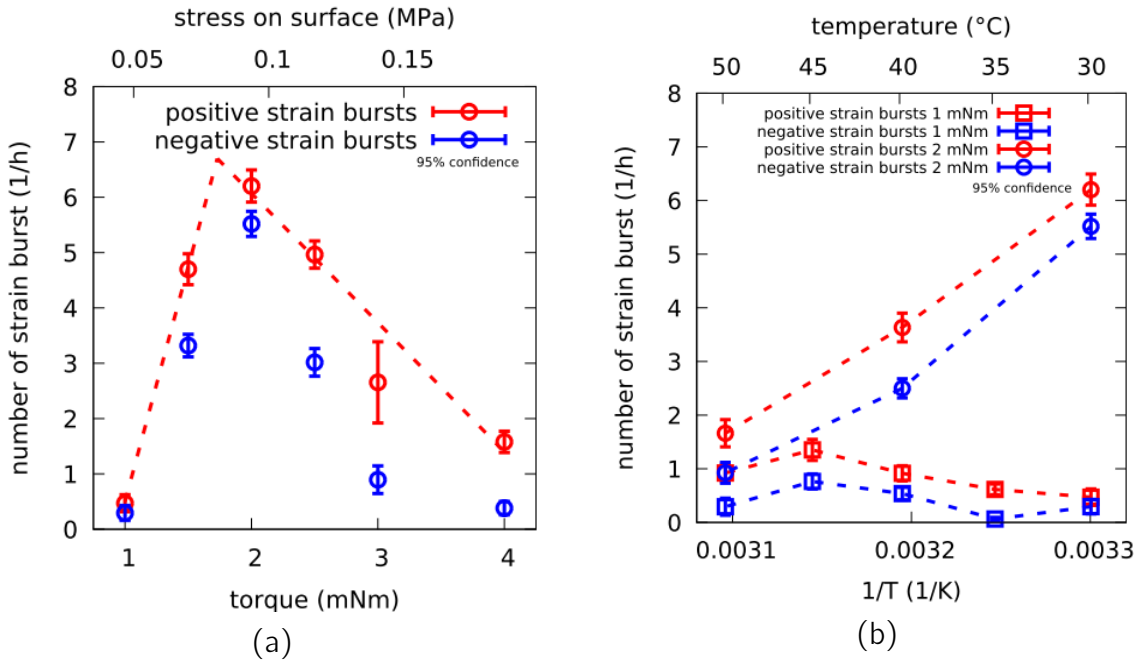

Figure 6.12.: *Number of strain bursts depending on torque (a) and temperature (b).*

eV with an activation volume $\nu \sim 2$ nm^3 for oriented PE-HD films [151] to 0.53 eV in experiments with small stress extrapolated to zero stress [152].

The activation energy for the generation of strain bursts was determined with a classical Arrhenius evaluation [153]

$$In(n) = In(A) - \frac{E_A}{R}\frac{1}{T} \tag{6.10}$$

with E_A being the activation energy, n the number of strain bursts and A the pre-exponential factor. This results in a activation energy of positive strain bursts $E_A = 0.59$ eV (Figure 6.13b), which is twice the measured activation energy of the creep process of the amorphous phase. In their nanoindentation creep experiments Li and Ngan found an activation energy of 0.22 eV for the strain bursts [89]. This value is even lower than the activation energy for creep of the amorphous phase and is therefore not realistic. Current nanoindentation creep experiments of Zare Ghomsheh et.al. [92], show that the activation energy for strain bursts in PE-HD is significantly higher. They found an activation energy of 0.64 eV which confirms the present results.

6.5.3. Stress and temperature dependence of strain bursts

It has been shown that strain bursts in nano-creep experiments occur only in a relatively small experimental window. With increasing stress, a maximum number of strain bursts

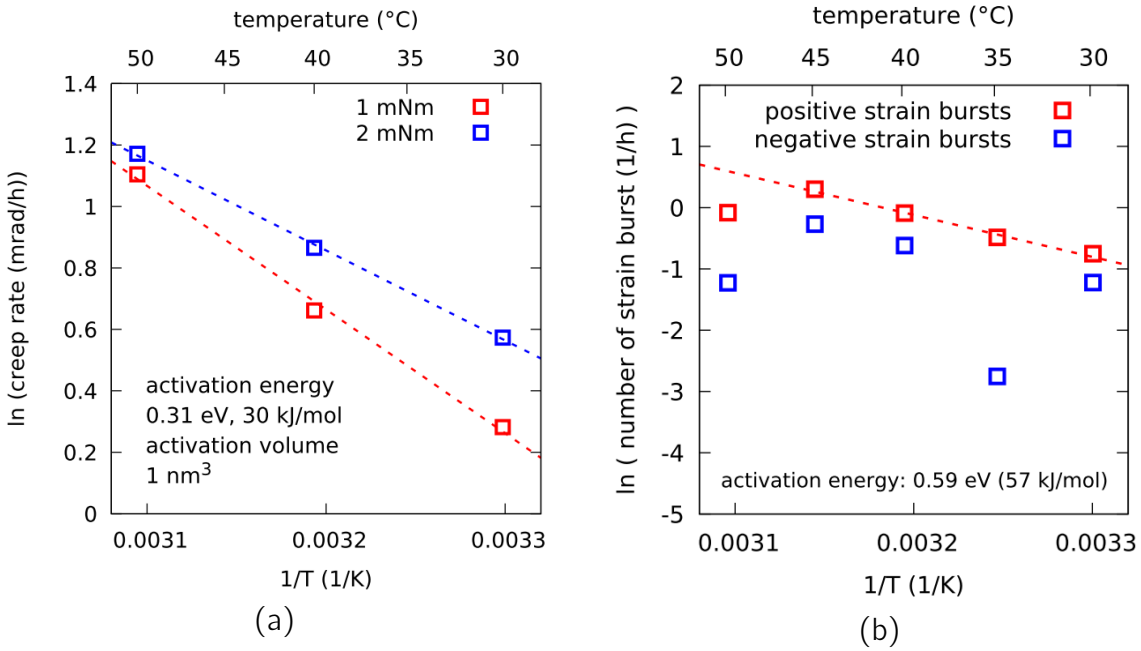

Figure 6.13.: *Arrhenius evaluation of actication energy for*
(a) amorphous creep, torque 1 and 2 mNm (stress 0.05 MPa/0.1 MPa on the sample surface),
(b) strain bursts, torque 1 mNm (stress 0.05 MPa on the sample surface).

is reached followed by a strong decrease (Figure 6.13b). One possible explanation is that the thermal activation of dislocations in the crystalline phase does not occur at all or only at a very limited way. This would mean a strengthening of the crystalline phase or of the interface (rigid amorphous phase) where the dislocations are generated. Such a strengthening of the interface could be explained by the larger deformation rate of the amorphous phase caused by the higher stress. It is more likely that the deformation in the crystalline phase is no longer caused by only local and limited dislocation avalanches and the deformation in the crystalline phase now occurs in a more homogeneous way (transition from coarse to fine slip). Therefore the deformation in the crystalline phase is no longer jerky and cannot be separated from the deformation of the amorphous phase. This is similar to the disappearance of strain bursts in metallic single crystals, where with increasing sample size, the jump height of the strain bursts decreases and the macroscopic deformation becomes smoother.

It is worth mentioning that at a loading of 1 mNm (stress 0.05 MPa on the sample surface) in the temperature range 30 - 40 °C we observe a typical Arrhenius behaviour, while at 2 mNm (stress 0.1 MPa on the sample surface) this is no longer the case (Figure 6.12b). This is an indication that there is a change of the deformation process. I.e. the thermal activation of the dislocations is no longer the rate controlling mechanism.

At a temperature of 50 °C with a loading of 1 mNm (stress 0.05 MPa on the sample

surface) also a change in the behaviour of the material occures. The number of strain bursts decreases, contrary to the Arrhenius behaviour (Figure 6.12 b). This temperature-dependent change in the behaviour is correlated with the alpha transition in PE-HD [17, 154, 155]. From polypropylene it is known that the dislocations annihilate in the area of the alpha transition and thus the dislocation density decreases strongly [84] which causes a decrease of the probability of dislocation avalanches.

6.5.4. Negative strain bursts

Surprisingly negative strain bursts occur in the nano-creep experiments. Negative strain bursts could not be observed in the nanoindentation creep experiments on PE-HD and are unknown in metals at all. Their behaviour is equal to the positive strain bursts with the difference that they occur less often (at least at the beginning of deformation) and only after a certain deformation. Basically, the deformation in semi-crystalline polymer is very inhomogeneous, since the two phases, especially above the glass transition temperature, have an extremely different strength. This may result in a locally more deformed amorphous phase than the crystalline one. Through entanglements and tie molecules this can lead to locally much higher stresses, which may also be directed against the loading direction (back stresses). This is also reflected in the strong recovery behaviour with increasing temperature of plastically deformed polymers [20, 125]. Such a back stress can obviously cause back deformations in the crystalline phase which manifest as negative strain bursts.

6.5.5. Line energies

With the calculations of Shadrake & Guiu for the line energy of a <001> screw dislocation in a polyethylene crystal $\mu b^2 = 9.59 \cdot 10^{-11} - 1.51 \cdot 10^{-10}$ J/m [59] the energy to generate a screw dislocation in a polyethylene lamella crystal with a thickness λ = 18 nm can be estimated as (outer cut off radius $R_0 = \lambda$, inner cut off radius $r_0 = b = 0.254$ nm, neglecting the elastic energy of the dislocation core).

$$E^{\perp} = \frac{\mu b^2}{4\pi} ln \left(\frac{R_0}{r_0} \right) \lambda = 1.5 - 2.6\ eV \tag{6.11}$$

Correctly, instead of the lamella thickness λ the stem length should be used and the equation is only valid in a limited temperature range [19]. But this point is irrelevant for an estimation of the magnitude of the line energy.

The, with equation 6.11 calculated, value for $E^{\perp}$ is much higher than the activation energy for the strain bursts (= dislocation movement) measured with nano-creep experiments. This supports the assumption that only the dislocation mobilisation can be thermally activated. To generate new dislocations an increased shear stress is necessary. Dislocation

density measurements on polypropylene (chapter 4 and 5) have shown that already undeformed samples have high dislocation densities ($\sim 10^{15}$ m^{-2}). Therefore, at least at low loadings, only the Peierls stress must be achieved for a plastic deformation. A significant increase in the dislocation density in compression tests occurs only at deformations $\varepsilon > 0.1$ and thus only after exceeding the yield stress. In both materials polypropylene (chapter 4 and 5) and PE-HD [156] the dislocation density increases significantly with increasing deformation.

6.5.6. Timing of strain burst after plastic pre-deformation

Another amazing observation concerns the timing of the strain bursts. In the standard nano-creep experiments the number of strain bursts is time independent (Figure 6.5). However, if the specimens are plastically deformed before the nano-creep experiment, a characteristic time sequence of the strain bursts can be observed. The larger the temporal distance from the pre-deformation, the more rarely the strain bursts occur (Figure 6.14).

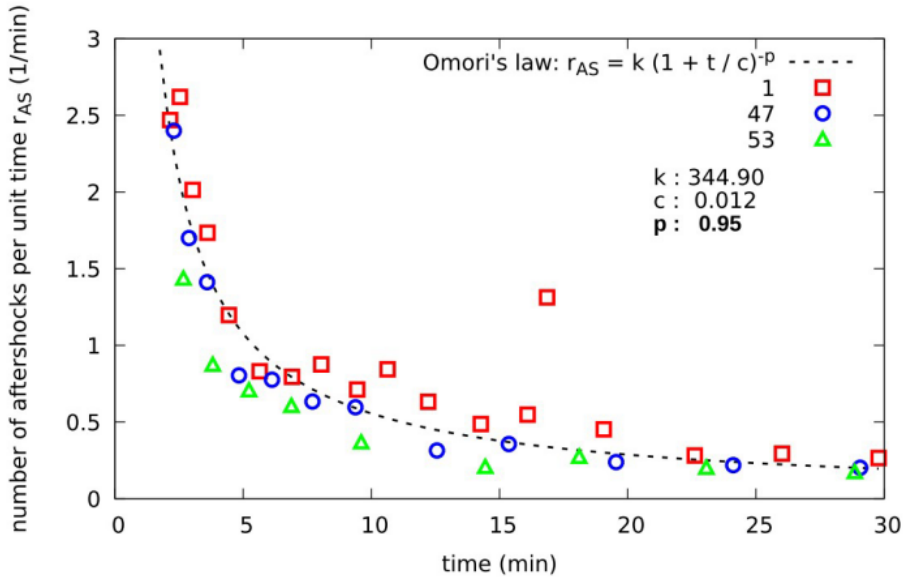

Figure 6.14.: *Number of aftershocks per unit time r_{AS} as a function of time distance t to to the main shock (= plastic pre-deformation at the begin of the creep experiment) load 1 mNm at 35 °C.*

After approximately 30 minutes, an equilibrium is obtained that corresponds to the level without plastic pre-deformation. Thereby the time behaviour of strain bursts after plastic pre-deformation follows Omori's law and is independent of the applied stress. Omori's law [157, 158] describes the number of aftershocks depending on the time after the main shock. Usually the modified version of Utsu [159] is used

$$a_{rs} = \frac{k}{\left(1 + \frac{t}{c}\right)^p} \tag{6.12}$$

where a_{rs} is the number of aftershocks per unit time, k and c are scaling factors, t is the time distance to the main shock and p modifies the decay rate.

For earthquakes the number of aftershocks is also independent of the magnitude of the main shock. Interestingly, the coefficient $p = 0.95$ for the strain bursts is in the same range as for standard earthquakes (typical $p = 0.75 \ldots 1.5$). It can be concluded that defects for deformation processes from km to nm scale play a decisive role and maybe follow the same physical laws.

6.6. Conclusions and summary

A new method for the investigation of the kinetics of dislocations in semi-crystalline polymers would be introduced. By means of the novel experimental setup via a torsion loading all the main disadvantages of nanoindentation creep experiment could be avoided. In addition, this also minimizes possible influences caused by temperature fluctuations. The use of hollow-cylinder specimens also results in a rather constant stress distribution over the cross section of the specimens. As a result, the activation energy for the dislocation movement could be determined with higher reliability compared to nanoindentation creep experiments.

By the cyclic execution of the nano-creep experiment the maximum deformation of the sample could be limited. Thereby, a sample can pass through many cycles without experiencing relevant structural changes and a specimen can be used for multiple measurements. The results clearly show that the performed nano-creep cycling experiment is a non-destructive test method.

A very surprising result was the appearance of negative strain bursts which could never be observed in other experiments and/or materials. This clearly shows that in the semi-crystalline polymers the interplay of two phases with very different mechanical properties causes complex and locally fluctuating stresses during deformation. This is the prerequisite for the formation of local forces, oppose to the macroscopic loading direction (back-stresses), which causes the negative strain bursts. This also shows that the amorphous phase above the glass transition temperature also affects the processes in the crystalline phase. It must be taken into account that the nano-creep experiments have been carried out with stresses < 1 % of yield stress, and thus the amorphous phase has not undergone any substantial changes such as orientations.

A further phenomenon, unknown with other experiments and/or materials, are the post-oscillations after a strain burst. In contrast to the strain burst observed in metals during

the deformation of very small single crystals, the lamellae (= single crystals) in the semi-crystalline polymers are surrounded via an interphase (rigid amorphous phase) by the amorphous phase. Since a strain burst is caused by dislocation avalanches, there are locally very large deformations which the surrounding amorphous phase must take part. Depending on the stiffness (viscosity) of the amorphous phase, it acts more as a damper (at low viscosity or slow strain rate) or more as a spring (at higher viscosity or high strain rate). If there is a large back deformation, as in the case of strong post-oscillations, the spring characteristics prevails. In the current example (Figure 6.7), the strong post-oscillations after a strain burst occur after relative long creep. Thus, one can assume that the amorphous phase is locally more stretched and stiffer, which reinforces the spring characteristics. For an exact clarification, however further specific experiments are necessary. By lowering the temperature closer to the glass transition temperature, the amorphous phase could be stiffened. This should increase the number of strain bursts with strong post-oscillations.

The total deformation of the sample surface during a single strain burst is in the order of magnitude of the lamellar thickness. One must assume that a single strain burst does not deform the whole sample homogeneously and the deformation is very localized. An estimation of the necessary mobile dislocation for the plastic deformation results in a deformed volume of approximately 113 μm^3 for a single strain burst. This shows that a strain burst is produced by the simultaneous plastic deformation of a very large number of lamellae and thus can cause considerable larger local deformations than the macroscopic one. This also explains why strong local back-stresses can arise, which can cause strong post-oscillations. The temporal sequence of the post-oscillations shows that this is a strain burst like deformation. The individual post-oscillations occur in a time interval ($\sim$ 0.1 s) comparable to that of the triggering strain burst.

Another unexpected result of the nano-creep experiments is that both the loading and the temperature can change the characteristics of the deformation process in the crystalline phase. For small loadings, a classical thermally activated process with an activation energy of 0.59 eV could be found up to a temperature of 45 °C. For higher temperatures as well as higher loadings (static loading > 2 mNm, σ > 0.1 MPa but still < 1 % yield stress) the behaviour changes (Figure 6.12). Instead of the expected increase of strain bursts with increasing temperature, the number of starin busts decreases with T (= increase with $1/T$). This means that either a non-thermally activated process becomes dominant, or that the deformation of the crystalline phase no longer proceeds jerkily via dislocation avalanches but more homogeneously (transition from coarse to fine slip). As a result, the deformations of the two phases can no longer be separated.

An additional question is, why strain bursts occur at such extreme low loadings (σ < 1 % of yield stress), since they represents the plastic deformation of the crystalline phase. One possible cause is the very small strain rate $\dot{\varepsilon}^{vM}$. Taking the average creep rate of the amorphous phase (Figure 6.10) with $\dot{\gamma} \sim 2$ mrad/h = $5.55 \cdot 10^{-7}$ rad/s as the macroscopic strain rate, then follows

$$\dot{\varepsilon}^{vM} = \frac{\dot{\gamma}}{\sqrt{3}} = 3.2 \cdot 10^{-7}\, s^{-1} \tag{6.13}$$

At these extremely small strain rates, which are corresponding to very small frequencies in mechanical spectroscopy, the relaxation processes are shifted to substantially lower temperatures. So the α-process can be shifted to temperatures less than the ambient temperature (Figure 6.15).

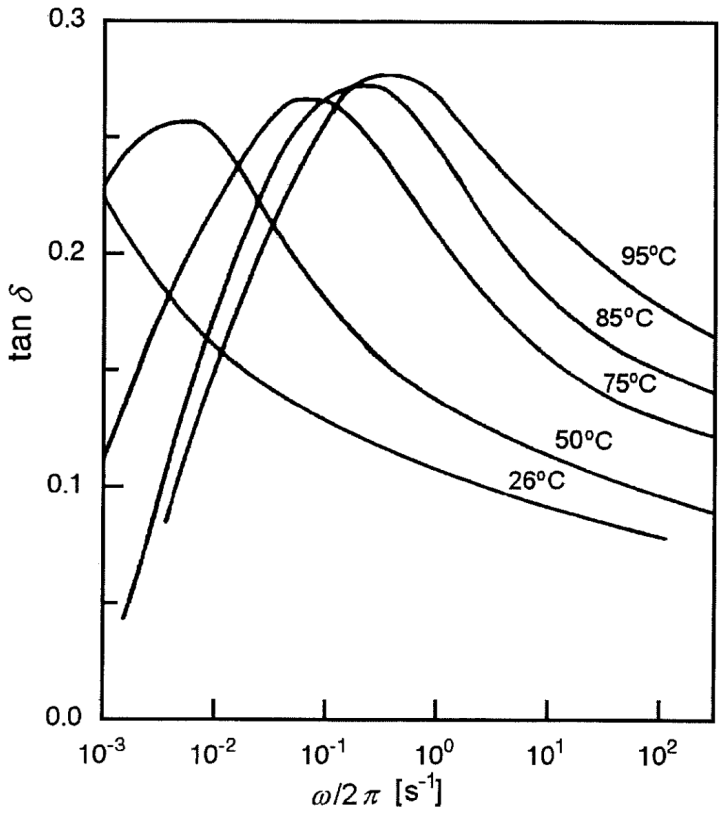

Figure 6.15.: *Loss tangent of mechanical α-process in PE-LD. From* [31].

The α-process in polyethylene is connected with additional translational mobility in the crystalline phase [160]. This is equivalent to a softening of the crystalline phase and therefore allows the plastic deformation of the lamellae to occur even at very small loadings.

The results suggest that at low stresses (as in nano-creep experiments) the plasticity in the crystalline phase is mainly influenced by the mobility of dislocations because sufficient thermally activated dislocations exist to allow localized deformations of lamella crystals (strain bursts caused by dislocation avalanches). But for a plastic flow of macroscopic samples (yield behaviour) the number of these thermally activated dislocations is too low and additional dislocations must be mechanically generated. Therefore the dislocation generation is crucial for the mechanical behaviour.

Part IV.

Summary and Outlook

7. Summary

At the beginning of this dissertation in 2001 the knowledge about dislocations in semi-crystalline polymers was relatively low, since methods for the analysis of dislocations were rarely. Although the existence of dislocations in semi-crystalline polymers is known from single crystals for a long time, the proof in samples crystallized from the melt was not possible at that time. Nevertheless the importance of dislocations for plastic deformation was generally accepted. With Young's dislocation model from 1974 it was possible to describe the plasticity of many semi-crystalline polymers realistically and this model was confirmed several times by experiments.

In order to improve the knowledge about dislocation in semi-crystalline polymers and to enable to study the significance for the plasticity the dissertation pursued two main objectives.

- Proof of dislocations and reliable measurement of dislocation density by X-ray diffraction.
- Investigation of the dislocation kinetics by a novel nano creep test.

7.1. Proof of dislocations by X-ray diffraction

For the proof of dislocations in semi-crystalline polymers by X-ray diffraction the MXPA, a novel method for dislocation analysis in metals, has been combined with the modified Williamson-Hall analysis. With the modified Williamson-Hall analysis, start values for the MXPA could be determined and the number of fit parameters for the MXPA reduced. This enabled the successful application of the MXPA to polypropylene for the first time (chapter 4). In a second step, the modified Williamson-Hall analysis was extended by additional constraints to limit the degree of freedom at the determination of the start values for the MXPA. Thus the quality of the start values for the MXPA could be improved. As a result, the effort for a MXPA was clearly reduced and the quality and reliability of the results could be significantly improved. By means of synchrotron radiation the dislocation density and the crystallite size (CSD size) could be determined in an in situ experiment during cyclic deformation (chapter 5).

Thereby it was possible to prove dislocations in melt-crystallized polypropylene and to measure the dislocation density as a function of the deformation. It could be shown that

in PP with increasing plastic deformation the dislocation density increases by about one order of magnitude. Thereby the distinct increase in the dislocation density originates from crystallographic slip processes which are accompanied by dislocation generation and motion which confirms Youngs's dislocation model for the description of plasticity in PP. It has been shown that the dislocation density in undeformed polypropylene is 10^{15} m^{-2}. If the plastic deformation exceeds $\varepsilon \sim 25$ %, the dislocation density increases up to one order of magnitude. The increase at deformations far beyond the yield point ($\varepsilon > \varepsilon_y \sim$ 10 %) shows that there is a sufficient number of dislocations and these have only to be mobilized.

The dislocations annihilate during unloading and the dislocation density decreases to the level of the undeformed sample. This clearly shows that for the determination of the dislocation density as a function of the deformation, in situ experiments have to be carried out. Only after a deformation $\varepsilon_{total} > 45$ % is there no longer a complete annihilation of the newly generated dislocations. It can be assumed that during the unloading the dislocation density decreases at least by a factor of 10, but not below the level of the undeformed sample. Thereby the annihilation of the dislocations depends on the molecular mobility in the amorphous and crystalline phase.

In principle, it can be summarized that in suitable semi-crystalline polymers the combination of the modified Williamson-Hall analysis with the MXPA can reliably determine the dislocation density and the crystallite size (CSD size). The evaluation process could be considerable shortened and the reliability of the results significantly improved. But further optimizations regarding the automatisation of the evaluation procedure are desirable. The evaluation procedure, developed in this dissertation, has already been successfully applied to α-PP, γ-PP , PHB and PA.

7.2. Investigation of the dislocation kinetics by a novel nano-creep test

For a better understanding of the processes responsible for plasticity (e.g. the generation of dislocations and their movement), the knowledge about their kinetics is also of decisive importance. For this purpose usually mechanical tests with strain rate jumps are carried out. Since semi-crystalline polymers consist of two phases and the macroscopic deformation cannot be easely attributed to the individual phases. Nevertheless Li and Ngan were able to show that at nanoindentation creep experiments on polyethylene, the deformation in the crystalline phase occurs jerky over dislocation avalanches. This allows the specification of the macroscopic deformation to that of the amorphous phase (uniform and smooth) and of the crystalline phase (jerky). Thus a direct observation of the crystalline phase by mechanical experiments was possible. But these nanoindentation creep experiments have some limitations (inconstant loading stress, inhomogeneous stress field, small test volume) which can lead to unrealistic results. Therefore, a new nano-creep test based

on torsional loading has been developed within the scope of this dissertation (chapter 6) which avoid all these ambiguities. With the new nano-creep experiment, the stress can be applied much more homogeneously in a larger sample volume, so that the kinetics of the dislocation movement can be examined much more detailed as in nanoindentation creep experiments. With this new approach a reliable value of 0.59 eV for the activation energy for the mobilization of dislocations could be determined for the first time. In addition to the measurement of the activation energy the following four previously unknown phenomena could be observed.

1. **Negative strain bursts.**
   The most surprising result was the appearance of negative strain bursts which could never be observed in other materials. This means that considerable back-stresses are generated in the amorphous phase, which can cause a deformation in opposite direction to the macroscopic deformation. This shows that the amorphous phase above the glass transition temperature T_g also affects the processes in the crystalline phase. This is particularly noteworthy, since the macroscopic stress at the nano-creep experiments is always lower than 1 % of the yield stress and one must assume that the amorphous phase has not undergone any significant structural changes.

2. **Post-oscillations after a strain burst.**
   An estimation of the necessary dislocation density for the plastic deformation results in a volume of approximately 113 μm^3 being deformed for a single strain burst. This means that, in spite of a macroscopically very small deformation (few nm), locally significant deformations must occur. To a similar extent these deformations must also occur in the surrounding amorphous phase. Thereby in the amorphous phase arise back-stresses which undo the entire deformation, and the dislocation avalanches can run several times in different directions through the crystal. Therefore, the strong post-oscillations can be interpreted as a sequence of positive and negative strain bursts.

3. **Strain bursts and thus plastic deformation in the crystalline phase already occur at stresses < 1 % of yield stress.**
   Considering classical plasticity models for different materials, a plastic deformation in the applied stress range should be excluded. However, polymers show a time-temperature superposition due to the weak and temperature-dependent Van der Waals bonds between the macromolecules. This means that at very low strain rates (in case of the nano-creep experiments is $\dot{\varepsilon}^{vM} = 3.2 \cdot 10^{-7}$) the relaxation processes can run also at significantly lower temperatures and thus the strength of the crystalline phase is substantially reduced even at room temperature. This allows plastic deformations in the crystalline phase at significantly lower stresses.

4. **There is only a very small stress and temperature range in which the strain bursts show Arrhenius behaviour.**
   At very low loadings and extremely small associated strain rates, the deformation of the crystalline phase can be separated from that of the amorphous phase. In this

range, the strain bursts also show the expected Arrhenius behaviour. But doubling of the loading, or a temperature rise exceeding 45 °C will change the appearance of the strain bursts completely. The deformation of the crystalline phase occurs no longer via dislocation avalanches but increasingly by homogeneous movement of dislocations (transition from coarse to fine slip) and thus individual strain bursts are more and more difficult to detect.

The results show that the plasticity in the crystalline phase at low stresses (as in nano-creep experiments) and the yield behaviour of macroscopic samples is mainly influenced by the mobility of dislocations because sufficient thermally activable dislocations exist to allow the deformation of lamella nano-crystals. But for plastic flow far beyond the yield point the number of these thermally activatable dislocations is too low and additional dislocations must be mechanically generated. Here, the generation of dislocation determines the mechanical behaviour.

8. Outlook

With the new methods developed within the scope of this dissertation, some fundamental questions concerning the dislocations in semi-crystalline polymers could be clarified. But new methods often raise new questions. The investigated materials alpha polypropylene and polyethylene are important model materials for basic research. However, other semi-crystalline polymers or crystal modifications may show a different behaviour. Therefore the new developed methods for the analysis of dislocation should be applied to other semi-crystalline polymers as well.

A very interesting, hardly investigated model material is gamma polypropylene. The morphology of γ-PP can be strongly influenced by the crystallization conditions [103, 104]. Also γ-PP shows no increase of dislocation density during plastic deformation [124]. The major deformation mechanism in γ-PP is the interlamellar shear of the lamellae within the amorphous phase [106], which is different to PE and α-PP. By first systematic investigations regarding the strength of γ-PP [139, 140], quite unexpected results were observed. The strength strongly depends on the crystallization temperature and the crystallization pressure. Although the crystallization at different pressures leads to a completely different spherulite structure (Figure 2.23), it does not necessary cause different strengths (Figure 8.1a). Due to the higher pressure, an increase in strength results at higher crystallization temperatures, but comparable strengths are obtained despite a completely different spherulite structure. Rather, in terms of Young's dislocation model the differences in the strength of the γ-PP can be explained by differences in the lamellar thickness (Figure 8.1b). But this does not explain the difference in strength between alpha and gamma polypropylene.

In principle, gamma polypropylene is comparable to polyhydroxybutyrate (PHB). PHB also has relatively small lamellar thicknesses below 10 nm and shows a similar behaviour during plastic deformation [80]. Like in γ-PP, there is no increase in the dislocation density during plastic deformation. This could also mean that Young's dislocation model is not applicable for very small lamella thicknesses. This conclusion also follows from the consideration that at equal crystallinity degree the thickness of the amorphous intermediate layer is reduced by a small lamellar thickness. Thus, the fraction of the rigid amorphous phase is very high over the entire amorphous phase. This leads to a solidification of the entire amorphous phase and can strongly influence the macroscopic strength. This means that for small lamellar thicknesses Young's dislocation model has to be added to a composite model (like [64, 88]), since it does not consider the amorphous phase which cannot be neglected even at temperatures far over T_g.

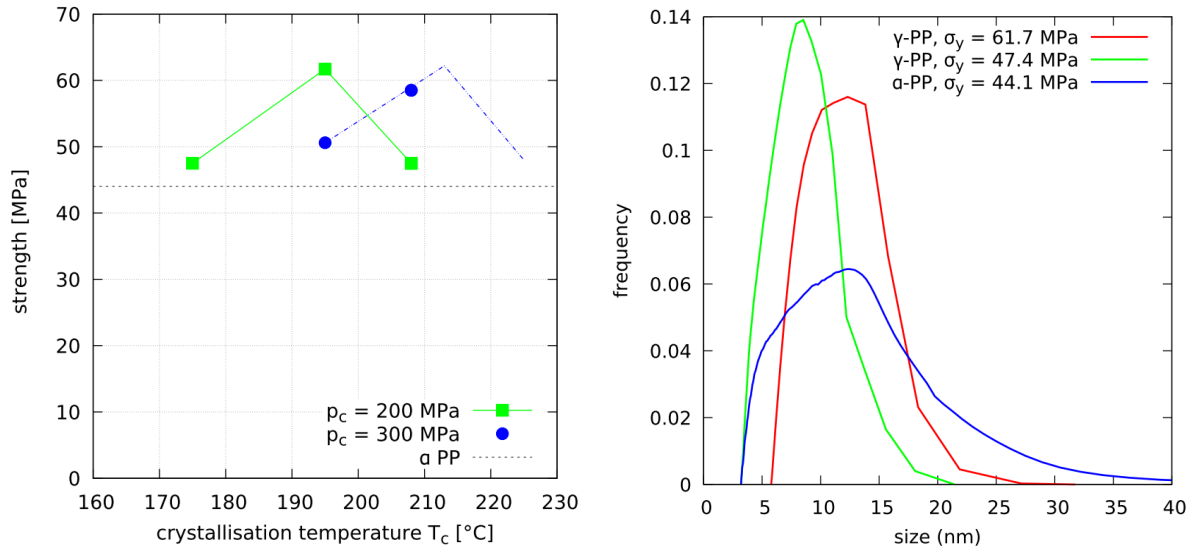

(a) (b)

Figure 8.1.: *Gamma polypropylene.*
(a) Strength dependence on crystallization pressure p_c und crystallization temperature T_c [31].
(b) Lamella thickness distribution from DSC for a sample with high (red) and low (green) strength.

Another aspect, in this context, is the behaviour of high density polyethylene (PE-HD). This semi-crystalline polymer shows no β relaxation (= glass transition) [17], which means there is no pronounced glass transition in the amorphous phase. Thus the amorphous phase should also be relatively stiff beyond T_g and considerably contribute to the macroscopic strength. However, the strength of PE-HD shows a good agreement with Young's dislocation model [51] which suggests that the amorphous phase does not affect the strength of semi-crystalline polymer, at least at temperatures above T_g.

On the other hand Rozanski and Galeski [161] could show that an additional stress in the amorphous phase decreases the macroscopic yield stress. The stress required for plastic deformation of crystals is equal to the measured yield stress plus the stress exerted by a swollen amorphous phase. Therefore, there are still open questions about the influence of the amorphous phase on the strength of semi-crystalline polymers.

Other interesting model materials are the terephthalates PET, PTT and PBT because they have a sufficient number of XRD reflections to analyse the defects by means of the MXPA. Furthermore, the rate of crystallization of PET is very small, thus the crystallinity can be controlled over the cooling conditions.

The MXPA has proven to be a very powerful method for the analysis of defects (dislocations) in semi-crystalline polymers. But their application to semi-crystalline polymers is still difficult because of the complex crystal systems with low symmetry. Further improve-

ments are therefore desirable. Through the calculation of the theoretical contrast factors, Spieckermann [23] could determine dislocation types (screw or edge) and slip directions (chain or transverse slip) by means of modified Williamson-Hall analysis. By integrating this approach into MXPA, the reliability of this method could be further increased. In addition, the distribution of the slip systems could be measured by means of a XRD texture measurement and thus the whole quality of the MXPA with respect to the reliability and resolution could be remarkably enhanced. Since for semi-crystalline polymers the lamellar thickness distribution can be measured by means of DSC, it is desirable to take this information into account at the MXPA. This could further reduce the number of fit parameters.

Unfortunately, the MXPA requires at least five XRD reflections. Therefore, the MXPA is not suitable for applying it to polyethylene (Figure 2.24). A relatively new method for defect analysis is the moment method developed by Groma [162–164], which allows a defect analysis on single X-ray reflection. This method is based on the asymptotic behaviour of the second and fourth order restricted moments. It can be considered as an advancement of the variance method originally proposed by Wilson [165]. In principle, by this method all semi-crystalline polymers can be analysed. Polt could showed that a quantitative analysis is possible at a background-to-peak-ratio of 10^{-3} [54]. In high density polyethylene, despite the high crystallinity of 80 %, the required signal quality cannot be achieved. Thus, an absolute defect density (dislocation density) cannot be determined but the analysis of the relative dislocation density development during the plastic deformation and of the annihilation behaviour is possible [54, 156].

Strain bursts in semi-crystalline polymers are a recently discovered phenomenon and, apart from this dissertation, only few nanoindentation creep experiments with polyethylene were carried out so far [89, 91]. Although a new nano-creep experiment, introduced by this dissertation, could be used to gain substantial new insights into strain bursts in semi-crystalline polymers, there are still open questions. Preliminary tests on polypropylene showed a similar behaviour as in polyethylene, it was also possible to induce strain bursts. Thus it is likely that strain bursts are a typical phenomenon in semi-crystalline polymers at small loadings, but further tests are necessary. An interesting approach is the calculation of the activation energy from the creep rate combined with a frequency evaluation [166] which could sucsessfuly applied by Zare Ghomsheh et al. [92] for nanoindentation creep experiments. Such an evaluation procedure may be also of interest for the nano-creep experiments.

9. Bibliography

[1] (access 30.12.2016). 2016. URL: http://www.plasticseurope.de.

[2] (access 30.12.2016). 2016. URL: http://www.worldsteel.org.

[3] G Gottstein. *Physical Foundations of Materials Science*. Springer, 2004.

[4] M Zehetbauer and YT Zhu, eds. *Bulk Nanostructured Materials*. 1st ed. Wiley-VCH, 2009.

[5] (access 30.12.2016). 2016. URL: http://www.doitpoms.ac.uk.

[6] (access 30.12.2016). 2016. URL: http://www.che.hw.ac.uk.

[7] (access 30.12.2016). 2016. URL: http://www.suggest-keywords.com.

[8] RJ Young and PA Lovell. *Introduction to Polymers*. 3rd ed. Taylor & Francis, 2011.

[9] Rolf Hosemann. "Crystalline and paracrystalline order in high polymers". In: *Journal of Applied Physics* 34.1 (1963), pp. 25–41.

[10] G Kanig. "Direkte beobachtung von polyäthylen-feinstrukturen und ihre veränderungen beim verstrecken und tempern". In: *Journal of Crystal Growth* 48.2 (1980), pp. 303–320.

[11] GW Ehrenstein, ed. *Polymer-Werkstoffe: Struktur – Eigenschaften – Anwendung*. 3rd ed. Carl Hanser Verlag, 2011.

[12] B Wunderlich. "Reversible crystallization and the rigid–amorphous phase in semicrystalline macromolecules". In: *Progress in Polymer Science* 28.3 (2003), pp. 383–450.

[13] Malgorzata Walczak. "Role and properties of the confined amorphous phase of polymers". PHD Thesis. Ecole nationale supérieure d'arts et métiers - ENSAM, 2012.

[14] (access 30.12.2016). 2016. URL: http://www.rheothing.com.

[15] B Crist. "Plastic deformation of polymers". In: *Structure and Properties of Polymers*. 12 vols. VCH Verlagsgesellschaft mbH, 1993. Chap. Nano and Micromechanics of Crystalline Polymers, 427—469.

[16] L Lin and AS Argon. "Structure and plastic deformation of polyethylene". In: *Journal of Materials Science* 29.2 (1994), pp. 294–323.

[17] IM Ward and J Sweeney. *An Introduction to the Mechanical Properties of Solid Polymers*. 2nd ed. John Wiley & Sons Ltd, 2004.

[18] AS Argon. *The Physics of Deformation and Fracture of Polymers*. Cambridge University Press, 2013.

[19] Z Bartczak and A Galeski. "Plasticity of Semicrystalline Polymers". In: *Macromolecular Symposia* 294.1 (2010), pp. 67–90. ISSN: 1521-3900.

[20] R Hiss et al. "Network stretching, slip processes, and fragmentation of crystallites during uniaxial drawing of polyethylene and related copolymers. A comparative study". In: *Macromolecules* 32.13 (1999), pp. 4390–4403.

[21] Z Bartczak. "Influence of molecular parameters on high-strain deformation of polyethylene in the plane-strain compression. Part II. Strain recovery". In: *Polymer* 46.23 (2005), pp. 10339–10354.

[22] R Seguela and F Rietsch. "Double yield point in polyethylene under tensile loading". In: *Journal of materials science letters* 9.1 (1990), pp. 46–47.

[23] F Spieckermann. "Investigation of Deformation Induced Changes of the Microstructure of Semicrystalline Polymers and their Impact on Mechanical Properties". PHD Thesis. University of Vienna, 2010.

[24] Andrzej Pawlak, Andrzej Galeski, and Artur Rozanski. "Cavitation during deformation of semicrystalline polymers". In: *Progress in polymer science* 39.5 (2014), pp. 921–958.

[25] Jun Mo Kim, Rebecca Locker, and Gregory C Rutledge. "Plastic deformation of semicrystalline polyethylene under extension, compression, and shear using molecular dynamics simulation". In: *Macromolecules* 47.7 (2014), pp. 2515–2528.

[26] A Galeski et al. "Morphological alterations during texture-producing plastic plane strain compression of high-density polyethylene". In: *Macromolecules* 25.21 (1992), pp. 5705–5718.

[27] S Nikolov and D Raabe. "Yielding of polyethylene through propagation of chain twist defects: Temperature, stem length and strain-rate dependence". In: *Polymer* 47.5 (2006), pp. 1696–1703.

[28] PB Bowden and RJ Young. "Deformation mechanisms in crystalline polymers". In: *Journal of Materials Science* 9.12 (1974), pp. 2034–2051.

[29] A Keller and DP Pope. "Identification of structural processes in deformation of oriented polyethylene". In: *Journal of Materials Science* 6.6 (1971), pp. 453–478.

[30] EF Oleinik. "Plasticity of semicrystalline flexible-chain polymers at the microscopic and mesoscopic levels". In: *Polymer science. Series C* 45 (2003), pp. 17–117.

[31] Gert R Strobl and Gert R Strobl. *The physics of polymers*. Vol. 2. Springer, 1997.

[32] A Galeski and G Regnier. "Nano- and micro-mechanics of polymer blends and composites". In: Hanser, 2009. Chap. Nano and Micromechanics of Crystalline Polymers.

[33] A Galeski, AS Argon, and Robert E Cohen. "Changes in the morphology of bulk spherulitic nylon 6 due to plastic deformation". In: *Macromolecules* 21.9 (1988), pp. 2761–2770.

[34] BJ Lee et al. "Simulation of large strain plastic deformation and texture evolution in high density polyethylene". In: *Polymer* 34.17 (1993), pp. 3555–3575.

[35] RN Haward and G 1 Thackray. "The use of a mathematical model to describe isothermal stress-strain curves in glassy thermoplastics". In: *Proceedings of the Royal Society of London A: Mathematical, Physical and Engineering Sciences*. Vol. 302. 1471. The Royal Society. 1968, pp. 453–472.

[36] Henry Eyring. "Viscosity, plasticity, and diffusion as examples of absolute reaction rates". In: *The Journal of chemical physics* 4.4 (1936), pp. 283–291.

[37] J Richeton et al. "Modeling and validation of the large deformation inelastic response of amorphous polymers over a wide range of temperatures and strain rates". In: *International journal of solids and structures* 44.24 (2007), pp. 7938–7954.

[38] A Peterlin. "Molecular model of drawing polyethylene and polypropylene". In: *Journal of materials science* 6.6 (1971), pp. 490–508.

[39] Paul J Flory. "Molecular morphology in semicrystalline polymers". In: *Nature* 272 (1978), pp. 226–229.

[40] LG Shadrake and F Guiu. "Dislocations in polyethylene crystals: line energies and deformation modes". In: *Philosophical Magazine* 34.4 (1976), pp. 565–581.

[41] Z Bartczak, RE Cohen, and AS Argon. "Evolution of the crystalline texture of high-density polyethylene during uniaxial compression". In: *Macromolecules* 25.18 (1992), pp. 4692–4704.

[42] Z Bartczak and A Galeski. "Yield and plastic resistance of α-crystals of isotactic polypropylene". In: *Polymer* 40.13 (1999), pp. 3677–3684.

[43] RWK Honeycombe. "The Plastic Deformation of Metals". In: (1968).

[44] Roland Séguéla. "Plasticity of semi-crystalline polymers: crystal slip versus melting-recrystallization". In: *e-Polymers* 7.1 (2007), pp. 382–401.

[45] H Gleiter and AS Argon. "Plastic deformation of polyethylene crystals". In: *Philosophical Magazine* 24.187 (1971), pp. 71–80.

[46] Z Bartczak, AS Argon, and RE Cohen. "Deformation mechanisms and plastic resistance in single-crystal-textured high-density polyethylene". In: *Macromolecules* 25.19 (1992), pp. 5036–5053.

[47] R Hill. *The Mathematical Theory of Plasticity*. Oxford, 1950.

[48] JR Hirsch and PT Wang. "Texture and strength evolution in deformed polypropylene". In: *Texture, Stress, and Microstructure* 13.2-3 (1991), pp. 101–122.

[49] S Ahzi, BJ Lee, and RJ Asaro. "Plasticity and anisotropy evolution in crystalline polymers". In: *Materials Science and Engineering: A* 189.1-2 (1994), pp. 35–44.

[50] Andrzej Galeski. "Strength and toughness of crystalline polymer systems". In: *Progress in Polymer Science* 28.12 (2003), pp. 1643–1699.

[51] T Kazmierczak, A Galeski, and AS Argon. "Plastic deformation of polyethylene crystals as a function of crystal thickness and compression rate". In: *Polymer* 46.21 (2005), pp. 8926–8936.

[52] FC Frank et al. "Deformation processes in polyethylene interpreted in terms of crystal plasticity". In: *Philosophical Magazine* 3.25 (1958), pp. 64–74.

[53] RJ Young and PB Bowden. "Twinning and martensitic transformations in oriented high-density polyethylene". In: *Philosophical magazine* 29.5 (1974), pp. 1061–1073.

[54] G Polt. "Dislocation mechanisms with respect to thermal relaxation and plastic deformation in semicrystalline polymers". PHD Thesis. University of Vienna, 2016.

[55] Joachim Rösler, Harald Harders, and Martin Bäker. *Mechanisches Verhalten der Werkstoffe*. Springer-Verlag, 2013.

[56] Thomas Chi-tsai Ting. *Anisotropic elasticity: theory and applications*. 45. Oxford University Press on Demand, 1996.

[57] D Hull and Bacon DJ. *Introduction to Dislocations*. 3rd ed. Pergamon Press, 1984.

[58] (access 06.01.2017). 2017. URL: `http://www.jrgreer.caltech.edu/content/teaching/MS116Files/Lectures/10a_Line\%20energy.pdf`.

[59] LG Shadrake and F Guiu. "Elastic line energies and line tensions of dislocations in polyethylene crystals". In: *Philosophical Magazine A* 39.6 (1979), pp. 785–796.

[60] JM Peterson. "Thermal initiation of screw dislocations in polymer crystal platelets". In: *Journal of Applied Physics* 37.11 (1966), pp. 4047–4050.

[61] James M Peterson. "Peierls stress for screw dislocations in polyethylene". In: *Journal of Applied Physics* 39.11 (1968), pp. 4920–4928.

[62] RJ Young. "A dislocation model for yield in polyethylene". In: *Philosophical Magazine* 30.1 (1974), pp. 85–94.

[63] Buckley Crist, Christopher J Fisher, and Paul R Howard. "Mechanical properties of model polyethylenes: tensile elastic modulus and yield stress". In: *Macromolecules* 22.4 (1989), pp. 1709–1718.

[64] Bijin Xiong et al. "Critical stress and thermal activation of crystal plasticity in polyethylene: Influence of crystal microstructure and chain topology". In: *Polymer* (2017).

[65] WJ O'Kane and RJ Young. "The role of dislocations in the yield of polypropylene". In: *Journal of materials science letters* 14.6 (1995), pp. 433–435.

[66] AS Argon, A Galeski, and T Kazmierczak. "Rate mechanisms of plasticity in semicrystalline polyethylene". In: *Polymer* 46.25 (2005), pp. 11798–11805.

[67] R Séguéla. "Dislocation approach to the plastic deformation of semicrystalline polymers: kinetic aspects for polyethylene and polypropylene". In: *Journal of Polymer Science Part B: Polymer Physics* 40.6 (2002), pp. 593–601.

[68] John Price Hirth and Jens Lothe Krieger. *Theory of Dislocations*. Jens Lothe Krieger, 1991.

[69] O Darras and R Séguéla. "Tensile yield of polyethylene in relation to crystal thickness". In: *Journal of Polymer Science Part B: Polymer Physics* 31.7 (1993), pp. 759–766.

[70] AW Agar, FC Prank, and A Keller. "Crystallinity effects in the electron microscopy of polyethylene". In: *Philosophical Magazine* 4.37 (1959), pp. 32–55.

[71] BE Warren. *X-ray Diffraction*. Dover Publications Inc., Reprint of the Addison-Wesley Publishing Company, Inc., 1991.

[72] MK Krivoglaz. *Theory of X-ray and Thermal Neutron Scattering by Real Crystals*. Plenum Press, 1996.

[73] BE Warren and BL Averbach. "The effect of cold-work distortion on X-ray patterns". In: *Journal of Applied Physics* 21.6 (1950), pp. 595–599.

[74] M Wilkens. "The determination of density and distribution of dislocations in deformed single crystals from broadened X-ray diffraction profiles". In: *Physica status solidi (a)* 2.2 (1970), pp. 359–370.

[75] GK Williamson and WH Hall. "X-ray line broadening from filed aluminium and wolfram". In: *Acta metallurgica* 1.1 (1953), pp. 22–31.

[76] T Ungár and A Borbély. "The effect of dislocation contrast on x-ray line broadening: A new approach to line profile analysis". In: *Applied Physics Letters* 69.21 (1996), pp. 3173–3175.

[77] T Ungár et al. "The contrast factors of dislocations in cubic crystals: the dislocation model of strain anisotropy in practice". In: *Journal of applied crystallography* 32.5 (1999), pp. 992–1002.

[78] Michael B Kerber et al. "X-ray line profile analysis—An ideal tool to quantify structural parameters of nanomaterials". In: *JOM* 63.7 (2011), pp. 61–70.

[79] H Wilhelm et al. "Evidence of dislocations in melt-crystallised and plastically deformed polypropylene". In: *Materials Science and Engineering: A* 387 (2004), pp. 1018–1022.

[80] F Spieckermann et al. "Plasticity and X-ray Line Profile Analysis of the semicrystalline polymer poly (3-hydroxybutyrate)". In: *Journal of Physics: Conference Series*. Vol. 240. 1. IOP Publishing. 2010, p. 012146.

[81] Florian Spieckermann et al. "Determination of lamella thickness distributions in isotactic polypropylene by X-ray line profile analysis". In: *Polymer* 51.18 (2010), pp. 4195–4199.

[82] Florian Spieckermann et al. "The role of dislocations for the plastic deformation of semicrystalline polymers as investigated by multireflection X-ray line profile analysis". In: *Journal of Applied Polymer Science* 125.6 (2012), pp. 4150–4154.

[83] G Polt et al. "Crystalline plasticity in isotactic polypropylene below and above the glass transition temperature." In: *Express Polymer Letters* 9.10 (2015).

[84] F Spieckermann et al. "Dislocation movement induced by molecular relaxations in isotactic Polypropylene". In: *submitted to Macromolecules* (2017).

[85] Yehia M Haddad. *Mechanical Behaviour of Engineering Materials: Volume 2: Dynamic Loading and Intelligent Material Systems*. Springer Science & Business Media, 2013.

[86] Robert C Scogna and Richard A Register. "Rate-dependence of yielding in ethylene–methacrylic acid copolymers". In: *Polymer* 49.4 (2008), pp. 992–998.

[87] George Halsey, Howard J White, and Henry Eyring. "Mechanical properties of textiles, I". In: *Textile Research Journal* 15.9 (1945), pp. 295–311.

[88] F Spieckermann et al. "Rate mechanism and dislocation generation in high density polyethylene and other semicrystalline polymers". In: *Polymer* 55.5 (2014), pp. 1217–1222.

[89] J Li and AHW Ngan. "Nanoscale fast relaxation events in polyethylene". In: *Scripta Materialia* 62.7 (2010), pp. 488–491.

[90] Michael D Uchic et al. "Sample dimensions influence strength and crystal plasticity". In: *Science* 305.5686 (2004), pp. 986–989.

[91] M Zare Ghomsheh et al. "Analysis of strain bursts during nanoindentation creep of high-density polyethylene". In: *Polymer International* 64.11 (2015), pp. 1537–1543.

[92] M Zare Ghomsheh et al. "Activation energy of strain bursts during nanoindentation creep on polyethylene". In: *in preparation for submission* (2017).

[93] B Poon, D Rittel, and G Ravichandran. "An analysis of nanoindentation in linearly elastic solids". In: *International Journal of Solids and Structures* 45.24 (2008), pp. 6018–6033.

[94] B Lotz, JC Wittmann, and AJ Lovinger. "Structure and morphology of poly (propylenes): a molecular analysis". In: *Polymer* 37.22 (1996), pp. 4979–4992.

[95] Zhenzhen Zhou et al. "An abnormal melting behavior of isotactic polypropylene spherulites grown at low temperatures". In: *Polymer* 111 (2017), pp. 183–191.

[96] Sergio Brückner et al. "Polymorphism in isotactic polypropylene". In: *Progress in Polymer Science* 16.2-3 (1991), pp. 361–404.

[97] J Morawiec et al. "Rolling of polymeric materials with side constraints". In: *Materials Science and Engineering: A* 317.1 (2001), pp. 21–27.

[98] S Vleeshouwers. "Simultaneous in-situ WAXS/SAXS and dsc study of the recrystallization and melting behaviour of the α and β form of iPP". In: *Polymer* 38.13 (1997), pp. 3213–3221.

[99] H Dragaun, H Hubeny, and H Muschik. "Shear-induced β-form crystallization in isotactic polypropylene". In: *Journal of Polymer Science: Polymer Physics Edition* 15.10 (1977), pp. 1779–1789.

[100] J Moitzi and P Skalicky. "Shear-induced crystallization of isotactic polypropylene melts: isothermal WAXS experiments with synchrotron radiation". In: *Polymer* 34.15 (1993), pp. 3168–3172.

[101] Ewa Piorkowska and Gregory C Rutledge. *Handbook of polymer crystallization*. John Wiley & Sons, 2013.

[102] Stefano Valdo Meille and Sergio Brückner. "Non-parallel chains in crystalline gamma-isotactic polypropylene". In: *Nature* 340 (1989), pp. 455–457.

[103] Khaled Mezghani and Paul J Phillips. "The γ-phase of high molecular weight isotactic polypropylene. II: The morphology of the γ-form crystallized at 200 MPa". In: *Polymer* 38.23 (1997), pp. 5725–5733.

[104] Khaled Mezghani and Paul J Phillips. "The γ-phase of high molecular weight isotactic polypropylene: III. The equilibrium melting point and the phase diagram". In: *Polymer* 39.16 (1998), pp. 3735–3744.

[105] C von Baeckmann et al. "The Influence of Different Crystallization Conditions on the Macromolecular Structure of γ-Polypropylene and the Development of Super-Sized Spherulites". In: *in preparation for submission* (2017).

[106] E Lezak, Z Bartczak, and A Galeski. "Plastic deformation of the γ phase in isotactic polypropylene in plane-strain compression". In: *Macromolecules* 39.14 (2006), pp. 4811–4819.

[107] EP Moore, ed. *Polypropylene Handbook*. Hanser Publishers, 1996.

[108] Stefano V Meille, S Bruckner, and W Porzio. "γ-Isotactic polypropylene. A structure with nonparallel chain axes". In: *Macromolecules* 23.18 (1990), pp. 4114–4121.

[109] Andrew Peacock. *Handbook of polyethylene: structures: properties, and applications*. CRC Press, 2000.

[110] (access 22.01.2017). 2011. URL: `http://www.esrf.eu/UsersAndScience/Experiments/CRG/BM26/SaxsWaxs/Hdpe`.

[111] J Petermann and H Gleiter. "Direct observation of dislocations in polyethylene crystals". In: *Philosophical Magazine* 25.4 (1972), pp. 813–816.

[112] N Brown. In: *Microplasticity*. Ed. by C.J. McMahon. New York: Wiley-Interscience, 1968, pp. 45–73.

[113] N Brown and S Rabinowitz. "Components of microstrain in polyethylene". In: *Journal of Polymer Science Part B: Polymer Physics* 40.23 (2002), pp. 2693–2701.

[114] E Schafler, M Zehetbauer, and T Ungár. "Measurement of screw and edge dislocation density by means of X-ray Bragg profile analysis". In: *Materials Science and Engineering: A* 319 (2001), pp. 220–223.

[115] T Ungár and G Tichy. "The Effect of Dislocation Contrast on X-Ray Line Profiles in Untextured Polycrystals". In: *physica status solidi (a)* 171.2 (1999), pp. 425–434.

[116] G Ribárik and T Ungár. *Unpublished results*. 2002.

[117] BE Warren. "X-ray studies of deformed metals". In: *Progress in metal physics* 8 (1959), pp. 147–202.

[118] G Ribárik, T Ungár, and J Gubicza. "MWP-fit: a program for multiple whole-profile fitting of diffraction peak profiles by ab initio theoretical functions". In: *Journal of Applied Crystallography* 34.5 (2001), pp. 669–676.

[119] Alfred Paris. "Anwendung der Bragg-Profilanalyse zur Bestimmung von verformungsinduzierten Versetzungen in Polypropylen". Diploma Thesis. University of Vienna, 2003.

[120] T Ungár. "Dislocation densities, arrangements and character from X-ray diffraction experiments". In: *Materials Science and Engineering: A* 309 (2001), pp. 14–22.

[121] JM Mark, ed. *Polymer Data Handbook*. 2nd ed. Oxford University Press, 1999.

[122] Jeno Gubicza and Tamás Ungár. "Characterization of defect structures in nanocrystalline materials by X-ray line profile analysis". In: *Zeitschrift für Kristallographie-Crystalline Materials* 222.11/2007 (2007), pp. 567–579.

[123] Jen Gubicza. *X-ray line profile analysis in materials science*. IGI Global, 2014.

[124] G Polt et al. "The role of dislocations in γ-iPP under plastic deformation investigated by X-ray line profile analysis". In: *Mechanics of Materials* 67 (2013), pp. 126–132.

[125] Florian Spieckermann et al. "Determination of critical strains in isotactic polypropylene by cyclic loading-unloading". In: *Journal of Engineering Materials and Technology* 131.1 (2009), p. 011109.

[126] Peng Li, Sheng Zhao, and Jenny Liu. "Characterizing Stress–Strain Relationships of Asphalt Treated Base". In: *Journal of Materials in Civil Engineering* 28.8 (2016), p. 04016045.

[127] Elizabeth J Clark and John D Hoffman. "Regime III crystallization in polypropylene". In: *Macromolecules* 17.4 (1984), pp. 878–885.

[128] Buckley Crist, Francis M Mirabella, et al. "Crystal thickness distributions from melting homopolymers or random copolymers". In: *Journal of Polymer Science Part B Polymer Physics* 37.21 (1999), pp. 3131–3140.

[129] N Alberola, JY Cavaille, and J Perez. "Mechanical spectrometry of alpha relaxations of high-density polyethylene". In: *Journal of Polymer Science Part B: Polymer Physics* 28.4 (1990), pp. 569–586.

[130] G Ribárik. "Modelling of diffraction patterns based on microstructural properties". PHD Thesis. Eotvos Lorand University, 2008.

[131] Michael B Kerber. "X-ray line profile analysis in theory and experiment". PHD Thesis. University of Vienna, 2012.

[132] W Ruland. "X-ray determination of crystallinity and diffuse disorder scattering". In: *Acta Crystallographica* 14.11 (1961), pp. 1180–1185.

[133] CG Vonk. "Computerization of Ruland's X-ray method for determination of the crystallinity in polymers". In: *Journal of Applied Crystallography* 6.2 (1973), pp. 148–152.

[134] Erik Parteder and Rolf Bünten. "Determination of flow curves by means of a compression test under sticking friction conditions using an iterative finite-element procedure". In: *Journal of materials processing technology* 74.1 (1998), pp. 227–233.

[135] Dima Libster, Abraham Aserin, and Nissim Garti. "Advanced nucleating agents for polypropylene". In: *Polymers for Advanced Technologies* 18.9 (2007), pp. 685–695.

[136] Przemyslaw Sowinski et al. "The role of nucleating agents in high-pressure-induced gamma crystallization in isotactic polypropylene". In: *Colloid and polymer science* 293.3 (2015), pp. 665–675.

[137] Dirk Willem Van Krevelen and Klaas Te Nijenhuis. *Properties of polymers: their correlation with chemical structure; their numerical estimation and prediction from additive group contributions*. Elsevier, 2009.

[138] Alfréd Kállay-Menyhárd et al. "Direct correlation between modulus and the crystalline structure in isotactic polypropylene". In: *Express Polymer Letters* 9.3 (2015), pp. 308–320.

[139] S Strobel. "Influence of the crystallization conditions on the strength of gamma polypropylene". Bachelor Thesis. University of Applied Sciences Upper Austria, 2017.

[140] Cornelia vonBaeckmann. "The role of high-pressure crystallization on the strength of γ-Polypropylene". Master Thesis. University of Vienna, 2016.

[141] S Rabinowitz and N Brown. "Microstrain investigation of polyethylene". In: *Journal of Polymer Science Part A-2: Polymer Physics* 5.1 (1967), pp. 143–156.

[142] Michael Zaiser. "Scale invariance in plastic flow of crystalline solids". In: *Advances in physics* 55.1-2 (2006), pp. 185–245.

[143] X Tong et al. "Shear avalanches in plastic deformation of a metallic glass composite". In: *International Journal of Plasticity* 77 (2016), pp. 141–155.

[144] (access 12.12.2016). 2016. URL: `http://www.matweb.com`.

[145] (access 12.12.2016). 2016. URL: `http://www.gnu.org/software/octave`.

[146] A Vinogradov and IS Yasnikov. "On the nature of acoustic emission and internal friction during cyclic deformation of metals". In: *Acta Materialia* 70 (2014), pp. 8–18.

[147] J Lai and A Bakker. "Analysis of the non-linear creep of high-density polyethylene". In: *Polymer* 36.1 (1995), pp. 93 –99.

[148] S Patlazhan and Y Remond. "Structural mechanics of semicrystalline polymers prior to the yield point: a review". In: *Journal of Materials Science* 47.19 (2012), pp. 6749–6767.

[149] GI Taylor. "The mechanism of plastic deformation of crystals. Part I. Theoretical". In: *Proceedings of the Royal Society of London. Series A, Containing Papers of a Mathematical and Physical Character* 145.855 (1934), pp. 362–387.

[150] Kohji Tashiro, Masamichi Kobayashi, and Hiroyuki Tadokoro. "Calculation of Three-Dimensional Elastic Constants of Polymer Crystals. 1. Method of Calculation". In: *Macromolecules* 11.5 (1978), pp. 908–913.

[151] Hongyi Zhou and Garth L Wilkes. "Creep behaviour of high density polyethylene films having well-defined morphologies of stacked lamellae with and without an observable row-nucleated fibril structure". In: *Polymer* 39.16 (1998), pp. 3597–3609.

[152] James E Sinclair and John W Edgemond. "Investigation of creep phenomena in polyethylene and polypropylene". In: *Journal of applied polymer science* 13.5 (1969), pp. 999–1012.

[153] Svante Arrhenius. "Über die Reaktionsgeschwindigkeit bei der Inversion von Rohrzucker durch Säuren". In: *Zeitschrift für physikalische Chemie* 4.1 (1889), pp. 226–248.

[154] Yongfeng Men et al. "Mechanical α-process in polyethylene". In: *Macromolecules* 36.13 (2003), pp. 4689–4691.

[155] EA Zubova, NK Balabaev, and LI Manevitch. "Molecular mechanisms of the chain diffusion between crystalline and amorphous fractions in polyethylene". In: *Polymer* 48.6 (2007), pp. 1802–1813.

[156] F Spieckermann et al. "Evidence for dislocation presence and multiplication from the Momentum Method". In: *in preparation for submission* (2017).

[157] Fusakichi Omori. "On the after-shocks of earthquakes". In: *Journal of the College of Science* 7 (1894), pp. 111–200.

[158] Carl Kisslinger. "Aftershocks and fault-zone properties". In: *Advances in geophysics* 38 (1996), pp. 1–36.

[159] T Utsu. "A statistical study on the occurrence of aftershocks." In: *Geophysical Magazine* 30.4 (1961).

[160] Richard H Boyd. "Relaxation processes in crystalline polymers: molecular interpretation—a review". In: *Polymer* 26.8 (1985), pp. 1123–1133.

[161] Artur Rozanski and Andrzej Galeski. “Plastic yielding of semicrystalline polymers affected by amorphous phase”. In: *International journal of plasticity* 41 (2013), pp. 14–29.

[162] I Groma. “X-ray line broadening due to an inhomogeneous dislocation distribution”. In: *Physical Review B* 57.13 (1998), p. 7535.

[163] I Groma and F Székely. “Analysis of the asymptotic properties of X-ray line broadening caused by dislocations”. In: *Journal of applied crystallography* 33.6 (2000), pp. 1329–1334.

[164] A Borbély and I Groma. “Variance method for the evaluation of particle size and dislocation density from x-ray Bragg peaks”. In: *Applied Physics Letters* 79.12 (2001), pp. 1772–1774.

[165] A JC Wilson. “The effects of dislocations on X-ray diffraction”. In: *Il Nuovo Cimento (1955-1965)* 1.2 (1955), pp. 277–283.

[166] VI Vettegren et al. “The distribution of creep activation energies in oriented polyethylene films”. In: *Technical Physics Letters* 29.10 (2003), pp. 848–850.